STIMULI-RESPONSIVE NANOPARTICLES FOR TREATMENT OF LUNG CANCER

by

ROSHNI IYER

DISSERTATION

Submitted in partial fulfillment of the requirements
for the degree of Doctor of Philosophy at
The University of Texas at Arlington

December, 2018

Arlington, Texas

Supervising committee:

Dr. Kytai T. Nguyen, Supervising professor

Dr. Yi Hong, Co-advisor

Dr. Debabrata Saha

Dr. Liping Tang

Dr. Wei Chen

ACKNOWLEDGEMENTS

I would like to take this opportunity to extend my sincere gratitude to all of those, who have helped and guided me on my path to achieving my doctoral degree. They all have provided me with exciting opportunities and helped me polish my research and analytical skills, which will be a very valuable asset for the future. First and foremost, I would like to thank my advisor, Dr. Kytai T. Nguyen for her advice, words of wisdom, patience and most importantly providing me with the resources that have played a key role in achieving success in my work. Without her support, I would not have been able to attend and present at several international bioengineering conferences that have provided me with insight and ideas for my research. I would also like to thank Dr. Yi Hong, not only for giving me the opportunity to use his glutathione-responsive polymer, but also for his encouragement and support that helped me develop the first part of my research. Furthermore, I would like to express my gratitude to Dr. Debabrata Saha for his guidance and expertise in radiation oncology that helped shape my research in radiation therapy. Thanks to him, I had the opportunity to learn from and work with experts in the field of cancer biology and radiation therapy from the University of Texas Southwestern Medical Center in Dallas. In addition to Dr. Nguyen and Dr. Hong, I would like to thank Dr. Liping Tang and Dr. Wei Chen, for taking time out of their busy schedules to be a part of my dissertation committee and helping me through the dissertation process. I would also like to acknowledge my co-authors for their help and support throughout the research. My sincere gratitude towards the Enhanced graduate teaching assistantship provided by the University of Texas at Arlington for financial support and the staff in the bioengineering department at UTA for their kind assistance. Finally, and most importantly, this work was supported by funding from the National Institute of Health grants.

DEDICATION

I would like to express gratitude towards my lab mates at the Nanomedicine and Drug Delivery Lab and the friends I made at UTA, for their words of encouragement and for all the small moments that we laughed together. I will always cherish those moments. I thank all my dear friends, especially Ms. Sonia Santimano, who stood by me all these years and supported me during happy and difficult times. Most importantly, I would like to thank my parents, Mr. Gopal Iyer and Mrs. Geeta Gopal for having the faith in me, for being patient and for supporting me emotionally and financially, without any doubt. Their undying love and support gave me the strength to pursue and complete my doctoral degree. Finally, thank you lord for bestowing upon me your words of wisdom and for your faith in me that have been a beacon of light and a source of encouragement throughout this journey.

ABSTRACT

STIMULI-RESPONSIVE NANOPARTICLES FOR TREATMENT OF LUNG CANCER

Roshni Iyer, PhD

The University of Texas at Arlington

Supervising professor: Kytai T. Nguyen

Despite extensive research and progress in anti-cancer therapeutics, an effective treatment for non-small cell lung cancer (NSCLC) remains elusive, resulting in poor 5-year patient survival rate. Towards this end, we have explored a therapeutic regimen to improve the effects of local concurrent chemo-radiation-therapy (CRT), by utilizing multifunctional stimuli-responsive nanoparticles (NPs) as drug carriers. We have also utilized lung cancer targeting strategies for site-specific drug delivery, mainly antibodies against the Ephrin-transmembrane receptor kinase (EphA2), that is over-expressed mainly on lung cancer cells, to promote the targeted delivery of drugs to only cancer cells, and eventually reduce the toxicity to healthy tissues. The overall goal of these NPs is to provide a triggered release of potent radiosensitizers (NU7441) upon exposure to radiation, followed by release of chemotherapeutic agents (cisplatin) in response to elevated glutathione levels in the lung cancer cells, to facilitate enhanced spatio-temporal drug release in the lung tumor environment for CRT. This design-driven research has been approached in three specific aims, each exploring the physico-chemical properties of the NPs and their *in vitro* and *in vivo* therapeutic efficacies and biodistribution; **Aim 1:** Cisplatin-loaded glutathione (GSH)-responsive nanoparticles (GNPs) for lung cancer chemotherapy, **Aim 2:** NU7441-loaded radiation (RT)-responsive NPs for lung cancer radiation therapy and **Aim 3:** Multifunctional dual drug-loaded, dual stimuli-responsive core-shell NPs (DSNPs) for CRT. Our results demonstrated the GSH- and radiation-responsive drug release characteristics of the NPs from Aim 1 and 2 respectively, the enhanced lung cancer cell targeting abilities of these NPs and finally their improved therapeutic efficacies compared to free drugs and untargeted NPs. Finally, a core-shell combination of these NPs observed synergistic drug release and therapeutic efficacies, concurrently with radiation therapy. These NPs could potentially be used to improve outcomes in patients with NSCLC when applying CRT to treat lung cancer.

LIST OF FIGURES

TABLE OF CONTENTS

CHAPTER 1: INTRODUCTION

1.1. LUNG CANCER

1.1.1 Lung cancer statistics

Cancer is one of the major causes of mortality world-wide, and the second largest cause of death in the United States. Cancer statistics for 2018, from the American Cancer Society predict over 1,735,000 cases, estimating over 4,000 new cases per day [1]. Additionally, over 600,000 Americans' have been estimated to die due to cancer in 2018, which is a shocking 1,700 deaths per day, emphasizing the severity of the disease [1]. Lung cancer is one of the most common causes of cancer-related mortality in the United States. The American Cancer Society has projected over 230,000 new cancer cases and about 150,000 deaths due to lung cancer for the year 2018 [1]. Additionally, the survival rate of patients suffering from lung cancer is one of the lowest, accounting for about 18% [1].

1.1.2 Lung cancer physiology

Lung cancer is broadly classified into two major types; small cell lung cancer (SCLC) and non-small cell (or large cell) lung cancer (NSCLC) based on their appearance. Non-small cell lung cancer (NSCLC) accounts for over 80 to 85% of total lung cancer cases and is one of the major causes of deaths due to lung cancer in the United States [2]. NSCLC can be further classified into

epidermoid, adenocarcinoma, broncho-alveolar, and squamous cell carcinoma [3]. SCLC on the other hand, is a less prominent but more aggressive form of lung cancer, and accounts for about 15 to 20% of lung cancer cases [2, 4]. NSCLC and SCLC experience variations in oncogene expression; for instance, K-RAS is mutated in over 30% of NSCLC cases, but never in SCLC [4]. The tumor suppressor gene (TSG) p53 is mutated in over 90% of SCLC cases, and over 50% NSCLC cases [5], whereas retinoblastoma TSG is inactivated in over 90% of SCLC cases, but in only 15% of NSCLC cases [4]. Thus, the oncogene expression can also be used as a biomarker for identification of the lung cancer type. Histologically, NSCLC tissues from former or current smokers, observe molecular abnormalities in the epithelium, such as hyperplasia, dysplasia and *in situ* carcinoma, all of which are minimal in SCLC tissues for the same population [4]. However, SCLC tissues from these patients experience more genetic damage in terms of significantly increased rate of allele loss, compared to that in NSCLC tissues [5].

1.1.3 Causes of lung cancer

Lung cancer is commonly caused by inhalation of toxic mutagenic agents. Tobacco is one of the major causes of lung cancer, due to the exposure of the lungs to toxic agents from the smoke [6, 7]. Adenocarcinoma, on the other hand is caused by inhalation of agents such as asbestos, or upon exposure to radiation such as radon [8, 9]. Besides these, lung cancer can also be caused by genetic alteration, familial predisposition, or bacterial infection like *Helicobacter pylori* [10, 11].

1.2. CANCER TREATMENT STRATEGIES

Standard lung cancer treatment strategies include chemotherapy, radiation therapy and surgery. Choice of treatment depends on the type of lung cancer. Initial stages of SCLC respond to chemotherapy and radiation therapy [2]. NSCLC, on the other hand, is less susceptible to these treatment modalities, but can be treated by surgery; however, this option is limited to early NSCLC patients only (stages I, II and IIIA) [2]. The later stages of NSCLC are then treated with chemotherapy and/or radiation therapy or a combination of these modalities. Overall improvement in surgical techniques, chemotherapy and radiation therapy have drastically improved the 1 year survival rate of lung cancer patients from 34% in 1975-1977 to 45% in 2008-2011 [12]. However, the 5-year survival rate of lung cancer patients still remains very low, limited to about 7% of SCLC patients and 21% of NSCLC patients [12]. There are several strategies that have been utilized to treat lung cancer [3, 13, 14]. The following section will review the most common lung cancer treatment strategies, including those that we have utilized in this research, and discuss their advantages and limitations.

1.2.1 Surgery

Treatment of early stage NSCLC usually involves surgical removal of the cancerous tissues. A 2016 statistical report of cancer treatment and survival observed that majority (over 69%) of stage I and II NSCLC patients undergo tumor resection surgery, whereas over 25% of the surgical cases also receiving chemotherapy and/or radiation therapy [12]. There are several

types of surgical procedures that can be implemented to treat NSCLC, such as pneumonectomy, which is surgical removal of an entire lung [15]. Lobectomy, on the other hand, involves removal of an entire lobe containing the tumor, while segmentectomy is removal of only the tumor affected part of the lobe and is usually implemented in patients with poor lung functions [16, 17]. A recent study investigating the survival and postoperative complications of lung cancer patients that underwent surgical resection of lung tumor reported the highest percentage of tumor resection via lobectomy (69%), followed by wedge resection (17%), segmentectomy (7%), pnemonectomy (3%) bilobectomy (3%) and sleeve lobectomy (1%) [18]. Surgical resection of lung tumors has several limitations, particularly reducing the quality of life for the patients post-operation and the risk of long-term disability [19]. Complications from lung surgery include air leak, pneumonia or mucus plugging, atrial fibrillation, right middle lobe torsion, hemorrhage, chylothorax and nerve injury [20]. In fact, a recent study observed that in over 50% of patients suffering from postoperative complications, the most common complication was acute respiratory distress syndrome (ARDS) [18].

1.2.2 Chemotherapy

Chemotherapy is intravenous administration of antineoplastic drugs, that circulate throughout the body and kill tumor cells [21]. Chemotherapy remains the first-line treatment for advanced stage NSCLC (stages IIIb and IV) [3]. A 2016 study reported over 53% of stages IIIb and IV NSCLC cases received chemotherapy with or without radiation therapy [12]. Multiple single and combined drug strategies have also been investigated clinically to obtain the highest

therapeutic efficacy. Commonly recommended chemotherapeutic strategies include platinum drugs such as cisplatin, carboplatin, and platinum doublets including cisplatin/gemcitabine, cisplatin/pemetrexed, pemetrexed/carboplatin and gemcitabine/carboplatin, all of which have shown modest clinical successes [3, 21, 22]. The antifolate agent pemetrexed is approved for treatment of non-squamous carcinomas only [22]. Addition of molecular targets such as bevacizumab that targets VEGF combined with paclitaxel/carboplatin further increased overall patient survival and has hence been approved for treatment of non-squamous carcinomas [23]. However, other clinical trials combining bevacizumab with other platinum doublets have observed evidences of excess toxicities [24]. Cetuximab, another monoclonal antibody against epidermal growth factor receptor (EGFR), did not improve patient outcomes, and thus has not yet received approval for treatment of NSCLC [25]. Approved second-line chemotherapeutic agents include, docetaxel, pemetrexed for non-squamous carcinoma, and the EGFR inhibitors like erlotinib and gefitinib [3]. Erlotinib, specifically observed significant improvement in patient survival and outcomes in a large randomized trial for the treatment of advanced NSCLC [26].

Chemotherapy suffers from several limitations, particularly toxicity in healthy tissues. For instance, cisplatin platinum-based drugs cause severe dose-limiting side-effects, such as nephrotoxicity, cardiotoxicity, peripheral neuropathy and anemia [21]. Besides these drawbacks, chemotherapy also causes side-effects such as fatigue, hair loss and nausea [21]. These limitations greatly limit the dose that can be administered to the patient and consequently reduce the therapeutic efficacy of the drugs. Another major disadvantage of chemotherapy, is the hydrophobic nature of the chemotherapeutic drugs that limits their administration to low doses, leading to low bioavailability [27, 28]. Additionally, chemo-resistance in cancer cells contributes

to the lack of therapeutic effectiveness of the drug [29]. Thus, there is an urgent need to improve the delivery of chemotherapeutic drugs and enhance their therapeutic efficacy while reducing off-target drug side-effects. In aim 1, we will investigate nanoparticles for delivery of cisplatin for improved lung cancer chemotherapy.

1.2.3 Radiation therapy

Radiation therapy (RT) is the treatment of choice in cases where surgery is not applicable [30, 31]. RT involves exposing solid tumors to ionizing radiations like x-rays, gamma rays and high energy particles [32]. RT kills tumor cells by generating free radicals (via excitation of the water molecules within cells) [33]. These free radicals then induce DNA double strand breaks (DSB), thereby causing DNA damage followed by cell death [33]. Some of the most common radiotherapy strategies are, stereotactic body radiation (SBRT) or stereotactic ablative RT (SABR) for stage I NSCLC and concurrent chemoradiation for stage III NSCLC [34, 35]. SABR involves subjecting the patient to fractionated high doses of radiation at the site of tumor [35]. Compared to conventional RT, SABR is advantageous as it can reduce the overall treatment time and produces a larger effective dose for treatment, a significant benefit for patients suffering from cardiopulmonary diseases and for the elderly [35]. SABR is usually supplemented with 4D computed tomography to determine the precise location for RT [35]. Hyper fractionation (HFX) exploits fractionated radiation doses that can control the growth of NSCLC, without risking damage to normal healthy tissues [35]. Chemoradiation therapy, on the other hand involves chemotherapy in addition to RT, a strategy which has proven superior compared to RT alone [36].

However, chemoradiation therapy is a feasible option only for patients devoid of any other chronic illness, young patients and those with other healthy organs [35].

The limitations associated with RT include low tolerance of normal tissues to radiation, which limits the dosage that can be used and radiation-induced lung injury, particularly lung fibrosis [37, 38]. Additionally, tumor cells undergoing RT may have the ability to repair their damaged DNA as a result of non-homogenous end joining process (NHEJ) and homologous recombination (HR), thus reducing the efficacy of RT [39]. DNA-dependent protein kinase (DNA-PK) is a nuclear serine/threonine kinase, that is a major component of NHEJ-induced DNA repair in cancer cells, that acts as a scaffolding protein to align the broken DNA strand and guide the repair factors involved in DNA repair [40, 41]. Thus, DNA-PK inhibitors, a class of radiosensitizers (RS), have been investigated to overcome the limitations by causing irreversible DNA damages and to potentially reduce the dose of radiation required for a therapeutic effect [38]. The most common approach uses highly potent small molecules like wortmannin (IC50: 5nM for PI3K), LY294002 (kinase domain inhibitor, IC50: 1.4μM), NU7026 (IC50: 0.23μM for DNA-PK and 13μM for PI3K) and NU7441 (IC50: 0.3μM for DNA-PK and 7μM for PI3K) that target the ATP binding sites on the kinases [40, 41]. However, these molecules have poor solubility in aqueous solutions, limited serum half-life, in addition to *in vivo* toxicity due to their non-selective nature, that limit their feasibility in the clinic [41]. In addition to small molecule DNA-PK inhibitors, nucleotides (example: GRN163L) and antibodies (example: ScFv 18-2) for radiosensitization have grabbed the interest of several researchers, due their biological nature that can overcome the issues of poor solubility and limited half-life [41]. In aim 2, we will explore the use of nanoparticles to deliver radiosensitizers and enhance the radiation therapy of lung cancer.

1.2.4 Combined chemotherapy-radiation therapy

Concurrent chemo-radiotherapy (CRT) is being explored clinically, with the intent to provide organ-preservation (a drawback of surgical treatment of cancer). This therapy often uses chemotherapeutic agents as radiation sensitizers, and as agents to systemically target distant micrometastasis [42, 43]. The use of chemotherapeutic drugs concurrently with radiation, can enhance the damage produced by radiation, inhibit post-radiation DNA repair, reduce radio-resistance in cancer cells and thus produce an additive effect [42]. Combinations of chemotherapeutic agents and radiation investigated include, those using EGFR inhibitors such as cisplatin, carboplatin, 5-fluorouracil, capecitabine, gemcitabine pemetrexed, hydroxyurea, taxane, mitomycin-C, tirapazamine and temozolomide [42-44]. For instance, elderly stage III NSCLC patients treated with chemoradiation observed a higher overall survival compared to that in patients receiving RT alone [45]. Several clinical trials utilizing cisplatin and etoposide with concurrent thoracic radiation have established the safety and tolerability of the treatment [46]. Similarly, a phase-II study established the tolerability and efficacy of RT combined with docetaxel (administered a post-chemotherapy regimen of cisplatin and etoposide), and reported a median survival rate of 26 months and an overall 5-year survival rate of 29% in patients with stage IIIB NSCLC [47]. In another study, comparing sequential therapy (RT administered after completion of chemotherapy regimen) and CRT, CRT observed a significantly higher response rate (84%) and median survival rate (16.5 months) compared to sequential therapy (response rate: 66% and median survival rate: 13.3 months) [48]. Furthermore, in cases such as lung cancer, where

locoregional control of cancer treatment is crucial to the success of the treatment, concurrent therapy has proven more successful compared to radiation alone [44, 49]. However, CRT has several associated limitations due high risk of complications and side–effects such as pulmonary hemorrhage, pneumonitis or esophagitis [46]. Thus, in aim 3, we will utilize the advantages of CRT towards developing a concurrent chemo-radiation therapy using nanoparticles that can enhance the individual treatment modalities synergistically to improve lung cancer therapy, while reducing their limitations.

1.3. STIMULI RESPONSIVE NANOPARTICLES FOR CANCER THERAPY

Drug delivery to cancer cells must overcome the following barriers to achieve their therapeutic potential: drug resistance in the tumor due to physiological barriers, cellular drug resistance, poor biodistribution and fast clearance of the drugs [50]. Nanotechnology is a constantly evolving field that has had profound effects on various research areas, particularly drug delivery. Nanotechnology provides various powerful and customizable tools for cancer biomarker detection, imaging, and delivery of anti-cancer drugs that have revolutionized the field of cancer therapy. NPs can overcome the cellular and non-cellular resistance to drug delivery and improve drug delivery specifically to the cancer cells while reducing toxicity to healthy tissues.

NPs are submicronic particles (<1 μM in diameter), which are used as carriers for drug delivery to the targeted tissues and/or intended cells. Encapsulating chemotherapeutic drugs into NPs enhance their bioavailability and internalization into cancer cells [50]. Additionally,

incorporation of targeting molecules can improve the site-specific drug delivery, biodistribution and internalization of the drugs. The other advantages of NPs for cancer drug delivery include their ability to encapsulate hydrophobic drugs, a feature commonly associated with anti-cancer drugs, and protect the drugs from clearance, particularly pulmonary clearance by macrophage phagocytosis and mucocilliary clearance [51]. Furthermore, drug release from NPs can be tailored to be within the drugs therapeutic window post-administration [50].

The long-term aim of cancer nanotechnology is to accelerate therapeutic efficacy, improve patient outcomes and minimize toxicity to healthy organs. Stimuli responsive NPs are a class of nanomaterials that maintain their original structure in normal body conditions and undergo reversible or irreversible physicochemical changes in response to a stimulus [52]. These changes in the structure induce the NPs to release their payload, and thus provide controlled drug delivery from these NPs. The tumor microenvironment is also a host for various endogenous drug release triggers such as acidic pH (~ 6.5 to 6.8) [53], hypoxia [54], and enzymes (e.g. matrix metalloproteinases) [55, 56]. The acidic tumor pH is a result of the extensive glycolysis by cancer cells for generating energy, while hypoxia is a result of deficient blood supply due to the aberrant vascular network in the tumor microenvironment [56]. Additionally, exogenous stimuli (usually in combination with an endogenous stimuli responsive polymer) like light [57], magnetic field [58] and ultrasound [59] can also be used to trigger the release of anticancer drugs from stimuli responsive NPs. Here, we will discuss two stimuli that are available to tailor drug release from nanoparticles, particularly those utilized in this research; i.e. endogenous redox (glutathione concentration) signals and exogenously supplied radiation that generates reactive oxygen species (ROS) to induce a trigger-controlled drug release from the nanoparticles.

1.3.1 Glutathione responsive nanoparticles

Glutathione (L-γ-glutamyl-L-cysteinyl-glycine; GSH) is a tripeptide of glutamic acid, cysteine and glycine, existing as either; (i) most commonly a reduced form of GSH or (ii) the oxidized form of GSH i.e. GSSG, which constitutes less than 1% of the total GSH concentrations [60]. The redox balance in cells is determined by the equilibrium between GSH and GSSG ratios. GSH is an antioxidant that protects cells from free radicals and plays a major role in regulating various carcinogenic mechanisms in cancer cells, such as cell proliferation, cell death and the sensitivity of cells to chemotherapeutic drugs and radiation [61]. GSH is significantly upregulated in the cancer microenvironment up to 100-1000 times more than normal healthy tissues and can thus, serve as an endogenous signal to trigger drug release from polymers that can undergo reduction in the presence of GSH [62, 63]. Thus, the elevated levels of GSH can be utilized as an endogenous stimulus to trigger the release of drugs from nanoparticles sensitive to the changes in the GSH concentration in the surrounding environment. Polymers comprising of disulfide linkages are highly prone to cleavage of these bonds due to GSH, thus triggering their degradation and subsequent release of their payload [62]. GSH responsive nanomaterials can be developed either by: self-assembly of micelles containing a disulfide backbone [64], polymer chains connected by a disulfide link [65], or utilizing a disulfide crosslinker in the shell or core of micelles [66, 67]. In this research, we have developed nanoparticles synthesized from polyurethane based elastomers comprising of disulfide linkages in the backbone of the polymer that undergo cleavage in response to changes in glutathione levels and trigger drug release [68].

1.3.2 ROS responsive and radiation responsive nanoparticles

Several types of polymers responsive to elevated levels of ROS in the cells have been widely researched for cancer drug delivery applications [69, 70]. ROS-responsive polymers commonly comprise of either thioether [71] or thioketal linkages [72] in the poloymer backbone, or may be doped with ROS responsive materials like selenium [73], tellurium [74], phenylboronic acid or phenylboronic ester [75], that get cleaved upon exposure to elevated intracellular ROS in the cancer cells. Imbalanced ROS levels and subsequent redox imbalance have been deemed the hallmarks of cancer progression and resistance to cancer treatments [76]. Elevated levels of ROS such as superoxide ($O_2^{\cdot -}$), nitric oxide ($NO^{\cdot}$), hydroxyl radicals ($^{\cdot}OH$) among others have been detected in most cancers, as a result of several cellular mechanisms such as high metabolic activity, peroxisomal activity, oncogene activation, increased cell receptor signaling and mitochondrial dysfunction among several other physiological changes in the cancer cells [76, 77]. The extracellular sources of ROS include pollution, tobacco, drugs and radiation exposure (or during radiation therapy to induce DNA damage and cell apoptosis), while intracellular ROS is generated by mitochondria, peroxisomes, the endoplasmic reticulum and the NADPH oxidase complex in cells [78]. Thus, taking advantage of the high levels of ROS in cancer cells, various ROS responsive polymers have been developed for cancer drug delivery applications. Since radiation produces ROS in the intracellular environment of the cancer cells to induce cell apoptosis, we will use this phenomenon to cleave our ROS responsive NPs and release the encapsulated radiosensitizers synergistically during radiation treatment to enhance the effects of radiation therapy. In this research, we have used hyaluronan based nanoparticles as a ROS responsive drug release platform for inducing release of radiosensitizers during radiation therapy. Hyaluronic acid

is a non-branched, non-sulfated glycosaminoglycan, comprised of glycosidic links that connect the repeated units of d-glucuronic acid-β-(1→3)-N-acetyl-d-glucosamine together [79]. These glyosidic bonds undergo hydrolytic scission due to the free radicals acquiring a hydrogen radical from hyaluronic acid, thus inducing degradation of the hyaluronic acid polymer [79].

1.4. TARGETING STRATEGIES FOR DRUG DELIVERY

Nano-carriers for cancer drug delivery face several obstacles, such as the mucus lining in the lung that hinder NP penetration into lung tumors and non-specific uptake into healthy cells leading to off-target toxicity [80]. Addition of targeting capabilities to the NPs can overcome these barriers and subsequently achieve their therapeutic goals. NP targeting can be achieved via passive targeting and active targeting approaches. Passive targeting utilizes the EPR effect in tumor tissues, specifically the leaky blood vessels and poor lymphatic drainage. The EPR effect is considered as a gold standard to study the efficacy of anti-cancer drugs and formulations [81, 82]. The unique characteristics of tumor blood vessels enhance the permeability of the blood vessels, and that of various macromolecules [82]. Additionally, the dense network of interstitial tissues limits the elimination of those macromolecules that have entered the tumor regions, thus improving their retention within the tumor tissues [81]. As a result of the EPR effect, drugs and NPs can accumulate in larger concentrations in tumor tissues compared to normal healthy tissues and plasma [83, 84]. However, passive targeting may not be effective in all cases due to the inhomogeneous nature of blood vessels across the tumor [85]. Active targeting involves incorporation of targeting ligands that can specifically bind to the cancer cells, followed by

receptor-mediated internalization of the NP before drug release [85]. Targeting agents are classified as proteins (antibodies), nucleic acids (aptamers) and other targeting ligands like peptides, vitamins and carbohydrates. In this section, we will explore two strategies that we have utilized to target nanomaterials to lung cancer cells in our research projects.

1.4.1 Antibodies and ligands against markers overexpressed on cancer cells

Targeted therapy can be achieved by targeting antibodies against markers overexpressed or exclusively expressed on the surface of cancer cells, but not on healthy/normal cells [86]. This allows the drug-loaded nano-carriers to localize specifically in the desired tissues to enhance drug enrichment in those tissue, and reduces off-target side-effects associated with drugs like anti-neoplastic drugs [86]. The most commonly investigated targeting strategy for lung cancer involves conjugation of targeting ligands like folic acid [87] and epidermal growth factor receptor (EGFR) [88], that are overexpressed on lung cancer cells. For example, Peng et al. [88], investigated single chain variable fragment anti-EGFR antibody to specifically target cisplatin-heparin nanoparticles to lung cancer cells. They observed significant enhancement in the intracellular delivery of cisplatin, in addition to improved circulation time and biodistribution of the targeted cisplatin compared to free cisplatin. Similarly, Menon et al. [87] observed enhanced therapeutic efficacy of folic acid-conjugated NPs made of poly(N-isopropylacrylamide)-carboxymethyl chitosan as a shell and poly(lactic-co-glycolic acid) as a core, and encapsulated gemcitabine hydrochloride and NU7441 for lung cancer chemo-radiotherapy compared to those of free drugs and radiation therapy alone. In this research, we will explore the enhanced targeting capabilities of anti-EphA2

antibodies to specifically bind to the Ephrin transmembrane receptor A2, that is highly overexpressed on the surface of lung cancer cells [89-91].

1.4.2 Cell membrane coated nanomaterials

Cell membrane coated NPs are now gaining popularity, due to their ability to mimic the surface properties of the host cell, including cancer homing capabilities of cancer cells, stem cells, platelets and macrophages [92]. Cell membrane coatings on the NP surface provide the following properties to the NPs; improving cell-specific targeting, prolonging circulation time of the NPs and enhancing immune cell targeting [93]. Various cell membranes have been investigated and used for targeting nanoparticles to tumor cells, such as cancer cell membranes, macrophage membranes, platelet membranes and RBC membranes [94]. For instance, paclitaxel loaded poly(caprolactone) NPs were coated with cells membranes extracted from 4T1 mammary breast cancer cells, a highly metastatic breast cancer cell line [95]. These NPs had the capability to specifically localize in the primary tumors and metastatic lesions of 4T1 orthotopic tumors, and significantly inhibit the growth of these tumors via paclitaxel delivery. However, it is not known if these cancer cell membranes could impart metastatic properties to the pre-existing primary tumor cells, and thus increase the chances of micro-metastasis. In this report we will investigate NPs functionalized with platelet cell membranes, that utilize the homing capabilities of platelets towards the lung tumor microenvironment for improved lung cancer targeting [96].

1.5. OVERVIEW OF RESEARCH PROJECT

This research project will examine strategies employing anti-cancer drug loaded stimuli-responsive NPs to improve the outcomes of conventional chemotherapy and radiation therapy. The long-term goal and specific aims are as described below:

1.5.1 Goals of research

The long-term goal of this project is to develop a composite NP system that can deliver chemotherapeutic drugs and radiation sensitizers for enhanced chemotherapy and radiation therapy for lung cancer treatment. To achieve this goal, we will utilize stimuli responsive NPs coupled with various lung cancer cell targeting strategies that provide drug release upon exposure to a stimulus. This strategy will ensure a timed release of the drug at the site of lung cancer, while sparing healthy tissues, thereby minimizing any toxicity and side-effects due to treatment.

1.5.2 Specific aims

The first step towards our long-term goal of developing stimuli-responsive targeted nano-carriers for lung cancer therapy will be achieved via the following specific aims;

Aim 1. To develop glutathione-responsive nano-carriers for lung cancer chemotherapy.

Nanoparticles responsive to elevated GSH levels in cancer cells will be used to deliver cisplatin for lung cancer chemotherapy **(Figure 1.1)**. NP functionalization with antibodies targeting the ephrin-transmembrane receptors overexpressed on lung cancer cells will enhance targeting of the NPs to lung tumor site.

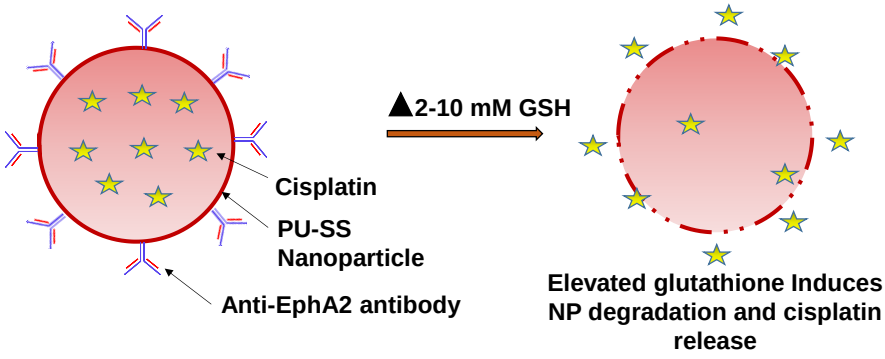

Figure 1.1 Schematic of anti-EphA2 antibody tagged GSH sensitive NPs for cisplatin delivery

Aim 2. To develop radiation-responsive nano-carriers for lung cancer radiation therapy.

Nanoparticles responsive to incident radiation will be used to deliver the radiation sensitizer NU7441 to intensify radiation therapy **(Figure 1.2).** Additionally, we will coat these NPs with platelet cell membranes and functionalize with antibodies against EphA2 to impart lung tumor targeting capabilities to the NPs.

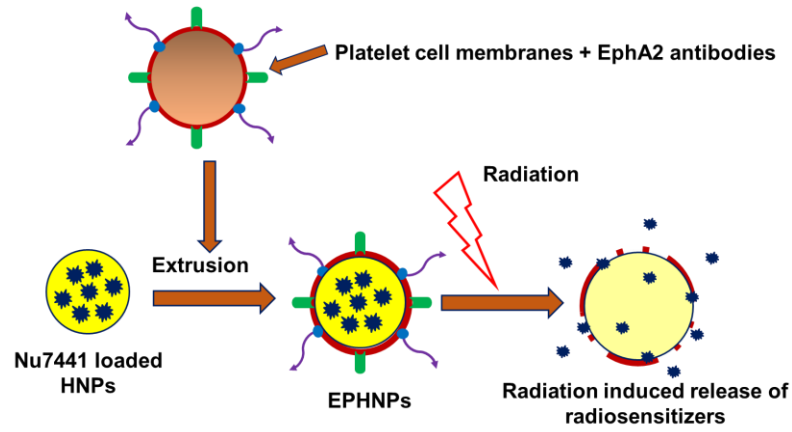

Figure 1.2 Schematic of anti-EphA2 and Platelet-membrane coated radiation-responsive NPs for lung cancer radiation therapy.

Aim 3. To develop dual-stimuli responsive nano-carriers for concurrent lung cancer chemo-radiation-therapy.

The NPs from aim 1 and that from aim 2 will comprise the core and shell of the composite NP respectively **(Figure 1.3)**, while utilizing the capability of anti-EphA2 conjugated on the NP surface to target lung cancer cells. These NPs will be utilized for concurrent chemo-radiation therapy for augmented lung cancer therapy.

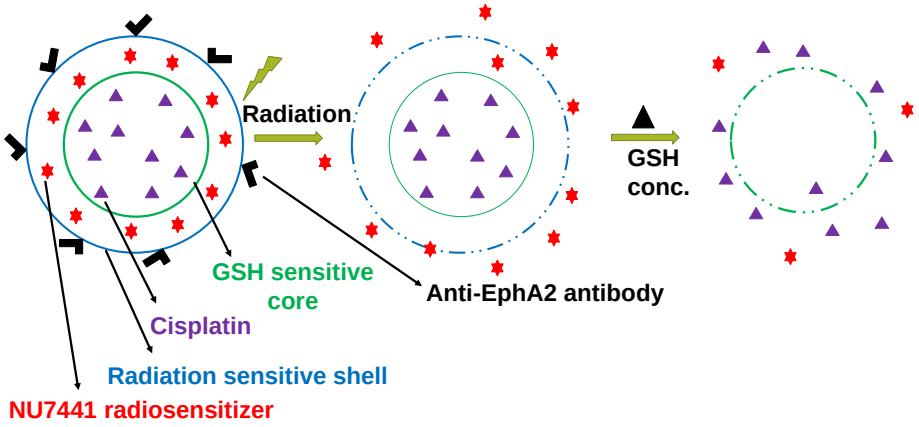

Figure 1.3 Dual stimuli responsive core-shell NPs encapsulating cisplatin and NU7441 for concurrent chemo-radiotherapy

1.5.3 Innovative aspects to this research

There are several innovative aspects to this research. We will explore novel stimuli-responsive polymers to develop nano-carriers for chemotherapy and radiation therapy applications. We will also explore various targeting strategies to improve localization of our NPs at the lung tumor site, to enhance their therapeutic efficacy while minimizing toxicity and side-effects to healthy cells. Finally, concurrent chemo-radiation-therapy via the composite NPs will further

enhance lung cancer treatment, and subsequently open new avenues for research in combined therapy strategies for lung cancer.

1.5.4 Successful outcomes from this research

The successful outcomes from this research will aid cancer researchers in developing more efficient strategies to treat lung cancer in addition to improving patient outcomes. Our stimuli-responsive NPs will provide on-demand drug release with spatio-temporal capabilities. Additionally, the targeting strategies implemented here will open new doors to enhancing lung cancer therapies, and reducing the side-effects typically associated with systemic drug and radiation-based lung cancer treatment. The composite NPs from aim 3 will further permit enhanced chemo-radiation therapy to strengthen our goal for improving lung cancer treatment.

CHAPTER 2: GLUTATHIONE RESPONSIVE NANOPARTICLES FOR LUNG CANCER TREATMENT

2.1. INTRODUCTION

The anti-neoplastic drug cisplatin (*cis*-diamminedichloroplatinum (II)), which has been widely and successfully investigated in the clinic to treat various solid tumors, such as head and neck squamous carcinoma and ovarian cancer, is the first-line FDA approved treatment for non-small cell lung cancer (NSCLC) [97]. Cisplatin has been highly successful at treating lung cancer, by decreasing the overall lung cancer associated mortality by 7% compared to untreated controls [98]. The mechanism of action of cisplatin involves crosslinking with the purine bases on double-strand DNA (ds-DNA), thus inducing damage to the DNA and resulting in cellular apoptosis [99]. Additionally, cisplatin has been observed to interact with various membrane and cytoplasmic components to induce further intracellular cytotoxicity [100]. Although cisplatin has been widely used in chemotherapy to effectively kill lung cancer cells, it has several drawbacks. For instance, this drug induces more harm than benefit, due to non-specific organ distribution. This, severely increases toxicity to the healthy tissues and in-adequate intratumor drug concentrations, needed to produce the desired therapeutic effects [88]. Furthermore, cisplatin is poorly soluble in aqueous solvents, that further affects its bioavailability and therapeutic index [101]. Besides the non-specific toxicity and side-effects associated with cisplatin, the efficacy of cisplatin is limited by innate and acquired drug resistance [97]. Cisplatin resistance has been classified into four categories: (1) poor or absence of cisplatin binding to DNA due to higher binding to cytoplasmic

components, also called as pre-target resistance, (2) on-target resistance due to repair of the DNA adducts, (3) post-target resistance due to alterations or defects in the signaling pathways that respond to DNA damage, and (4) off-target cellular mechanisms that prevent the cells from responding to cisplatin induced apoptosis [102]. For example, Sarin et al. [97] observed significant differences in cisplatin induced apoptosis in A549 lung cancer cells and its sub-line, cisplatin resistant $A549^r$ cells, with A549 cells exhibiting a 6-fold increase in apoptosis, while $A549^r$ cells exhibited a 2-fold increase in apoptosis and a 2-fold higher EC50 value. Consequently, one treatment strategy involving cisplatin may not be sufficient to produce the desired therapeutic effects.

These limitations of chemotherapy drugs, particularly off-target toxicity and poor bioavailability and biodistribution, can be overcome by encapsulating these drugs into NPs. NPs as a drug carrier for chemotherapy has achieved tremendous popularity, specifically due to their small size, improved solubility of the hydrophobic chemotherapeutic agents and customizability to enhance NP accumulation in the tumor tissues, thereby improving drug bioavailability and drug distribution in the tumors [87]. Nanoparticles also provide high encapsulation efficiencies for chemo-drugs, sustained drug release characteristics and escape from macrophage clearance [101]. Additionally, recent studies utilizing nanoparticles such as lipid assisted nanoparticles have been formulated to deliver cisplatin to cancer cells, while improving their intracellular uptake and drug concentrations, leading to increased DNA adducts and improved DNA damage [103]. Stimuli responsive nanoparticles are a class of nanoparticles that observe poor drug release in normal physiological conditions, and enhanced drug delivery at the targeted site upon exposure to a stimulus rendering spatial, temporal and dose-controlled drug release ability to the NPs [62]. Due

to these qualities, stimuli responsive nanoparticles are gaining significant insights for treating various cancers that consist of various endogenous stimuli to trigger the drug release from these nanoparticles, including changes in pH and enzymes like protease, phospholipase and glycosidase that are overexpressed in the tumor microenvironment [104]. Besides these, the cancer microenvironment also hosts enhanced levels of other molecules, namely antioxidants like glutathione (GSH), that are upregulated in response to high levels of oxidative stress within the cancer tissues [60]. In fact, the GSH levels in cancer cells are over 100-1000 times higher (e.g. 2-10 mM) than that outside the cancer cells (e.g. 2-10 μM in normal physiological environments) [62]. This observation, has led to the development of redox-responsive polymers comprising of disulfide bonds in the backbone, that undergo reduction-mediated cleavage in response to increased levels of GSH, thereby releasing their payload [62, 104]. For example, diblock copolymers comprising of a hydrophilic PEG block and hydrophobic polyphosphoester (PPE) block bearing disulfide bonds were utilized to synthesize micelles that underwent disassembly in elevated GSH conditions such as the tumor microenvironment [105]. The cleavage of the disulfide bonds in the polymer backbone resulted in transition of the hydrophobic PPE block to a hydrophilic state, subsequently dismantling the micelles and releasing their payload.

In this article, we will explore nanoparticles made of a biodegradable polyurethane polymers named as PU-SS synthesized in our lab [68]. These polymers comprise of disulfide linkages in the backbone of the polymer, that upon exposure to elevated levels of GSH undergo reduction of disulfide bonds that induce nanoparticle degradation and release of the encapsulated drugs. The PU-SS polymer was chosen from a library of GSH responsive polymers developed in our lab, as a result of its highest degradation rate in GSH, cytocompatibility and biocompatibility.

The chemotherapeutic drug encapsulated within these NPs is cisplatin, which has been approved by the FDA for lung cancer chemotherapy. Furthermore, these NPs are surface-coated with antibodies targeting the Ephrin-transmembrane receptors [89], that are overexpressed on the surface of lung cancer cells, but poorly on healthy cells, thus fortifying the specific lung cancer targeting ability of the NPs **(Figure 1.1)**. We investigated the GSH responsiveness of these NPs, particularly the drug release kinetics of cisplatin from these NPs in response to varying GSH concentrations, followed by evaluating the *in vitro* and *in vivo* therapeutic efficacies of these NPs at killing lung cancer cells and reducing the lung tumor volumes in murine subcutaneous lung cancer models.

2.2. EXPERIMENTAL SECTION

2.2.1 Fabrication of PU-SS nanoparticles

Glutathione-sensitive PU-SS polymer was synthesized using polycaprolactone and 1,6-Hexamethylene diisocyanate, with hydroxyethyl disulfide in molar ratios of 0.2:2:1.8, as described elsewhere [68]. PU-SS NPs (GNPs) were prepared by a standard emulsion technique. Briefly, a 10% solution of cisplatin (Cayman Chemicals) in 200µL of dimethyl sulfoxide (DMSO; MilliporeSigma) was added to a 2% solution of PU-SS dissolved in a solvent mixture of 95% dichloromethane (DCM; MilliporeSigma) and 5% hexafluoroisopropanol (HFIP; MilliporeSigma). This solution was then sonicated using a microtip sonicator at 10 watts for 5 minutes, and then added dropwise to 4mL of 5% polyvinyl alcohol (PVA; MilliporeSigma),

followed by sonication using an ultrasonicator at 30 watts for 5 minutes. Following overnight stirring, the NPs were washed with deionized water and collected by ultacentrifugation at 15,000 RPM for 30 minutes and lyophilized for 2 days. Cyanine-7 (Lumiprobe) and coumarin-6 (MilliporeSigma) loaded GNPs (1% w/w of dye to polymer) were also synthesized in the same process as above for the *in vivo* biodistribution and *in vitro* cell uptake studies respectively.

2.2.2 Coating Anti-EphA2 antibody on GNPs

Cisplatin loaded GNPs (CGNP) were coated with anti-EphA2 antibodies (BioLegend) by layer-by-layer electrostatic technique developed in our lab. Briefly, 5 mg of lyophilized CGNPs were dispersed in 5mL of 10mM Nacl solution, following which 250 µL of polyallylamine hydrochloride (PAH, MilliporeSigma) at a concentration of 100 µg/mL was added to the CGNP solution and allowed to coat onto the CGNPs for 30 minutes at room temperature under constant rotation. PAH coated CGNPs were collected by ultracentrifugation, and the pellet dispersed in 5 mL of 2-ethanesulfonic acid (MES; MilliporeSigma) buffer (pH 5.0). 10 µg of Anti-EphA2 antibodies were then added to this solution, and stirred overnight at 4°C. Anti-EphA2 coated CGNPs (CEGNPs) were then collected the following day by ultracentrifugation at 15,000 RPM for 30 minutes and lyophilized for 2 days. Bare GNPs (without cisplatin loading), cyanine-7 loaded GNPs and coumarin-6 loaded GNPs were also conjugated with anti-EphA2 antibodies in the same process as above. Bare GNPs conjugated with anti-EphA2 antibodies will be annotated as EGNPs in the rest of the manuscript.

2.2.3 Characterization of nanoparticles

Particle size, size distribution, and surface charges were measured using the Dynamic Light Scattering (DLS) technique (ZetaPALS zeta potential analyzer, Brookhaven Instruments Inc.). Transmission electron microscopy (TEM, JOEL 1200EX) and scanning electron microscopy (SEM, Hitachi S-4800 II FE SEM) were used to visualize the morphology of the NPs. Antibody conjugation efficiency was determined by Bradford protein assay (Bio-Rad Inc.), where amount of antibody remaining in the supernatant was determined via a standard of EphA2-antibody. Antibody coating efficiency was determined indirectly by the following:

$$Ab\ coating\ efficiency = \frac{Amount\ of\ Ab\ used - amount\ of\ Ab\ in\ supernatant}{Amount\ of\ Ab\ used} X\ 100\%$$

…. (2.1)

Cisplatin loading efficiency for each GNP was determined by an indirect method. Briefly, cisplatin in the supernatant in the formation process was quantified by an o-phenylenediamine (OPDA, MilliporeSigma) based spectrometric detection technique [106]. Briefly, 250µL of the cisplatin solution was mixed with 1mL of 1X-PBS (pH 6.8) and 1mL of OPDA solution (18 mg/mL in 1X-PBS, pH 6.8). The resulting solution was heated at 100˚C for 10 minutes, cooled down and supplemented with 7mL of dimethyl formamide (MilliporeSigma). The change in color as a result of the interaction between OPDA and cisplatin was analyzed by a UV-Vis spectrophotometer at 703 nm (Infinite M200, Tecan Group Ltd). The loading efficiency (LE) of cisplatin into the NPs was determined by the following;

$$Cisplatin\ LE = \frac{Cisplatin\ amount\ used - Cisplatin\ in\ supernatant}{Cisplatin\ amount\ used}\ X\ 100\%$$

…. (2.2)

To study the glutathione triggered cisplatin release kinetics from the GNPs, the lyophilized NPs were re-suspended in either 0 mM, 5 mM, or 10 mM of glutathione (Cayman Chemicals) in 1X-PBS (pH 7.4) in a 1 mg/ml concentration. 1 ml of the NP suspension was added to a microcentrifuge tube (4 replicates were used for each glutathione concentration) and incubated at 37 °C. At pre-determined time points, the GNP suspensions were centrifuged, supernatants were collected, and the pellets were resuspended in the same glutathione solutions as earlier and incubated at 37°C until the next time point. The amount of cisplatin released was quantified by the OPDA chemistry as described earlier. A standard curve of known cisplatin concentrations was used to determine the cumulative cisplatin release. Stability of the GNPs was determined by measuring the NP size using DLS when incubated in either cell culture media (RPMI, MilliporeSigma) supplemented with 10% fetal bovine serum (FBS), 0.9% sodium chloride (NaCl), or gamble's solution (simulated human lung fluid) at body temperature (37˚C) over a period of 3 days as previously described [87]. A sample size of n=3 per group was used for this study.

2.2.4 Cellular uptake of nanoparticles

Cellular uptake of EGNPs and GNPs was determined by measuring the amount of fluorescently-labeled GNPs internalized by lung cancer cells. EGNPs and GNPs loaded with a fluorescent dye, coumarin-6, were synthesized as described earlier. Coumarin-6 was used here to

facilitate fluorescent mediated detection of the NPs in the cells. To study *in vitro* cellular particle uptake, A549 human lung cancer cells (ATCC) were seeded at a seeding density of 10,000 cells/well in 96 micro-well plate and allowed to attach overnight. Next day, the cells were incubated with EGNPs and GNPs at different concentrations (0, 25, 50, 100, 250 and 500 µg/ml) at 37°C for 2 hours (n=4 per group). Post 2 hours, the cells were washed 3X with sterile 1X-PBS and lysed using 1% Triton X-100. The amount of NPs internalized were determined by measuring the fluorescence intensity of coumarin-6 (translated to µg of NPs) at a wavelength of λex 458 nm and λem 540 nm and normalized against the amount of total protein from cells per well, determined using bicinchonic acid assays (BCA) per manufacturer's instructions (Pierce™ BCA Protein Assay Kit, Thermo Scientific).

NP targeting of GNPs and EGNPs to A549 lung cancer cells were also determined by fluorescence imaging. A549 cells were seeded at a cell seeding density of 150,000 cells on glass coverslips and allowed to attach overnight. The following day, the A549 cells were exposed to 1mg/mL of coumarin-6 loaded GNPs or coumarin-6 loaded EGNPs for 2 hours, following which they were washed three times with 1X-PBS, and fixed for 15 minutes in 4% paraformaldehyde (MilliporeSigma). The fixed cells were washed with 1X-PBS to remove excess paraformaldehyde, and visualized under a fluorescence microscope (Cytoviva Inc.).

2.2.5 In vitro A549 cancer cell killing studies

The *in vitro* therapeutic efficacy of CEGNPs were determined by lactate dehydrogenase (LDH) cytotoxicity assays. Briefly, A549 lung cancer cells were seeded at a seeding density of 20,000 cells/well in a 48 micro-well plate and allowed to attach overnight. The following day,

cells were treated with free cisplatin (3 µg/mL and 5 µg/mL drug concentration) or NPs: CEGNPs, CGNPs, EGNPs and cisplatin loaded PLGA NPs (CPNPs) (concentration equivalent to 3 µg/mL and 5 µg/mL of cisplatin determined from the drug release kinetics) for 72 hours (n= 4 per group). Untreated cells and cells treated with 1% Triton X-100 were regarded as the negative and positive controls respectively. 72 hours later, cell death was determined by lactate dehydrogenase (LDH) cytotoxicity assays via the manufacturer's protocol. Furthermore, *in vitro* therapeutic efficacy was also confirmed by live/dead cell staining (Enzo Lifesciences) following the company's instructions.

In vitro therapeutic efficacy was also confirmed by quantifying the caspase-3 expression, as a marker for cell apoptosis after treatment. Briefly, A549 lung cancer cells were seeded at an initial seeding density of 250,000 cells/flask in T-25 flasks. Once the cells reached confluency they were treated with free cisplatin (5 µg/mL), or NPs: EGNPs, CGNPs, CEGNPs and CPNPs (concentration equivalent to 5 µg/mL of cisplatin determined from the drug release kinetics) for 72 hours (n= 4 per group). Untreated cells and cells exposed to 10% DMSO for the same period as the treatment groups served as the negative and positive control respectively. 72 hours later, caspase-3 expression was determined per the manufacturer's protocol.

To observe the survival of lung cancer cells upon exposure to the CEGNP NPs, we also performed clonogenic assays or colony formation assays (CFA). Clonogenic assays were implemented to determine the survival of A549 cancer cell colonies. Clonogenic assay or colony formation assay (CFA) is used to establish the ability of individual cells to survive and undergo cellular division, forming their individual colonies [107]. The effect of the therapeutic reagents is reflected in the ability of the cancer cells to form their colonies after exposure to the therapeutic agents. Colonies comprising of more than 50 cells are considered as one colony and counted. To

perform these studies, A549 lung cancer cells were seeded on 60mm petridishes, and *in vitro* CFA studies were performed as described previously [108]. The cells were treated with free cisplatin (100 ng/dish), or NPs: EGNPs, CGNPs, CEGNPs and CPNPs (concentration equivalent to 100 ng/dish of cisplatin determined from the drug release kinetics) and incubated at 37˚C for 10 days (n= 3 per group). A549 lung cancer cells not exposed to any treatment were included as negative controls. Once the cancer cell colonies had reached a colony of at least 50 cells, the cells were washed with phosphate buffered saline, and stained with crystal violet (MilliporeSigma) dye (0.5% w/v in 6% v/v glutaraldehyde). The number of colonies in each dish were then counted. A sample size of n=3 per group was used for this study.

2.2.6 Cytotoxicity analysis of nanoparticles

Healthy lung alveolar Type 1 (AT1) epithelial cells (Abmgood) were seeded at a density of 8,000 cells/well in a 96 microwell plate and incubated overnight to facilitate cell attachment. Next day, the cells were incubated with varying concentrations of non-drug loaded GNPs (0, 50, 100, 200, 500, and 1000 µg/ml; n= 4 per group). Following 24 hours incubation, the cell viability was determined using MTS cell viability assays (CellTiter 96®AQueous One Solution Cell Proliferation Assay, Promega Corporation) and validated using a live-dead assay (LIVE/DEAD ® Viability/Cytotoxicity Kit for mammalian cells, ThermoFisher Scientific) according to the manufacturer's instructions.

2.2.7 Hemo-compatibility analysis of nanoparticles

A hemolysis evaluation of the non-drug loaded GNPs was conducted as described previously [109]. Human blood from a donor was acquired following methods approved by the Institutional Review Board at the University of Texas at Arlington. After collection, human blood was incubated with GNPs at concentrations of either 100 µg/ml or 1000 µg/ml, 0.9% saline (as negative control), or distilled water (as positive control) for 2 hours at 37˚C. The samples were then centrifuged at 1000 g, following which absorbance (abs) readings were taken at 545 nm using a UV-Vis spectrophotometer. The percentage of hemolysis was calculated as below:

$$Hemolysis = \frac{Abs\ of\ sample\ -\ Abs\ of\ negative\ control}{Abs\ of\ positive\ control - Abs\ of\ negative\ control}\ X\ 100\%$$

…. (2.3)

To study the blood clotting kinetics, non-drug loaded GNPs at concentrations of either 100 or 1000 µg/ml) were added to blood activated with 0.1M calcium chloride ($CaCl_2$) and incubated at room temperature. At pre-determined time points (10, 20, 30, and 60 minutes), water was added to the tubes to lyse the red blood cells (RBCs) that were not a part of the formed clot. Absorbance readings of supernatant were taken at 540 nm using a UV-Vis spectrophotometer. The absorbance readings are inversely proportional to the size of the resulting clot. A sample size of n=8 per group was used for the hemolysis and hemocompatibility study.

2.2.8 In vivo biodistribution of fluorescently labeled NPs

To test the *in vivo* biodistribution of the EphA2 tagged GNPs (EGNPs) and untagged GNPs, athymic nude mice (Foxn1^{nu}, Jackson labs) were implanted with A549 lung cancer cells (2 million cells) subcutaneously in the hindlimb, following the protocol approved by The Institutional Animal Care and Use Committee (IACUC) at The University of Texas at Arlington. Once the tumors reached a diameter of approximately 10 mm, the NPs were administered. 0.9% saline served as the negative control, while cyanine-7 loaded GNPs either tagged with EphA2 antibodies or untagged served as the study groups. Animals were injected with saline or 1.5 mg of the NPs (n=4 per group comprising of randomly allocated 2 male and 2 female mice) intravenously. 24 hours later the mice were euthanized, and their tumors and visceral organs excised for further analysis. Tumor dimensions and tissue weights were recorded and imaged *ex vivo* in a fluorescence bioimager (Kodak In vivo Fx Pro system). The tissues were also homogenized using a tissue homogenizer (Precellys evolution, Bertin Instruments), and the amount (mg) of NPs retained in the tissues was quantified spectrophometrically.

2.2.9 In vivo therapeutic efficacy

To test the *in vivo* therapeutic efficacy of the CEGNPs, A549 lung cancer cells (2 million cells) were subcutaneously in the hindlimb of athymic nude mice (Foxn1^{nu}, Jackson labs), following the protocol approved by the Institutional Animal Care and Use Committee (IACUC) at The University of Texas at Arlington. Once the tumors reached a diameter of 7 mm, treatment was commenced. The saline (0.9%) served as a negative control. The study groups included free cisplatin (2.5 mg of cisplatin/kg of animal) and NPs: EGNPs, CGNPs and CEGNPs (at an

equivalent dose of 2.5 mg of cisplatin/kg of animal). We used 6 randomly allocated mice per group for this study (3 males and 3 females). Since cisplatin-loaded PLGA NPs observed significantly lower cancer cell death *in vitro*, they were excluded from *in vivo* assessment of therapeutic efficacy. Animals were injected with the control or study groups via tail vein injection with 2 times per week. Body weight (g) and tumor diameters (mm) were measured before each dosing regimen. Once the tumors on the control group reached a diameter of 20 mm, the study was considered to reach endpoint, post which the animals were euthanized, and their tumors excised and fixed in 4% paraformaldehyde (4% PFA). The lungs, heart, kidneys, liver and spleen were also collected and fixed in 4% PFA to evaluate the toxicity due to the treatment. The tumor volumes were determined as described earlier [110, 111], using the modified ellipsoid formula below:

$$Tumor\ volume = {((2 * tumor\ width) * tumor\ length)}/{2}$$

…. (2.4)

Relative tumor volumes (RTV: V/V_0) were calculated by normalizing tumor volumes (V) at a specific time to the tumor volume at start of NP/drug administration (V_0) using equation:

$$Relative\ tumor\ volume = {V}/{V0}$$

…. (2.5)

2.2.10 Statistical analysis

Results were analyzed statistically using 2-way ANOVA and Fisher's post-hoc analysis (GraphPad Prism) with $p<0.05$ considered as a significant value, unless specified otherwise. All results are displayed as mean ± SD, and quadruplet (n = 4) samples were used for each experiment if not specified.

2.3. RESULTS

2.3.1 Nanoparticle characteristics

A)

	Nanoparticle size (nm)	Zeta potential (mV)
Bare GSH NPs (GNP)	189 ± 21	-14±4
Cisplatin GNP (CGNP)	245 ± 20	-12± 2
Anti-EphA2 Ab conjugated CGNPs (E-CGNP)	300 ± 26	-14± 7

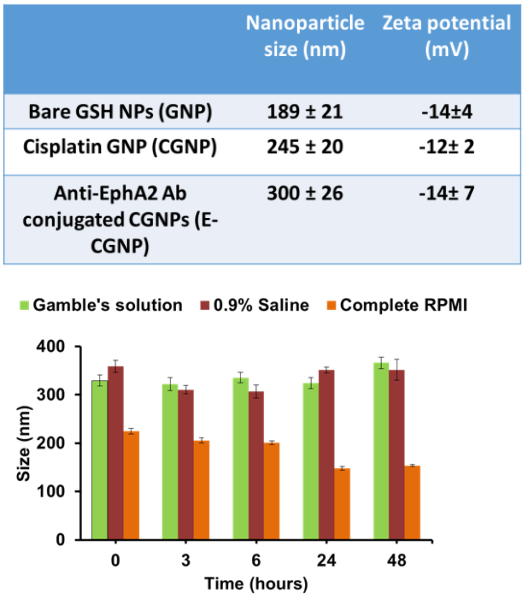

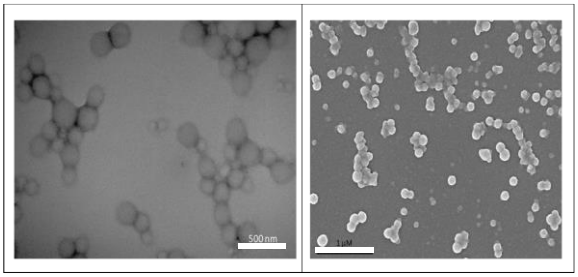

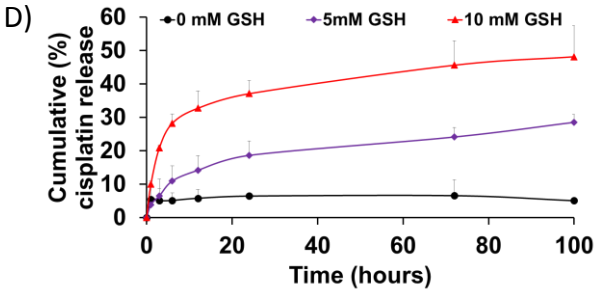

Figure 2.1. Nanoparticle characterization. **A)** Size and zeta potential of GSH sensitive NPs via DLS. **B)** TEM (left; scale: 500 nm) and SEM (right; scale: 1 µm) images of GSH sensitive NPs observe smooth NP morphology. **C)** NP stability evaluated by changes in the NP size observed stability up to 48 hours in gamble's solution, saline and complete media. **D)** GNPs observed 5-times enhanced drug release upon exposure to 10 mM of GSH compared to 0 mM of GSH.

EGNPs and CEGNPs had a mean diameter of 189±21 nm and 300±26 nm respectively **(Figure 2A)**. Additionally, the zeta potential of EGNPs and GNPs was determined to be -14±4

mV and -12±2 mV respectively **(Figure 2.1A)**. SEM and TEM microscopy imaging revealed a smooth morphology of the NPs **(Figure 2.1B)**. The EGNPs also observed an antibody coating efficiency **(using equation 2.1)** of about 84%, as detected by Bradford protein assays, confirming the successful coating of the antibodies on the NP surface using our antibody coating strategy.

Stability of the GNPs in 0.9% saline, complete media (supplemented with 10% FBS) and gamble's solution was determined by measuring the NP size at various time points using dynamic light scattering **(Figure 2.1C)**. Stability analysis of the NPs observed stable NP sizes up to 48 hours in all the three solutions. The drug loading efficiency of cisplatin was measured indirectly **(using equation 2.1)** using OPDA chemistry to be about 55%. The cisplatin release kinetics observed enhanced drug release when exposed to 5mM and 10 mM of GSH compared to that of 0mM GSH (nearly 5 times and 8 times higher drug release up 100 hours) **(Figure 2.1D)**. The enhanced drug release upon exposure to GSH, confirm the GSH responsiveness of the nanoparticle formulation.

2.3.2 In vitro therapeutic efficacy of E-GNPs

The therapeutic efficacy of CEGNPs were determined by exposing A549 lung cancer cells to the cisplatin loaded NPs, and determining the treatment induced cell death via cytotoxicity assays and clonogenic assays. The lactate dehydrogenase assay (LDH) observed cisplatin dose-dependent cell death of the A549 lung cancer cells over a 72-hour exposure to the treatment groups. Importantly, the cells treated with CEGNPs consisted of significant cancer cell death (~85%), especially at higher drug concentrations (5 µg/mL of cisplatin), compared to that by non-targeted

NPs (~70%), free cisplatin (~ 60%) and CPNPs (~ 30%) **(Figure 2.2A)**. The higher cell death could potentially be due to the enhanced targeting of lung cancer cells by the anti-EphA2 antibodies that might improve NP internalization into the cells, and subsequently enhance cell death. Furthermore, the therapeutic efficacy of the CEGNPs were determined by detecting the amount of caspase-3 produced due to the treatment over 72 hours. Caspase-3 production was used as a marker of cellular apoptosis, thereby indicating cell death. Similar to that observed by LDH assays, CEGNP treatment significantly augmented the caspase-3 production by A549 cells (~ 98%), compared to that by non-targeted NPs (~ 86%), free cisplatin (~83%) and the CPNPs (~80%) **(Figure 2.2B)**.

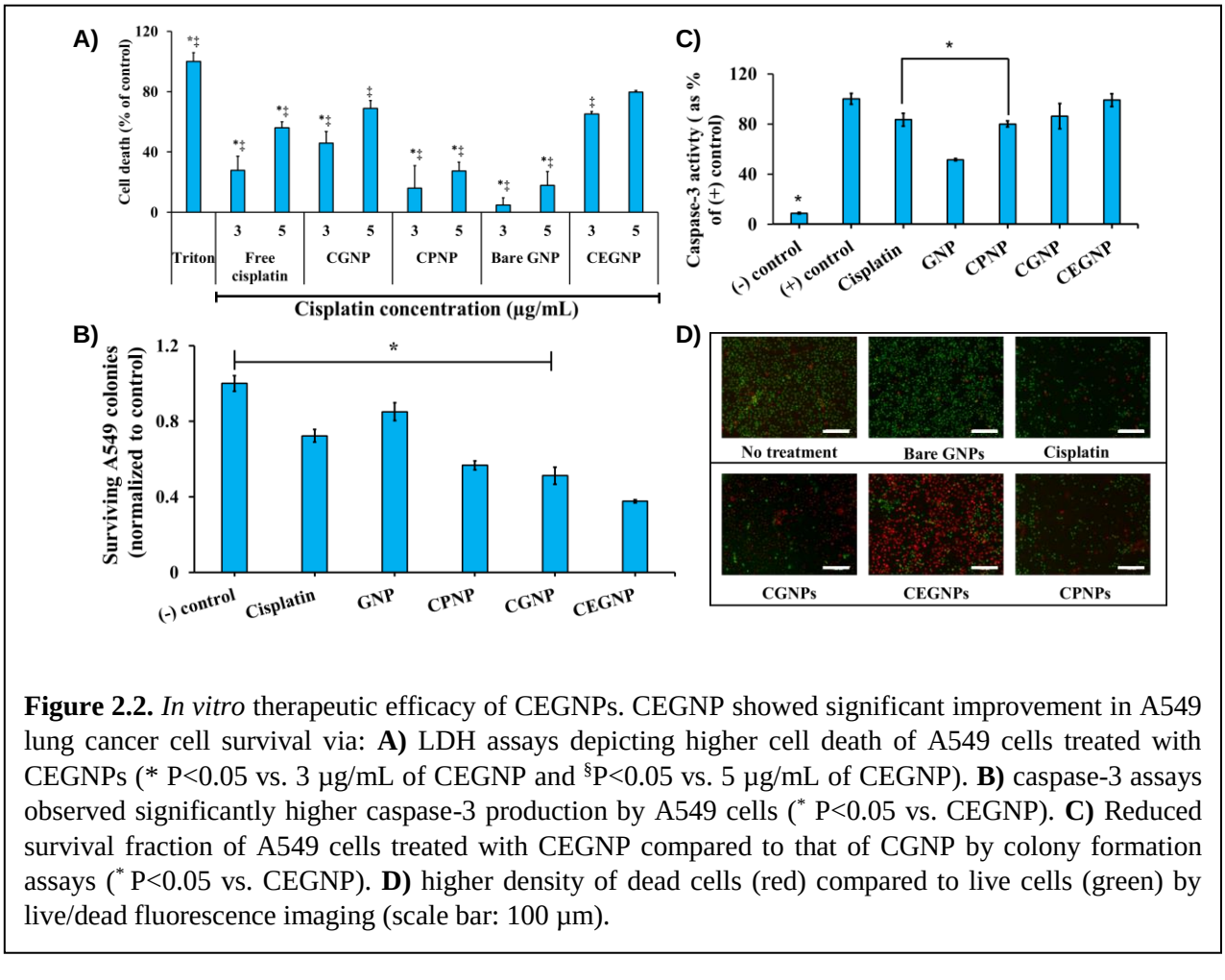

Figure 2.2. *In vitro* therapeutic efficacy of CEGNPs. CEGNP showed significant improvement in A549 lung cancer cell survival via: **A)** LDH assays depicting higher cell death of A549 cells treated with CEGNPs (* P<0.05 vs. 3 µg/mL of CEGNP and §P<0.05 vs. 5 µg/mL of CEGNP). **B)** caspase-3 assays observed significantly higher caspase-3 production by A549 cells (* P<0.05 vs. CEGNP). **C)** Reduced survival fraction of A549 cells treated with CEGNP compared to that of CGNP by colony formation assays (* P<0.05 vs. CEGNP). **D)** higher density of dead cells (red) compared to live cells (green) by live/dead fluorescence imaging (scale bar: 100 µm).

Clonogenic assays were implemented to determine the survival of A549 cancer cell colonies. We observed the colony formation ability of A549 cells exposed to CEGNPs and determined the A549 cell survival fraction over 10 days of treatment. Cells treated with CEGNPs significantly reduced the survival fraction (0.37), compared to that by untargeted CGNPS (0.51), free cisplatin (0.72) and CPNPs (0.56) **(Figure 2.2C)**. The *in vitro* therapeutic results signify the advantage of specific targeting of the CNGPs via the anti-EphA2 Abs. Additionally, the CEGNPs significantly improved therapeutic efficacy compared to that by CPNPs, which is conventionally used as a carrier for various chemotherapeutic drugs. Similar trend in results were observed via live/dead staining where CEGNPs observed a larger number of dead cells (red colored cells) compared to those treated with CGNPs and free cisplatin **(Figure 2.2D)**. CGNPs and CEGNPs also out-performed CPNPs, by significantly improving *in vitro* therapeutic efficacy.

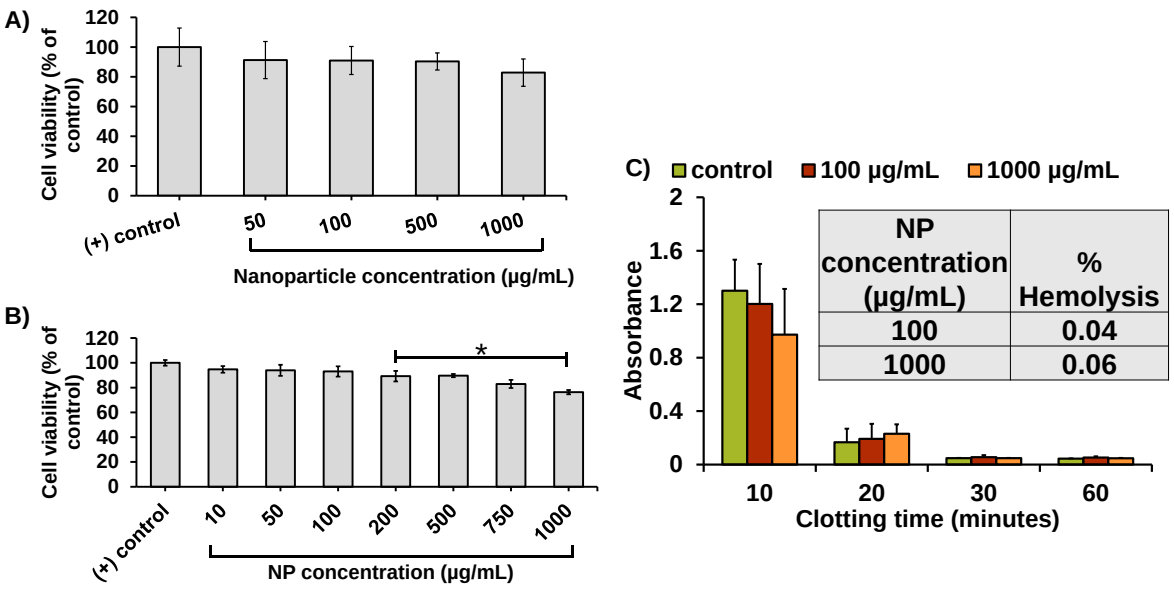

Figure 2.3. *In vitro* characterization of GNPs. **A)** *In vitro* cyto-compatibility studies of GNPs observed over 80% viability of alveolar type-I cells via MTS assays. **B)** LIVE/DEAD cell viability assays also observed AT1 survival over 90% of AT1 survival at the highest NP concentration (* $p < 0.05$ vs. (+) control/complete media). **C)** GNPs observed low hemolysis (inset), and a blood clotting trend similar to that of saline control confirmed by the blood clotting profile.

2.3.3 In vitro characterization of GNPs

The cytotoxicity of GNPs at increasing concentrations were determined by MTS **(Figure 2.3A)** and live/dead **(Figure 2.3B)** cytotoxicity assays. The GNPs observed over 90% cyto-compatibility up to 500 µg/mL, and more than 80% cell viability at the highest NP concentration of 1000 µg/mL to AT1, confirming the cyto-compatibility of the NPs to healthy lung cells. Hemocompatibility of the GNPs were analyzed by studying the hemolysis of blood and blood clotting profile of whole blood exposed to the NPs. Hemolysis analysis **(using equation 2.3)** of GNPs showed hemolysis of less than 1%, which is well below the acceptable range for NP induced hemolysis **(Figure 2.3C inset)**. Additionally, the blood clotting trend was observed to be similar to that of 0.9% saline exposed blood over 60 minutes, with blood clotting beginning within 20 minutes of exposure. These results confirm the hemocompatibility of the GNPs **(Figure 2.3C)**.

The uptake of EGNPs and GNPs were determined the measuring the fluorescence (as an indicator of NPs internalized into cells) normalized to the amount of proteins (as a determinant of cell number) using a spectrophotometer **(Figure 2.4A)**. EGNPs

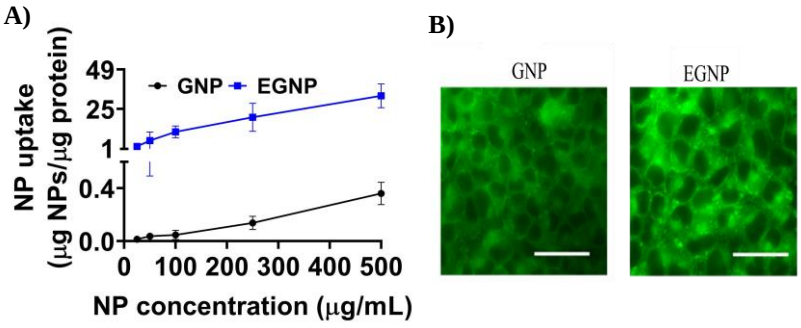

Figure 2.4. *In vitro* uptake study of EGNPs. **A)** Fluorescently-labeled GNPs observed poor targeting to A549 cells, while EGNPs observed significantly higher NP cellular uptake by A549 cells, with over 50-fold increase in the targeting efficiency compared to the untargeted GNPs. **B)** representative fluorescence microscopy images observed higher signal (green color) from the EGNPs in the lung cell microenvironment. Scale bar: 50 µM.

observed significantly improved internalization (nearly 50-fold) into A549 lung cancer cells, as a characteristic of the specific targeting capability of anti-EphA2 antibodies to the lung cancer cells. These results reaffirm the lung cancer cell targeting specificity of anti-EphA2 antibodies. Fluorescence imaging also observed higher localization of EGNPs (characterized by bright green dots) in the lung tumor environment compared to those of untagged GNPs **(Figure 2.4B)**.

2.3.4 In vivo biodistribution of EGNPs

In vivo biodistribution studies were performed to determine the localization of the EGNPs at the tumor site. Nude mice bearing subcutaneously implanted A549 lung tumors were injected with cyanine-7 loaded GNPs and EGNPs to compare their targeting efficacy (with saline serving as the background control). 24 hours after NP administration the mice, the tumors and visceral tissues were imaged *ex vivo* **(Figure 2.5A)**. Mice administered with EGNPs exhibited significantly increased signs of NP enrichment in the tumors, compared to that of mice administered with GNPs. However, we also observed NP localization in the liver, kidneys and visceral organs possibly due to the presence of small and very large NPs that escape and

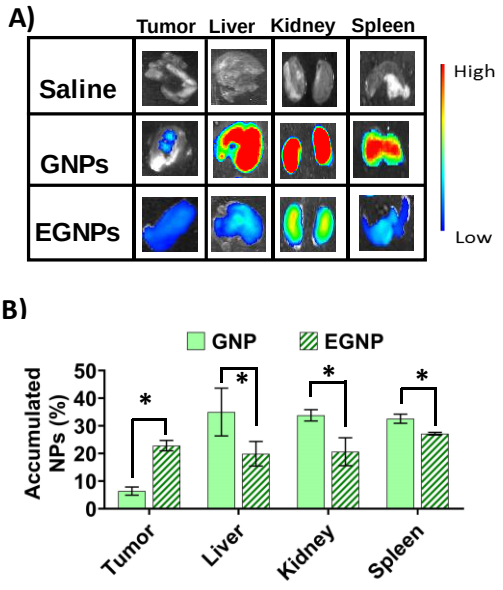

Figure 2.5 *In vivo* biodistribution study. **A)** *In vivo* fluorescence imaging observed localization of EGNPs in a subcutaneous A549 lung tumor model, with negligible GNP localization in the tumors. **B)** *ex vivo* analysis of tumor homogenates observed about 3X higher EGNP accumulation in the lung tumor site compared to untargeted GNPs (*P<0.05 vs. EGNPs accumulated in the same organ type).

accumulate in the liver, kidneys and spleen for elimination. Importantly, these signals were significantly lower in the tissues excised from the EGNP group, compared to those from the GNP group. Our observations from the images correlated with analysis of homogenized tissues, that noted about 23% EGNP concentrated in the tumors, while only 6% of GNPs were collected in the tumors **(Figure 2.5B)**. Visceral organs such as the liver, kidneys and spleen also exhibited high amounts of NP (both EGNP and GNP) accumulation; however these numbers were significantly lower for the EGNPs compared to the GNPs.

2.3.5 In vivo tumor reduction study

In vivo therapeutic efficacy studies were performed to determine the therapeutic efficacy of CEGNPs **(Figure 2.6)**. RTVs (calculated by **Equation 2.5**) of mice treated with saline and bare NPs exhibited an increase in relative tumor volume with time. RTV of mice administered with saline increased from 1 to 5.7, while those administered with bare GNPs increased from 1 to 5.18 indicating no effect of the bare NPs. Mice administered with free cisplatin also exhibited an increase in the relative tumor volume; however slower than that of saline and the bare NPs (1 to 3.4). Mice administered with CEGNPs, showed a significant reduction in the tumor growth rate compared to those by free cisplatin at the same equivalent dose. CGNPs observed a RTV of 1 to 1.15 within 14 days indicating reduced tumor volumes, while CEGNPs observed a RTV of 1 to

0.5 indicating a 50% reduction in tumor volumes over 14 days. These results were also confirmed by *ex vivo* representative photographs of tumors excised from the various groups that exhibit the differences in tumor sizes across the groups **(Figure 2.6B)**. Although we did not observe significant therapeutic differences between the untargeted and targeted NPs, we speculate that considering the benefit/risk ratio, we could potentially reduce the side-effects associated with cisplatin by improving the localization of these targeted NPs in the tumor microenvironment only.

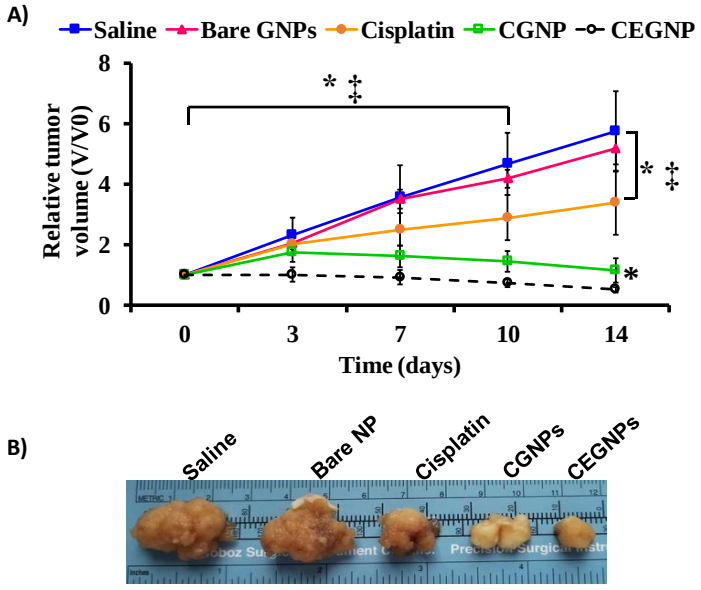

Figure 2.6. *In vivo* therapeutic efficacy study. **A)** A549 tumor growth rate significantly declined and slowed down in mice treated with the EphA2 targeting NPs encapsulating cisplatin, compared to those by the nontargeted cisplatin-loaded NPs, free cisplatin, bare NPs and saline (control). *P < 0.05 vs. EGNPs_14 days and ‡P< 0.1 vs. EGNPs_14 days. **B)** *ex vivo* photographical representation of excised tumors post-sacrifice, observed smaller tumor sizes in the mice administered with CEGNPs.

2.4. DISCUSSION

Over the last decade, GSH-sensitive bio-/nanomaterials have been developed and used as drug carriers for cancer therapies to release the drug payload in response to the endogenous GSH in the tumor microenvironment. The GSH/glutathione disulfide (GSSG) is the major redox couple

in mammalian cells, and it is a major determinant of the anti-oxidative capacities of cells, while extending cell-protection against free radicals [112]. The intracellular GSH/GSSG levels are regulated by various redox couples, like $NADH/NAD^+$, $NADPH/NADP^+$ and $thioredoxin_{red}/thioredoxin_{ox}$ [112]. GSH dysregulation plays a key role in human cancers, often increasing cellular resistance to several chemotherapeutic drugs [61]. Since tumor tissues express immensely higher levels of glutathione (~ 2-10 mM) compared to normal tissues (~ 2-10 µM), glutathione is a valuable endogenous tool to trigger drug release from polymers exhibiting GSH-responsive behaviors [62, 112].

The most common approach to developing GSH-responsive materials, involves incorporation of disulfide linkages in the polymer backbone that scavenge GSH, undergo reduction and subsequent disassembly to release their payload. For example, amphiphilic copolymers containing disulfide linkages were utilized for drug release in response to elevated GSH levels [113]. However, these micelles observed poor sensitivity to GSH levels, even up to 10 mM of GSH, followed by increased drug release upon treatment with 30 mM of GSH. Additionally, amphiphilic graft copolymers of hydrophobic poly(amidoamine) and poly (ethylene glycol) incorporating disulfide linkages observed nearly 100% release within 10h of exposure to 1 mM of DTT [64]. However, over 25% of drug was released within the same time in the absence of DTT, which is significantly higher compared to our observation (5% within 100 hours in the absence of GSH). In another approach, mesoporous silica NPs capped with disulfide linkages on their surface, were coated with N-acetylated heparin encapsulating doxorubicin [114]. These NPs also observed a GSH concentration sensitive increase in doxorubicin with approximately 100% release within 24 hours upon exposure to 10 mM of GSH, and ~20% release in the absence of GSH, which is

significantly higher than that observed from our NPs (~ 5% cisplatin release in the absence of GSH). Our NPs observed distinctive sensitivity to GSH levels at 5mM and 10 mM of GSH, with 5-times and 10-times more drug release compared to 0mM of GSH. These results highlight the sensitivity of our NPs towards GSH levels. The improved GSH sensitivity is potentially due to higher disulfide bonds in the parent polymer, which increases the hydrophilicity of the polymer [68].

To utilize NPs for cancer chemotherapy applications, it is imperative to study their therapeutic efficacy. To this end, we have utilized several *in vitro* studies that each indicated reduced viability, increased caspase-3 (apoptosis marker) production and reduced survival fraction of A549 lung cancer cells and their colonies upon treatment with CEGNPs. Additionally, EGNPs and GNPs also significantly out-performed cisplatin-loaded PLGA NPs that are conventionally used as drug carriers for chemotherapy due to their biodegradable and biocompatible natures [115]. Moreno et al. [116], observed an increase in tumor volume in mice treated with cisplatin-loaded PLGA NPs, while those treated with free cisplatin observed a relatively unchanging trend in tumor volumes, indicating better treatment response from these carriers. However, our observation of *in vivo* therapeutic efficacies witnessed significantly lower tumor growth rates in mice treated with CEGNPs (10-times lower) when compared to free cisplatin at the same drug dose. These results could potentially be due to the stimuli-responsive "on-demand" drug release from the GSH-responsive nanoparticles. Similarly, Ryu et al [113], observed about 80% viability of MCF-7 breast cancer cells treated with doxorubicin-loaded GSH-responsive micelles. Addition of exogenous GSH further decreased the cell viability, to 30% for cells treated with 20 mM of GSH in addition to the Dox-loaded micelles. Contrary to these results, our results observed that C

EGNPs significantly reduced the viability of A549 lung cancer cells (up to 80% cell death) compared to free cisplatin (up to 60% cell death) at equivalent concentrations without the addition of GSH. Additionally, as discussed in the earlier paragraph, our NPs showed higher sensitivity of GSH concentrations, unlike those synthesized by Ryu et al [113]. These findings could contribute to the enhanced therapeutic efficacy of our GNPs and EGNPs.

The other prominent feature of our NP design is the incorporation of lung tumor targeting capabilities *via* antibodies specifically targeting the Ephrin transmembrane receptor 2, overexpressed on lung cancer cells. Receptors of the Ephrin family belong to the tyrosine kinase family and are key regulators of various cellular functions [117]. Various lung cancer cell lines like A549, H460, H1299 and H1975 among others, have been observed to show high mRNA and protein levels of EphA2, often in correlation with smoking, K-RAS mutation, brain metastasis, tumor angiogenesis and poor survival of lung cancer patients [89, 117, 118]. In fact, knockdown of EphA2 has also been observed to inhibit the proliferation, motility and survival of lung cancer cells [118]. Taking advantage of the overexpression of EphA2 on lung cancer cells, antibodies and peptides targeting EphA2 can specifically deliver their cargo to lung cancer cells. For example, lipid nanoparticles coated with peptides against EphA2, and encapsulating anti-cancer agents, docetaxel and DIM-C-pPhC6H5 were generated to target and treat lung cancer cells [89]. This NP formulation observed 35% more uptake into tumor cells, and about 23% more reduction in tumor volume compared to untargeted NPs. Additionally, *in vivo* biodistribution studies observed about 40-60% improvement in NP localization compared to the untargeted NP variation. On the other hand, our NP formulation incorporating antibodies against EphA2, observed over 50-fold higher uptake into lung cancer cells and about 56% reduction in tumor volume. Furthermore,

EGNPs also observed about 4X increase in NP localization in the lung tumors compared to the untargeted GNPs.

Beside EphA2 ligands and/or antibodies, other lung cancer specific drug delivery approaches such as those using folic acid and anti-EGFR have also studied for targeting lung cancer cells. Alvarez-Berrios et al. [119] investigated folic acid (FA) conjugated mesoporous silica NPs for delivery of cisplatin to target and treat HeLa cells. These NPs were successfully internalized into HeLa cells and exhibited a significant decrease in HeLa cell viability upon treatment. However, the FA conjugated cisplatin loaded-NPs could not out-perform free cisplatin, with cell viability remaining higher at most concentrations. On the other hand, our NPs significantly outperformed the therapeutic efficacy of free cisplatin, even at lower drug concentrations, potentially due to the stimuli responsive nature of the NPs and improved targeting of our NPs. Additionally, a major disadvantage of using folic acid is competitive-binding of free folate in serum that may reduce the targeting efficacy of the NPs [120]. Peng et al. [88] developed cisplatin loaded heparin NPs, conjugated with single-chain antibodies against EGFR (ScFvEGFR) to target and treat lung cancers. Similar to our results, these NPs also significantly reduced tumor volume compared to free cisplatin. However, EGFR is also expressed on normal tissues, which majorly limits the targeting efficacy of antibodies or peptides against EGFR [121]. Thus, receptors of the ephrin family, such as EphA2 are valuable alternatives for targeted drug delivery.

2.5. SUMMARY

To summarize, glutathione-responsive NPs specifically targeting the lung cancer cells were formulated and characterized. The particles exhibited a hydrodynamic diameter of about 300 nm, and a zeta potential about -14 mV. Furthermore, they were stable up to 48 hours, and observed a glutathione concentration-dependent release of cisplatin. They were cyto-compatible to AT1 healthy lung cells and hemo-compatibile to human blood. Importantly, the presence of anti-EphA2 Ab on the NP surface, significantly enhanced the uptake of the NPs into lung cancer cells. Additionally, the targeted NPs also significantly augmented *in vitro* lung cancer cell death, and reduced tumor growth rate *in vivo*. These NPs also exhibited superior localization in the tumor regions compared to the untargeted GNPs. Thus, the cisplatin loaded glutathione-responsive NPs coated with anti-EphA2 antibodies can potentially be utilized as a chemotherapeutic strategy for lung cancer treatment. The limitations of this research include the use of a subcutaneous model for studying the biodistribution and tumor killing abilities of the NPs. An orthotopic tumor model (tumor cells implanted in the lungs) would be a more realistic *in vivo* model to use.

CHAPTER 3: EphA2 FUNCTIONALIZED-PLATELET-MEMBRANE COATED RADIATION-RESPONSIVE NPs FOR LUNG CANCER RADIATION THERAPY

3.1. INTRODUCTION

Radiation therapy (RT) is one of the common treatment strategies employed to treat lung cancer, with over 50% of all cancer patients receiving RT [33]. RT involves exposing cancerous tissues to high intensity beam of radiation, often as several fractions over a course of several weeks [33]. RT induces apoptosis in tumor cells by generating intracellular free radicals (via excitation of the water molecules within cells) [33]. These free radicals induce DNA double strand breaks (DSB), which then initiates a global response that causes DNA damage followed by cell death [33, 122]. Some of the most common radiotherapy strategies are, stereotactic body radiation (SBRT) or stereotactic ablative RT (SABR) for stage I NSCLC and concurrent chemoradiation for stage III NSCLC [34, 35]. However, radiation therapy suffers from several limitations, particularly reduced therapeutic efficacy as a result of the non-homologous end joining (NHEJ) repair mechanisms of cancer cells and inadequate oxygen levels, which curtails the effectiveness of the radiation regimen [122].

Radiation therapy for cancer treatment can be improved by addition of radiosensitizers that enhance the effects of radiation by inhibiting DNA repair in cells, thereby inducing cell apoptosis. Various radiosensitizers, including metal based radiosensitizers and small molecule radiosensitizers have been widely investigated to boost radiation therapy of various cancers. One such radiosensitizer, 8-dibenzothiophen-4-yl-2-morpholin-4-yl-chromen-4-one (NU7441), has

been proven to inhibit the DNA-dependent kinases that regulate the non-homogenous end joining process of DNA double strand repair after radiation therapy, in addition to providing an excellent radio-sensitization *in vitro* and *in vivo* [123, 124]. However, this radiosensitizer is extremely toxic and poorly soluble in aqueous solvents, which reduces its *in vivo* bioavailability [125]. Thus, there is an urgent need to circumvent these issues and develop alternatives to improve the delivery of NU7441 for radio-sensitization of lung tumors. Encapsulation of NU7411 into NPs can circumvent most of these limitations, and subsequently improve its therapeutic efficacy. The recent years have witnessed a surge in research involving nanoparticles as radiosensitizers or carriers for radiosensitizers; however, there have been very few reports involving encapsulation of NU7441 into NPs. For instance, PLGA NPs encapsulating NU7441, were conjugated with R11 peptide to target and enhance the radio-sensitivity of prostate cancer cells [126]. These NPs observed enhanced radio-sensitization of PC3 prostate cancer cells compared to that by radiation alone, signifying the advantages of using NU7441, in addition to targeting to treat cancers.

In this research project, we will use hyaluronic acid-based NPs that release NU7441 encapsulated within NPs, responding to radiation exposure, as a result from degradation of their glycosidic bonds due to ROS generated during radiation therapy [79, 127]. Furthermore, we will utilize platelet cell membranes to coat these NPs, to impart targeting to the lung cancer microenvironment. Platelets can migrate towards the cancer microenvironment, following which they adhere to the tumor cells, forming protective cloaks via tumor cell-induced platelet aggregation (TCIPA), a process that facilitates their metastasis via tumor cell extravasation [128, 129]. Previous research has also shown lung cancer cells to promote platelet activation and aggregation onto lung cancer cells via secretion of various chemokines in the tumor

microenvironment [129, 130]. Thus, our goal is to take advantage of these events to specifically target the drug-loaded nanoparticles to the lung cancer cells, thereby reducing off-target side effects of NU7441 and enhancing the effects of localized radiation therapy in the lung cancer microenvironment **(Figure 1.2)**. We will also incorporate antibodies against the EphA2 receptors that are highly expressed on lung cancer cells [91, 118], to further enhance the targeting of the radiation-responsive NPs towards the lung tumor site. In this report, we investigated the radiation responsiveness of these NPs, study the drug release kinetics of NU7441 from these NPs in response to varying radiation doses, and evaluated the *in vitro* therapeutic efficacy of these NPs at killing lung cancer cells.

3.2. EXPERIMENTAL SECTION

3.2.1 Fabrication of hyaluronic acid (HA) nanoparticles (HNPs)

It has been well-known that NP size has dramatic effects on the therapeutic efficacy of drug carriers influencing their capacity to cross biological barriers and to be up taken by cancer cells. However, little has been done to investigate factors affecting the size of HA NPs. In this study, various synthesis parameters influencing the HA NP size were studied to optimize the NP size. A relationship between NP size and synthesis parameters, namely HA concentration (%), oil to water ratio (Vo/Vw), sonication power (watts), and swelling time (hours), was quantified using Design Expert software (Stat-Ease Inc.). Hyaluronic acid NPs encapsulating NU7441 were synthesized by a reverse single emulsion technique. This process involves crosslinking of HA

using adipic acid dihydrazide (ADH; MilliporeSigma) via activation of the carboxylic acid groups on HA by 1-Ethyl-3-(3-dimethylaminopropyl) carbodiimide (EDC; MilliporeSigma). To perform factorial analysis, three major synthesis parameters **(Figure 3.1)**, namely HA swelling time (6 hours and 24 hours), oil-to-water ratio (1:1 and 2:1) and sonication power (10 watts and 30 watts) were investigated for their roles in NP size.

To synthesize HNPs, 50 mg of hyaluronic acid (~ 200 KDa; Lifecore Biomedical) was dissolved in PVA (5% w/v) at a concentration of 10 mg/mL and allowed to swell at a predetermined time (6 or 24 hours) at room temperature on a rotator. 2.5 mg of ADH was then added to this solution and allowed to react for 30 minutes, following which 2 mg of EDC was added to crosslink the HA. The HA solution was then added dropwise to DCM at a pre-determined ratio (1:1 or 2:1 oil-to-water) while stirring. This emulsion was sonicated using an ultrasonicator for 10 minutes at pre-determined power (10 watts or 30 watts) and stirred overnight in a fume hood to facilitate solvent evaporation. HNPs were obtained the following day via centrifugation at 15,000 RPM for 30 minutes, followed by lyophilization. For NPs encapsulating NU7441 (Tocris), 2 mg of NU7441 was dissolved in 200 µL of dimethyl sulfoxide (DMSO; MilliporeSigma) to constitute the drug phase. The NU7441 solution was then added to the HA solution, followed by

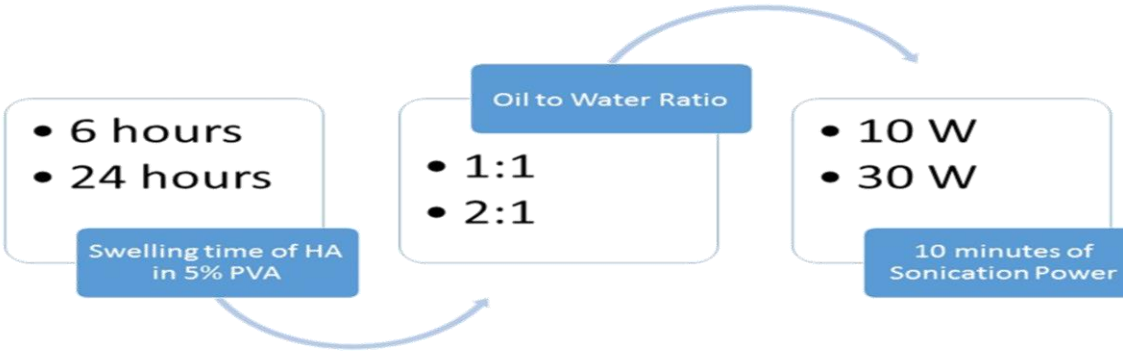

Figure 3.1. Factors varied during synthesis of HA NPs.

sonication using a microtip sonicator at 30 watts for 1 minute, prior to addition of ADH. The rest of the NP synthesis was performed as above.

To perform factorial analysis, NP sizes for various combinations were determined by dynamic light scattering technique, and the outcomes were entered into a factorial analysis software (Design expert), which was then used to generate a predictive equation and 3D plots to study the effects of multiple parameters on HNP size. The outcomes from these plots for selected as ideal parameters for synthesis of HNPs and used for future HNP formulations.

3.2.2 Isolation of platelets and platelet membranes

Platelets and platelet membranes were isolated by a freeze-thaw technique described previously [131]. Human platelet rich plasma (PRP) was purchased from Innovative Research. To collect platelets, PRP was firstly centrifuged at 100 x g for 15 minutes at room temperature to separate red blood cells and white blood cells in the PRP. The supernatant was collected and diluted 2-fold in cold 1X-PBS supplemented with 1 mM of Ethylenediaminetetraacetic acid (EDTA; MilliporeSigma) and centrifuged at 800 x g for 15 minutes at room temperature. The supernatant was discarded, and the pellet containing platelets was resuspended in cold 1X-PBS supplemented with 1mM of EDTA and protease inhibitor cocktail (MilliporeSigma) to preserve platelet proteins. Platelet membranes were isolated via a repeated-freeze thaw method, by firstly freezing the platelet solution at -80˚C for 15 minutes, followed by thawing at room temperature for 15 minutes. This process was repeated 7 times, to ensure complete rupture of platelet cell

membranes. The platelet membranes were then isolated via centrifugation at 4000 x g for 10 minutes, and the pellet was resuspended in 1X-PBS containing a protease inhibitor cocktail.

3.2.3 Functionalizing HNPs with platelet membranes and EphA2 antibodies

To insert anti-EphA2 antibodies (Biolegend) on the surface of the platelet membranes, we used palmitated-protein A (PPA; ProSpec), which had a high affinity to bind to the Fc region of IgG, thus functioning as a docking point for antibodies (Abs) on cell membranes [132]. Briefly, 1 mg/mL of protein A was resuspended in a 1X-PBS solution (pH 7.4) and supplemented with 0.3% sodium deoxycholate (MilliporeSigma), 0.1% sodium bicarbonate (MilliporeSigma) and 0.1% sodium azide (MilliporeSigma). Palmitic acid (MilliporeSigma) was dissolved at a concentration of 10 mg/mL in 100% ethanol. This solution was then heated to 50°C, following which 10 µL of this solution was added to the protein solution at 37°C. This complex was then incubated while shaking for 18h, followed by filtration to separate the free proteins or lipid mixtures. The PPA mixture was then added to the extracted platelet membranes (50 µg/mL of PPA to membranes from 3.0 million cells), incubated at 37°C for 10 minutes, and washed to remove unbound PPA. Platelet cell membranes (± PPA) were then coated onto the HNPs via extrusion technique. Briefly, amount of proteins in the platelet membrane solution were determined by BCA protein assay (Thermofisher scientific), before complexation with PPA. The platelet membrane coated HNPs (PHNPs) were formulated by mixing drug loaded HA NPs with the membrane extract (at a ratio of 1:2 of NPs: protein in membranes) and co-extruded about 22 times through a 400 nm polycarbonate porous membrane using a mini-extruder (Avanti Polar) to cloak these the platelet

membranes onto HNPs. Insertion of antibodies using PPA was performed as described earlier [133]. Briefly, PPA-platelet membrane coated HNPs were incubated with 100 µg/mL of anti-EphA2 antibody on ice for 1 hour, followed by centrifugation to collect the EphA2 tagged platelet membrane coated HNPs (EPHNPs).

EphA2 Abs were conjugated on HNPs via carbodiimide chemistry. Briefly, 5mg of lyophilized NPs was suspended in 4mL of 2% 2-ethanesulfonic acid (MES; MilliporeSigma) buffer (~ pH 5.0), and 20 mg of EDC was added to this suspension and allowed to react at room temperature for 30 minutes. Twenty mg of N-hydroxysuccinimide (NHS; MilliporeSigma) was then added to this suspension and allowed to react at room temperature for another 30 minutes. This reaction activated ester groups on the NP surface for conjugating of ligands/antibodies onto NPs. Eleven µg of Ab solution was then added to the above solution, and the conjugation reaction performed overnight 4°C, followed by dialysis to remove unconjugated Abs, and lyophilization to obtain the Ab/targeting ligand-conjugated NPs. Antibody conjugation efficiency was determined by Bradford protein assays and calculated by the equation;

$$Ab\ coating\ efficiency = \frac{Amount\ of\ Ab\ used - amount\ of\ Ab\ in\ supernatant}{Amount\ of\ Ab\ used} X\ 100\%$$

…. (3.1)

Retention of platelet markers on PHNPs was determined by flow cytometry. Briefly, 1 mg of non-drug loaded HNPs and PHNPs were resuspended in 1X-PBS (with 0.1% sodium azide(MilliporeSigma)) and labeled with fluorescently labeled antibodies against CD62p (labeled with APC, activated platelet marker) and CD42a (labeled with PE, platelet identification marker)

to detect via flow cytometry (BD LSR II Flow Cytometer). Platelets labeled with these antibodies were included as controls.

3.2.4 Characterization of nanoparticles

Particle size, size distribution, and surface charges were measured using the Dynamic Light Scattering (DLS) technique (ZetaPALS zeta potential analyzer, Brookhaven Instruments Inc.). Transmission electron microscopy (TEM, JOEL 1200EX) was used to visualize the morphology of the platelet membrane coated and uncoated HNPs.

NU7441 loading efficiency for HNPs were determined by indirect method. Briefly, the amount of NU7441 in the supernatants was collected by a UV-Vis spectrophotometer (Tecan) at an absorbance of 234 nm. The amount of NU7441 loaded into the NPs was determined by the following equation;

$$NU7441\ loading\ efficacy = \frac{NU7441\ amount\ used - NU7441\ \ in\ supernatant}{NU7441\ \ amount\ used}\ X\ 100\%$$

…. (3.2)

Radiation sensitivity of HNPs and EPHNPs was determined by exposing NU7441 loaded NPs to increasing radiation doses (0 Gy, 2 Gy, 5 Gy and 10 Gy). To study the radiation triggered NU7441 release kinetics from HNPs and PHNPs, the lyophilized NPs were first re-suspended in 1X-PBS (pH 7.4) in a 1 mg/ml concentration. NP suspensions were added to dialysis bags (10 KDa, Spectrum laboratories), and subjected to radiation (3 replicates for each radiation dose). The dialysis bags were then inserted into a 1X-PBS bath of 10 mL each, and incubated at 37˚C, to

simulate the body temperature. At pre-determined time points, 1 mL of 1X-PBS solution from the 1X-PBS bath was extracted and stored at -20˚C, 1 mL fresh 1X-PBS was replenished, and the dialysis bags were incubated at 37°C until the next time point. The amount of NU7441 released was quantified by a UV-Vis spectrophotometer at 280nm. A standard curve of known NU7441 concentrations was used to determine the cumulative NU7441 release. A sample size of n=3 per group was used for this study.

3.2.5 Cellular uptake of nanoparticles

Cellular uptake of HNPs and EPHNPs was determined by measuring the amount of fluorescently-labeled NPs that get internalized by lung cancer cells. HNPs and EPHNPs loaded with a fluorescent dye, fluorescein isothiocyanate (FITC; MilliporeSigma) were synthesized as described earlier. FITC was used here for detection of NPs in the cells. To study *in vitro* cellular uptake of NPs, A549 human lung cancer cells were seeded at a seeding density of 10,000 cells/well in 96 micro-well plate and allowed to attach overnight. Next day, the cells were incubated with HNPs and EPHNPs at different concentrations (0, 50, 100, 250, 500 and 1000 µg/ml; n= 4 per group) at 37°C for 2 hours. Post 2 hours, cells were washed 3X with sterile 1X-PBS and lysed using 1% Triton X-100. The amount of NPs internalized were determined by measuring the fluorescence intensity of FITC (translated to µg of NPs) at a wavelength of λex 495 nm and λem 519 nm and normalized against the amount of total protein from cells per well, determined using bicinchonic acid assays (BCA) per manufacturer's protocol (Pierce™ BCA Protein Assay Kit, ThermoFisher Scientific). NP uptake of HNPs and EPHNPs to A549 lung cancer cells and AT1

cells was also determined by fluorescence imaging. A549 and AT1 cells were seeded at a cell seeding density of 150,000 cells on glass coverslips and allowed for attaching overnight. The following day, A549 cells were exposed to 1mg/mL of FITC-loaded HNPs or FITC loaded EPHNPs for 2 hours, following which they were washed 3X with 1X-PBS, and fixed for 15 minutes in 4% paraformaldehyde (MilliporeSigma). The fixed cells were washed with 1X-PBS to remove excess paraformaldehyde and their nucleus stained with nucBlue® (ThermoFisher Scientific). The cells were then observed under a fluorescence microscope (Cytoviva Inc).

3.2.6 In vitro therapeutic efficacy

The *in vitro* therapeutic efficacy of HNPs combined with radiation were determined by MTS cell viability assays. Briefly, A549 lung cancer cells (ATCC) were seeded at a seeding density of 20,000 cells/well in a 48 micro-well plate and allowed to attach overnight. The following day, cells (n= 4 per group) were treated with free NU7441 (1 µg/mL drug concentration) or NU7441 loaded NPs: EPHNPs and HNPs (concentration equivalent to 1 µg/mL of NU7441 determined from the drug release kinetics). Untreated cells and cells treated with 1% Triton X-100 were regarded as the negative and positive controls, respectively. Two groups of these treatments were prepared, where one group was exposed to 5 Gy radiation dose, and the other group was not exposed to radiation. 2 hours after drug treatment, cells were subjected to radiation. 72 hours later, cell death was determined by MTS cell viability assays (Promega Corporation) per the manufacturer's protocol.

To observe the survival of lung cancer cells upon exposure to the EPHNPs, we performed clonogenic assays or colony formation assays (CFA). To perform these studies, A549 lung cancer

cells were seeded on 60mm petridishes, and *in vitro* CFA studies were performed as described previously [108]. The cells were treated with free NU7441 (500 ng/dish), or NPs: HNPs, PHNPs and EPHNPs (concentration equivalent to 500 ng/dish of cisplatin from the drug release kinetics) and incubated at 37˚C for 2 hours. A549 lung cancer cells not exposed to any treatment and A549 cells exposed to radiation only were included as negative controls. Like the MTS assays performed above, two groups of treatments were prepared, where one group was exposed to radiation (2,5 and 10 Gy), and the other did not receive any radiation exposure. Post-radiation treatment, the petridishes were further incubated at 37˚C for 10 days. Once the cancer cell colonies had reached a colony of at least 50 cells, the cells were washed with phosphate buffered saline, and stained with crystal violet (MilliporeSigma) dye (0.5% w/v in 6% v/v glutaraldehyde). The number of colonies in each dish were then counted. Survival fraction was calculated by normalizing the number of surviving colonies at a certain radiation dose (S_D) to the number of surviving colonies at 0 Gy radiation (S_0). A sample size of n=3 per group was used for this study.

3.2.7 Cytotoxicity analysis of nanoparticles

Healthy lung alveolar Type 1 (AT1) epithelial cells (Abmgood) were seeded at a density of 8000 cells/well in a 96 microwell plate and incubated overnight to facilitate cell attachment. Next day, the cells were incubated with varying concentrations of non-drug loaded HNPs and PHNPs (0, 50, 100, 200, 500, and 1000 µg/ml). Following 24 hour incubation, the cell viability was determined using MTS cell viability assays (CellTiter 96®AQueous One Solution Cell Proliferation Assay, Promega Corporation).

3.2.8 Hemo-compatibility analysis of nanoparticles

A hemolysis evaluation of the non-drug loaded HNPs and PHNPs was conducted as described previously [109]. Human blood from a donor was acquired following methods approved by the Institutional Review Board at the University of Texas at Arlington. After collection, human blood was incubated with HNPs and PHNPs at a NP concentration of 100 µg/ml or 1000 µg/ml, 0.9% saline (as negative control), or distilled water (as positive control) for 2 hours at 37˚C. The samples were then centrifuged at 1000 g, following which absorbance readings were taken at 545 nm using a UV-Vis spectrophotometer. The percentage of hemolysis was calculated using the following equation:

$$Hemolysis = \frac{Abs\ of\ sample - Abs\ of\ negative\ control}{Abs\ of\ positive\ control - Abs\ of\ negative\ control} \times 100\% \quad \textbf{…. (3.3)}$$

To study the blood clotting kinetics, non-drug loaded PHNPs and HNPs at concentrations of 100 or 1000 µg/ml, water (negative control) and 0.9% saline (positive control) were added to blood activated with 0.1M calcium chloride ($CaCl_2$) and incubated at room temperature. At pre-determined time points (10, 20, 30, and 60 minutes), water was added to the tubes to lyse the red blood cells (RBCs) that were not a part of the formed clot. Absorbance readings of supernatant were taken at 540 nm using a UV-Vis spectrophotometer. The absorbance readings are inversely proportional to the size of the resulting clot. The blood clotting kinetics were also observed

visually, and photographs acquired. A sample size of n=8 per group was used for the hemolysis and blood clotting study.

Hemo-compatibility of HNPs and PHNPs was further investigated by determining potential platelet aggregation and activation upon exposure to the NPs. To conduct these studies, platelet rich plasma (PRP) was firstly isolated from whole blood. Platelet aggregation was determined via turbidity testing. Briefly, 100 µL of PRP was exposed to NP solution (1mg/mL concentration), or controls (no treatment: negative control and 20µM of adenosine diphosphate: positive control) for 5 minutes, followed by analysis via a spectrophotometer at an absorbance of 650nm. Decrease in absorbance is a sign of PRP turbidity, and an indicator of platelet aggregation. Thus, higher the absorbance, higher the turbidity and thus lower the platelet aggregation. Platelet activation studies were conducted via flow cytometry to detect the expression of activated platelet markers (CD62p or P-selectin) and platelet markers (CD42a or GP1X) on the surface of platelets exposed to HNPs and PHNPs, compared to that by positive control (20µM of adenosine diphosphate). Briefly, PRP was diluted in 2-fold in 1X-PBS, and 100 µL of the diluted PRP was exposed to the NP solutions (1mg/mL concentration) or controls (no treatment: negative control and 20µM of adenosine diphosphate: positive control) for 5 minutes. Platelets were then fixed in 0.5% w/v paraformaldehyde (in 1X-PBS containing 1% bovine serum albumin and 0.1% sodium azide, also called as staining buffer) for 20 minutes, followed by centrifugation at 1400 x g for 10 minutes to pellet the platelets. The platelets were then resuspended in staining buffer and labeled with antibodies against P-selectin (CD62p-APC) and GP1X (CD42a-PE). Isotypes for both antibodies were also included. After 20 minutes, cells were washed, resuspended in staining buffer and analyzed using a flow cytometer (BD LSRII Flow Cytometer).

3.2.9 In vivo biodistribution of fluorescently labeled NPs

To test the *in vivo* biodistribution of HNPs, EphA2 antibody-tagged HNPs (EHNPs) and EphA2-tagged platelet membrane coated HNPs (EPHNPs), athymic nude mice (Foxn1^{nu}, Jackson labs) were subcutaneously implanted (at the hindlimb) with A549 lung cancer cells (2 million cells), following the protocol approved by The Institutional Animal Care and Use Committee (IACUC) at The University of Texas at Arlington. EHNPs were included as a control against EPHNPs to show the enhanced biodistribution of the dual targeting moieties (platelet membranes and anti-EphA2 antibody) vs. that by anti-EphA2 alone. Once the tumors reached a diameter of approximately 10 mm, treatment was commenced. 0.9% saline served as the negative control, while cyanine-7 loaded HNPs, EHNPs and EPHNPs were the study groups. Since PHNPs did not observe a significant improvement in the CFA studies, we did not include PHNPs in the biodistribution study. Animals wereadministered with either saline or 1.5 mg of the NPs (n=4 per group comprising of randomly allocated 2 male and 2 female mice) via intravenous injection. 24 hours later the mice were euthanized, and their tumors and visceral organs (liver, kidneys and spleen) were collected for analysis. Tumor dimensions and tissue weights were recorded, following which they were imaged *ex vivo* in the fluorescence bioimager (Kodak *In vivo* Fx Pro system). The tissues were then homogenized using a tissue homogenizer (Precellys evolution, Bertin Instruments), and the amount (mg) of NPs retained in the tissues was quantified using a spectrophometer.

3.2.10 Statistical analysis

Results were analyzed statistically using 2-way ANOVA and Fisher's post-hoc analysis (Statview 5.0 software) with $p<0.05$ considered as a significant value. All results are displayed as mean ± SD, and quadruplet samples (n=4) were used for each experiment if not specified.

3.3. RESULTS

3.3.1 Effects of synthesis factors on NP sizes

Factorial analysis was performed to select the ideal parameters for synthesizing HNPs and understanding their roles in determining the size of HNPs. It was found that the sonication power

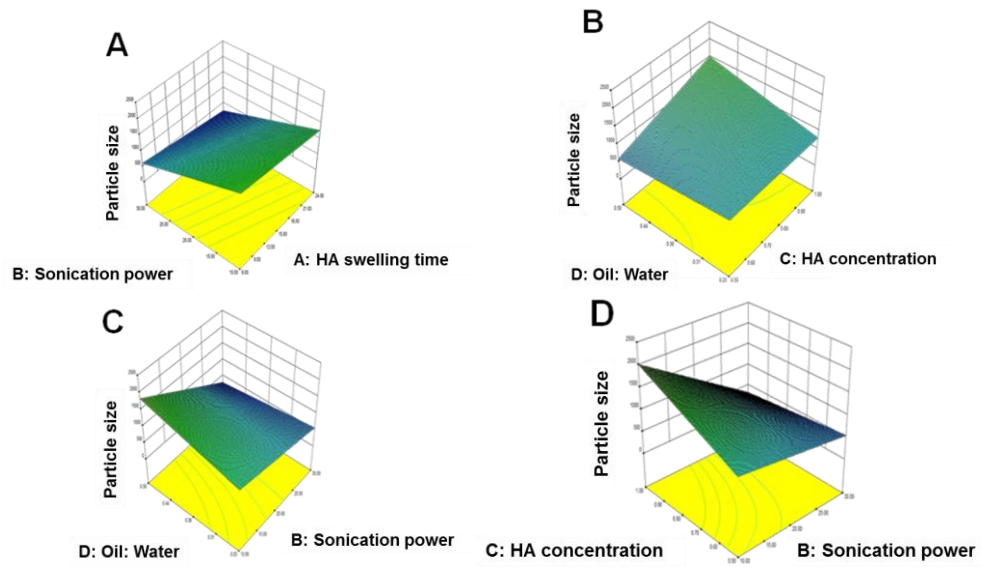

Figure 3.2. 3D Plot depicting the effects of multiple formulation factors on particle size. **A)** Effects of sonication power and HA swelling time: particle size is the smallest at the highest sonication power, i.e. 30W, and longest swelling time, i.e. 24 hours, indicating an inverse relationship. **B)** Effects of oil to water ratio and HA concentration: smallest particles are achieved at a lower O: W ratio and a lower HA concentration, depicting a direct relationship. **C)** Effects of oil to water ratio and Sonication Power: smaller sized particles are obtained at a higher O: W ratio and a higher sonication power of 30W. **D)** Effects of sonication power and HA concentration: smallest nanoparticles were obtained at the maximum HA Concentration and a sonication power of 30W.

and HA concentration significantly affected the NP size **(Figure 3.2)**. Based on the predicted trends, we performed an experiment to validate our formulation model. The model predicted a NP size of 189 nm with a certain formula **(Equation 3.3 below)**; the actual size achieved from using that formula was 191±38 nm, a less than 2.25% error between the predicted and actual sizes.

The predictive equation obtained from factorial analysis is as follows:

Particle Size = +961.50 -189.44* A -524.56* B + 212.74* C + 107.18* D - 106.29*A*C - 327.77* B*C - 251.4*B*D + 248.17*C*D + 176.00*A*B*C + 118.17*A*B*D + 254.83*A*C*D - 256.82*B*C*D - 332.95*A*B*C*D

Where: A-HA swelling time, B-sonication power, C-HA concentration, D-Oil: water

…. (3.4)

3.3.2 Nanoparticle characterization

NU7441-loaded HNPs and PHNPs observed a diameter of 190 ± 23 nm and 247 ±51 nm respectively, by dynamic light scattering technique. Additionally, TEM imaging of HNPs and PHNPs observed

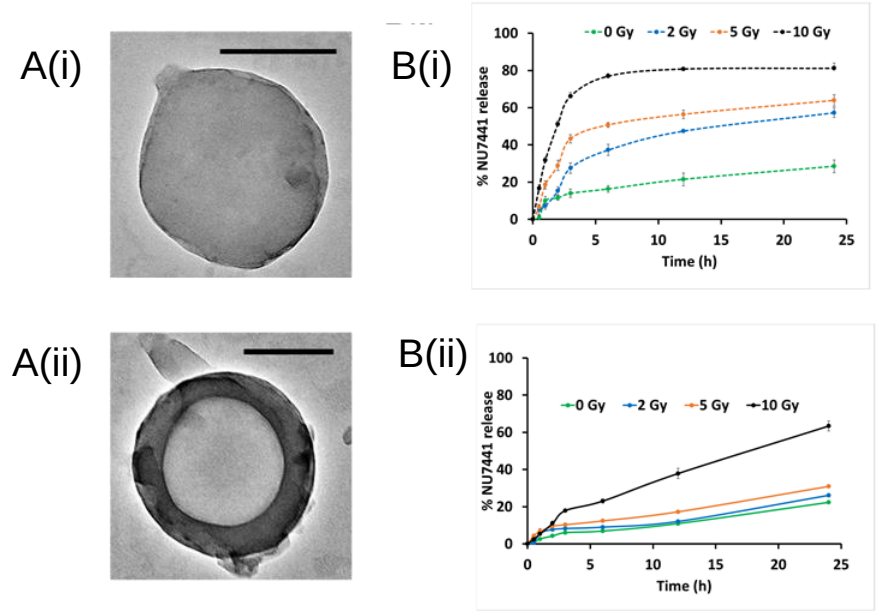

Figure 3.3: Characterization of NPs. **A)** TEM image of (i) HNPs and (ii) PHNPs showing successful coating of the cell membrane on the surface of HNPs. Scale bar: 200nm. **B)** Radiation responsive release of NU7441 from the HNPs (i) and PHNPs (ii), which shows significant increase in drug release as the radiation dose increases.

successful coating of the platelet membrane on the surface of the HNPs, as evidenced by the core-shell structure of PHNPs **(Figure 3.3A)**.

3.3.3 Drug loading efficiency and drug release characteristics of HNPs and PHNPs

NU7441 loading efficacy into HNPs was calculated indirectly via a UV *Vis* spectrophotometer at an absorbance of 288nm and was calculated to be about 63%. HNPs and PHNPs also exhibited radiation responsive drug characteristics, where an increase in exposed radiation dose, significantly increased drug release from the NPs **(Fig 3.3B)**. Radiation responsive release of NU7441 from HNPs **(Figure 3.3B (i))** and PHNPs **(Figure 3.3B (ii))**, which shows significant increase in drug release as the radiation dose increases. Almost 100% of the drug was released when exposed to 10 Gy radiation compared to about 30% released when not exposed to radiation from HNPs. PHNPs showed a slower drug release, with about 60% and less than 20% drug released at 10Gy radiation exposure and in the absence of radiation, respectively. Although, the membrane coating on the HNPs did not affect the radiation responsiveness of NPs, it slowed down NU7441 release from these NPs, thus exerting a barrier against premature drug release in the absence of radiation.

3.3.4 Flow cytometry analysis for detection of platelet markers on PHNPs

Flow cytometry analysis was employed to determine the retention of platelet markers on the surface of PHNPs. Since platelets markers, especially those of activated platelets are essential for homing towards the tumor microenvironment and for binding to the tumor cells, it is essential to retain them on the NP surface [134]. For proof-of-concept, we aim to identify the retention of platelet identification marker CD42a and platelet activation marker P-selectin on the surface of PHNPs using flow cytometry. Compared to uncoated HNPs, the PHNPs observed a significant shift in CD42a and P-selectin markers, a response similar to that of platelets **(Fig 3.4)**.

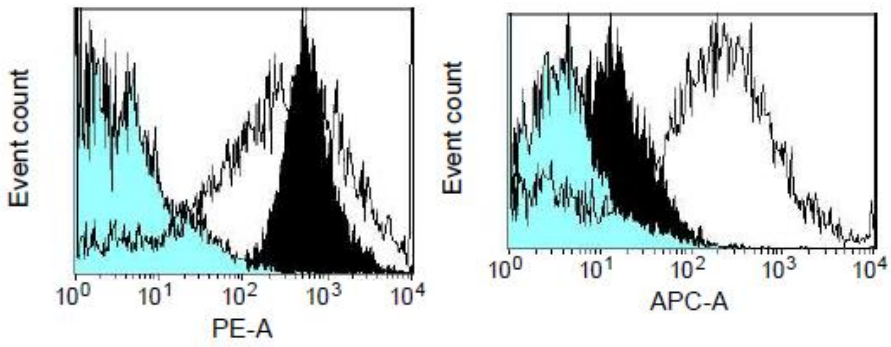

Figure 3.4. Confirmation of membrane coating on NPs. Flow cytometry analysis to identify platelet markers on the surface of PHNPs observed increased signal intensities for CD42a (PE-A) and CD62p (APC-A) platelet markers compared to uncoated NPs. (Black: platelets, blue: HNPs and clear: PHNPs).

3.3.5 In vitro characterization

The cytotoxicity of HNPs and PHNPs at increasing concentrations were determined by MTS cell viability assays. AT1 Cells exposed to HNPs and PHNPs were over 90% viable even at the highest NP concentration of 1000µg/mL, confirming the cyto-compatibility of the NPs to healthy lung cells **(Figure 3.5A)**.

Hemo-compatibility of the HNPs and PHNPs was analyzed by studying the hemolysis of blood and clotting profile of whole blood exposed to these NPs. Hemolysis analysis of HNPs and PHNPs showed hemolysis of less than 5%, which is well below the acceptable range for NP induced hemolysis. Hemolysis results also observed an increase in hemolysis with increase in NP concentration being exposed to blood. HNPs exhibited a hemolysis of about 2% and 4% at a NP concentration of 0.1 mg/mL and 1 mg/mL respectively, while PHNPs exhibited a hemolysis of 0.4% and 3% at a NP concentration of 0.1 mg/mL and 1 mg/mL, respectively. Platelet membrane coating also reduced hemolysis compared to that by HNPs. Additionally, the blood clotting trend was observed to be like that of 0.9% saline exposed blood over 60 minutes, with blood clotting within 30 minutes **(Figure 3.5B)**. These results confirm the hemo-compatibility of the HNPs and PHNPs.

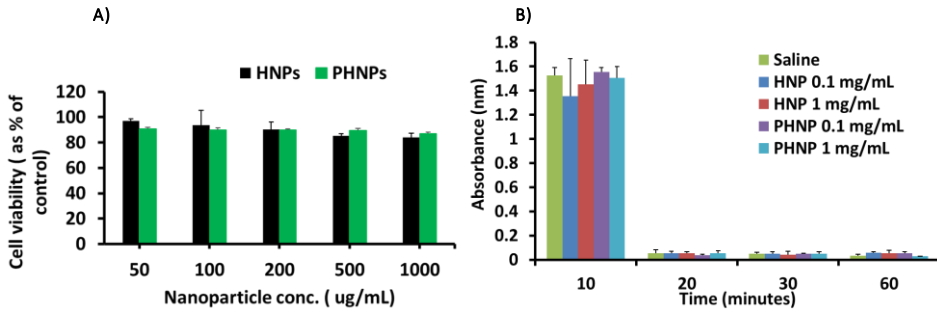

Figure 3.5. *In vitro* characterization of NPs. **A)** *In vitro* cyto-compatibility of the NPs observed over 90% alveolar type-I cell viability via MTS assays. **B)** HNPs observed a blood clotting trend like that of saline control.

To further investigate the hemo-compatibility of NPs, we conducted platelet activation and platelet aggregation studies using platelet rich plasma isolated from human blood. Since we observe platelet identification and activation markers on the PHNPs, it is imperative to confirm that the PHNPs will not induce either platelet aggregation or activation upon administration into the patient. Platelet aggregation study was performed via turbidity analysis of PRP exposed to these NPs via spectrophotometric analysis, compared to those exposed to adenosine diphosphate

as the positive control. Platelet aggregation studies observed similar absorbance values of PRP exposed to of PHNPs (1 mg/mL), HNPs (1 mg/mL) and untreated platelets (absorbance values of 0.129, 0.131 and 0.117, respectively). The positive control, on the other hand, observed significantly lower absorbance values (absorbance value of 0.05), indicating lesser turbidity and hence higher platelet aggregation. Additionally, the platelet activation study was performed using flow cytometry to determine the expression of platelet activation markers on platelets exposed to the NPs **(Figure 3.6)**. Signals obtained from isotypes and resting platelets observed absence of background signals for CD62p and CD42a, thus eliminating the possibility of non-specific binding. Platelets exposed to positive control exhibited a positive shift in the population compared to those exposed to isotypes, resting platelets, PHNPs and HNPs for CD62p, indicating the absence of CD62p activation. Platelets exposed to positive control, negative control and those exposed to the NPs, observed similar signals for platelet identification marker CD42a.

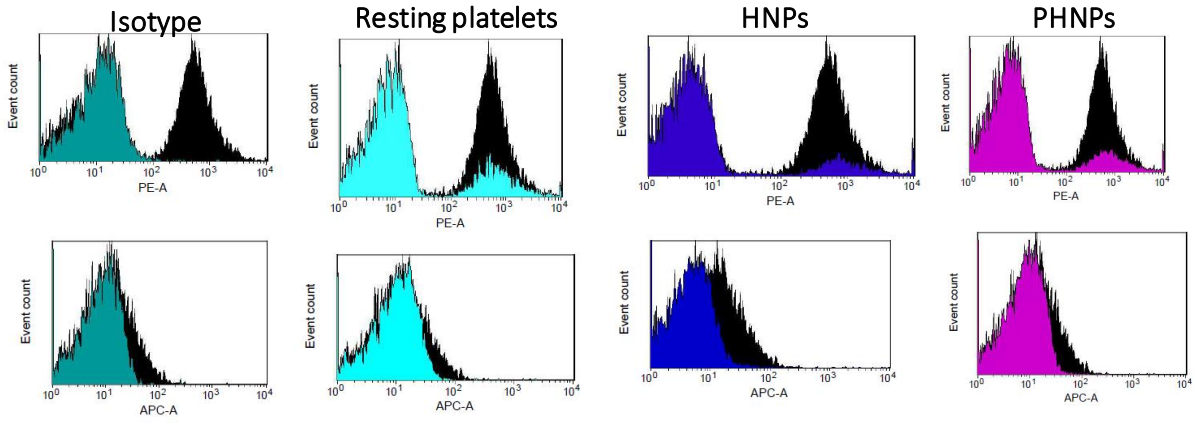

Figure 3.6. Confirmation of hemocompatibility using platelet activation study. Flow cytometry analysis did not observe activation of the resident platelets exposed to HNPs and PHNPs compared to that of positive control. PE-A indicates CD42a (platelet marker) and APC-A indicated CD62p (platelet activation marker). Black color: positive control, colored regions : listed groups.

The uptake of HNPs and PHNPs were determined by measuring the fluorescence (as an indicator of NPs internalized into cells) normalized to the amount of proteins (as a determinant of

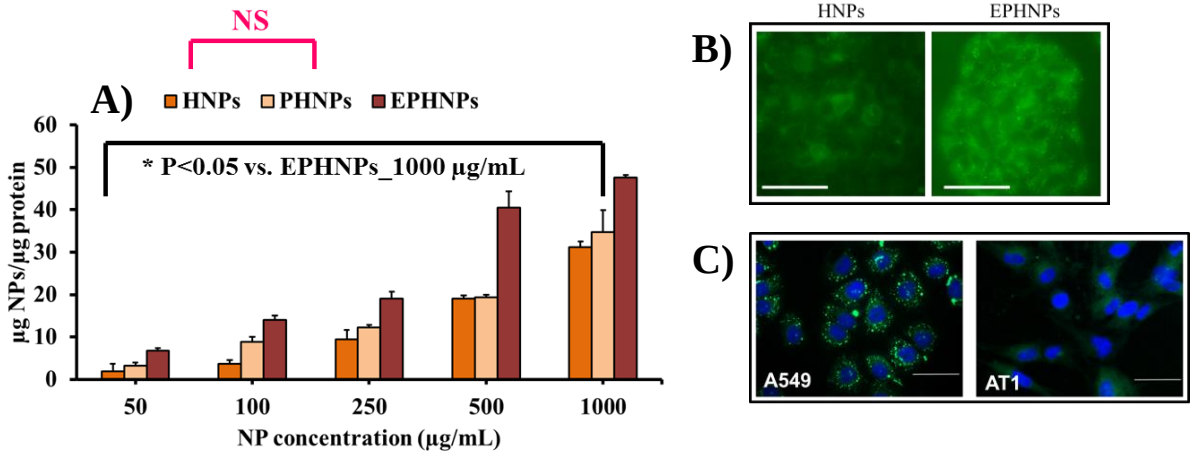

Figure 3.7. *In vitro* uptake studies. **A)** EPHNPs observed enhanced uptake into A549 cells compared to that by HNPs and PHNPs. **B)** EPHNPs observed greater localization in the lung tumor cell environment compared to that of HNPs. **C)** Inclusion of antibodies against EphA2 improved the specific uptake of the NPs in the lung tumor cells, while having minimal localization in the AT1 cells. Scale bar: 50µm.

cell number). HNPs, PHNPs and EPHNPs observed enhanced uptake into A549 lung cancer cells in a dose-dependent manner **(Figure 3.7A)**. However, the uptake into the lung cancer cells did not show a large difference between the uncoated and platelet membrane coated NPs. The inclusion of EphA2 membranes on the other hand, significantly enhanced the uptake of the NPs compared to those uncoated (bare) HNPs. Fluorescence microscopy further supported these findings, by illustrating the enhanced NP localization (green dots as a characteristic of FITC in the NPs) in the cancer cells because of the platelet membranes and the EphA2 antibodies **(Figure 3.7B)**. Furthermore, the EPHNPs observed improved localization in the A549 cells; however the localization of these NPs in healthy AT1 cells was significantly less **(Figure 3.7C)**. These results reaffirm the lung cancer cell targeting specificity of anti-EphA2 antibodies.

3.3.6 In vitro therapeutic efficacy of NPs

The therapeutic efficacy of NU7441 loaded EPHNPs and HNPs were investigated by exposing A549 and H460 lung cancer cells to these NPs, and determining the treatment induced cell death via MTS cell viability assays. MTS assays observed a NU7441 dose-dependent cell death of the A549 and H460 lung cancer cells over a 72-hour exposure. A549 and H460 cells exposed to radiation only exhibited a cell death of about 87% and 79%, respectively, while those exposed to the NP treatment groups in combination with radiation observed a significant reduction in cell viability compared to those exposed to the treatment groups alone in the absence of radiation **(Figure 3.8)**. NU7441 loaded HNPs and EPHNPs observed a decrease in cell viability compared to free drug alone. The higher cell death could potentially be due to the enhanced targeting of the platelet membranes coatings and EphA2 antibodies towards lung cancer cells, that might improve NP internalization into the cells, and subsequently enhance cell death. The poor response of A549 cells to radiation treatment could be potentially due to the radiation resistant nature of A549 cells. H460 cells, on the other hand, observed greater sensitivity to radiation treatment combined with NU7441 treatment due to their radiation-sensitive nature.

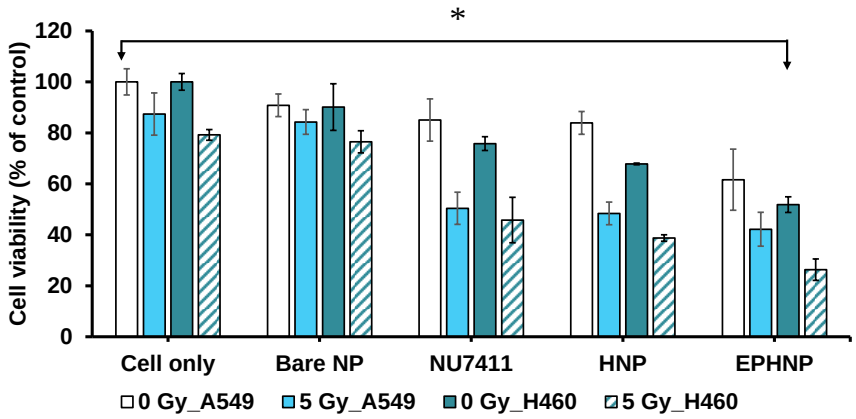

Figure 3.8. *In vitro* therapeutic efficacy. EPHNPs showed concentration dependent improvement in A549 and H460 lung cancer cell death via MTS assay when combined with radiation exposure. *P < 0.05 vs. H460 cell treated with EPHNPs + 5 Gy radiation exposure.

Clonogenic assays were implemented to determine the survival of A549 cancer cell colonies. Overall, survival fraction (SF) of the cells observed a radiation dose dependent decline, which further declined upon treatment with EPHNPs **(Figure 3.9)**. A549 cells treated NU7441 loaded EPHNPs experienced more than a fold-reduction in survival fraction when exposed to 10 Gy dose of radiation (SF: 0.62, 0.27, 0.21 and 0.13 upon exposure to 0, 2, 5 and 10 Gy radiation). Effects of radiation on SF of A549 cells alone was observed to be about 0.82 (2 Gy), 0.63 (5 Gy) and 0.61 (10 Gy). Cells treated with EPHNPs in conjunction with 10 Gy radiation also significantly reduced survival fraction (SF: 0.20) compared to that for HNPs + 10 Gy (SF: 0.38) and free NU7441 + 10 Gy (SF: 0.47). These results further emphasize the cancer killing advantages of the targeting trategies in combination with the radiation responsiveness of the NPs.

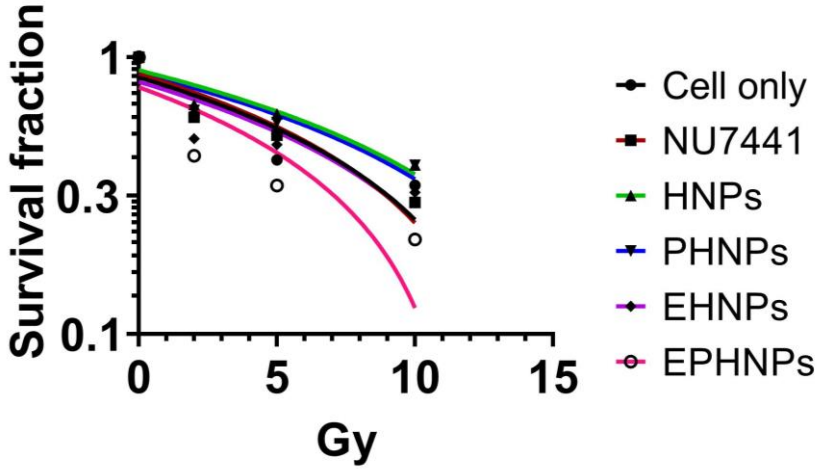

Figure 3.9. Investigation of *in vitro* therapeutic efficacy using colony formation assays. NU7441 loaded HA NPs and NU7441 loaded platelet-HA NPs in combination with radiation significantly reduced A549 lung cancer cell survival fraction via colony formation assays.

3.3.7 In vivo biodistribution of EPHNPs

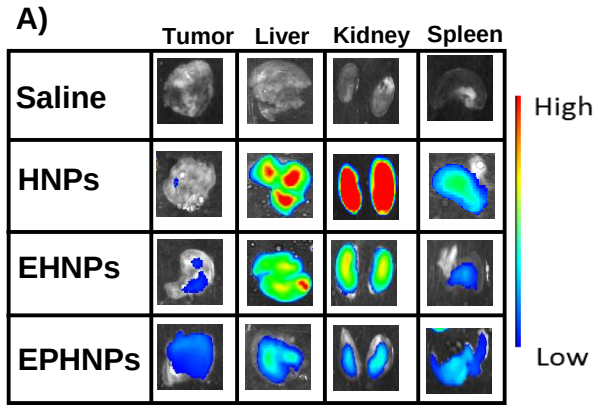

Figure 3.10. *In vivo* biodistribution study. **A)** *In vivo* fluorescence imaging observed localization of EPHNPs in a subcutaneous A549 lung tumor model, with negligible HNP localization in the tumors. **B)** *ex vivo* analysis of tumor homogenates observed about 2-fold higher EPHNP accumulation in the lung tumor site compared to untargeted HNPs and a fold higher than EHNPs (*P< 0.05 vs. EPHNPs_tumor).

In vivo biodistribution studies were performed to determine the targeting efficacy of the EPHNPs. Nude mice bearing subcutaneously implanted A549 lung tumors were injected with cyanine-7 loaded HNPs, EHNPs and EPHNPs to compare their targeting efficacy (with saline serving as the background control). 24 hours after NP administration the mice were imaged under anesthesia using an *in vivo* bioimager **(Figure 3.10A)**. Fluorescence imaging observed a significantly higher EPHNP enrichment in the tumor, compared to that of HNPs and EHNPs. Although, we observed NP accumulation in the visceral organs, namely liver, kidneys and spleen, the intensity was significantly higher in the untagged HNPs and EHNPs, than that for the EPHNPs. Furthermore, spectrophotometric analysis of homogenized tumor tissues observed over 4-times higher EPHNP localization (20% of injected NPs) in the tumors compared to untargeted HNPs (5% of injected NPs) and 2-times higher than EHNPs (10% of injected NPs) **(Figure 3.10B)**. Spectrophotometric analysis also correlated with the observations from the *ex vivo* imaging data, where EPHNPs showed lower localization in the visceral organs compared to that by the HNPs and EHNPs.

3.4. DISCUSSION

Novel radiation responsive polymers exhibiting induced drug release characteristics in response to radiation levels have been developed as carriers for radiosensitizers. This is the first report of NPs that release radiosensitizers in synergy with radiation therapy, while sensitizing the lung cancer cells for enhanced radiation therapy. Additionally, bio-functionalization of the NPs with platelets membranes and antibodies against the EphA2 receptors, ensure the migration of these NPs to the lung tumor microenvironment and facilitates enhanced NP enrichment in the tumor environment. The successful coating of platelet membranes on the NPs were confirmed via increase in the hydrodynamic diameters of the NPs via dynamic light scattering and via TEM imaging, that observed core-shell structure of HNPs in the core and platelet membrane shell on the HNPs similar to those observed for cell membrane coated NPs investigated by other groups [135]. Additionally, flow cytometry also observed retention of platelet markers on the surface of the platelet membrane coated PHNPs, indicating retention of platelet membrane markers sfter membrane extraction and NP extrusion. Importantly, these NPs also observed radiation-responsive drug release characteristics, with significantly higher amount of NU7441 being released as the radiation dose increased. Interestingly, the platelet membranes act as barriers to the drug release, with significantly lower NU7441 release upon radiation exposure as well as in the absence of radiation. This feature protects the drug from premature drug leakage in the absence of radiation and ensures maximal drug availability during radiation therapy. Platelet and erythrocyte hybrid membrane coated NPs by Hu et al. [136], also observed the impaired release of

chemotherapeutic drug doxorubicin from the membrane coated NPs compared to drug release from uncoated NPs, thus supporting our findings.

Due to its excellent characteristics such as biocompatibility, biodegradability, low-toxicity and non-immunogenicity, Hyaluronic acid (HA), a glycosaminoglycan, as one of the major components of extracellular matrix, has been widely utilized as a carrier for drug delivery [137]. Hyaluronic acid comprises of repeating disaccharide units of N-acetyl-D-glucosamine and D-glucuronic acid, linked via alternating β-(1→4) and β-(1→3) glyosidic bonds [138]. HA also targets CD44 receptors, that are overexpressed on cancer cells, thus imparting tumor targeting capabilities to the drug delivery system [139]. ROS produced in response to stress or radiation, degrade the glyosidic bonds of HA materials, by attracting a hydrogen radical from HA and resulting in the formation of a macroradical and a water molecule [140]. The ROS responsiveness of HA has been studied by Lee et al. [141]. The gold NP doped HA NPs labeled with fluorescein, exhibited about 86% and 61% fluorescence recovery within 2h of exposure to superoxide and hydroxyl radicals respectively. Our NP design makes use of the ROS produced during radiation therapy to degrade the HA NPs and release the encapsulated NU7441 during radiation therapy. This hypothesis was confirmed by the drug release kinetics study and the therapeutic studies where NU7441 loaded HNP and EPHNP mediated higher lung cancer cell death upon exposure to radiation compared to that without radiation exposure.

Circulating platelets have been extensively investigated for their role in cancer progression, due to their interactions with resident and circulating tumor cells. Cancer cells have the ability to cause aggregation of platelets due to a process called as tumor cell-induced platelet aggregation (TCIPA), that extends several advantages to tumor survival and metastasis [134]. Platelets have

also been observed to protect tumor cells from TNFα induced cytotoxicity and shield tumor cells from shear stress due to blood flow [142]. Platelets also bind to tumor cells via p-selectin binding to CD44 receptors on tumor cells, forming tumor cell aggregates that facilitate the extravasation of tumor cells into the vasculature [143, 144]. Thus, membranes derived from platelets may localize at the tumor site and adhere to tumor cells, and act as carriers to specifically deliver their cargo at the tumor site. A fusion of erythrocyte (RBC) and platelet membranes were investigated by Dehaini et al. [135], were coated on poly(lactic-co-glycolic acid) NPs to impart target specificity to the NPs and thereby improve NP localization at the cancer site. The RBC-platelet membrane coatings significantly augmented NP binding to the cancer cells compared to that of RBC membrane (only) coated NPs, but lower than that observed for NPs coated with just platelet membranes, emphasizing the benefits of platelet membrane coatings for cancer targeting applications. Our platelet-membrane functionalized NPs also observed higher uptake into lung cancer cells, in addition to improving the therapeutic efficacy of radiation compared with those of uncoated NPs combined with radiation and radiation alone. Inclusion of anti-EphA2 antibodies on NPs further enhanced lung cancer specificity (~ 4-times improved localization in the lung tumors compared to untagged HNPs). Thus, the EPHNPs reported here could potentially be employed for enhanced local radiation therapy at the tumor site, while sparing healthy tissues.

Hyaluronic acid has been widely investigated as a cancer cell targeting moiety, due to the high expression of CD44 in its backbone, that binds to CD44 receptors, often overexpressed on cancer cell lines like A549 lung cancer cells [145]. Tran et al. [146], decorated vorinostat loaded solid lipid NPs (SLNPs) decorated with HA to target A549 cells via CD44 receptors and subsequently enhance the therapeutic efficacy of the NPs. While they observed enhanced uptake

of the HA coated SLNPs into A549 lung cancer cells compared to the uncoated SLNPs, we observed differing results where the HNPs observed very poor uptake into A549 cells. This is potentially because while our uncoated HNPs were about 200nm in diameter, the size of the HA coated SLNPs was around 100 nm in diameter [147], thus exhibiting better uptake into the cells. However, upon functionalizing these NPs with platelet membranes and antibodies against EphA2, we were able to improve the uptake of the HA NPs. The combination of cell membrane and antibody functionalized NPs for cancer therapy has also been explored for enhanced tumor targeting and therapy. Platelet cell membranes coupled with TRAIL (to bind to death receptors DR4 and DR5 on cancer cells) functionalized onto doxorubicin (DOX) loaded nanogels were employed for localized treatment of breast cancer [144]. Similar to our observation of *in vitro* NP uptake and *in vivo* biodistribution, the platelet membrane and TRAIL coated NPs improved internalization of the NPs into MDA-MB-231 breast cancer cells, leading to localization in the tumor environment and significant reduction in cell viability compared to uncoated NPs. However, these NPs did not observe a difference in the drug release kinetics of DOX from the membrane coated NPs and that from uncoated NPs, potentially due to insufficient membrane coatings on the NPs and thus a marginal barrier to the drug release.

The recent years have witnessed a surge in research radiosensitizers for enhances the effects of radiation therapy. NU7441 is a DNA-PK inhibitor, which inhibits DNA repair after radiation therapy [87]. Thus, administration of NU7441 improves the efficacy of radiation therapy and enhances tumor cell apoptosis. Although NU7441 has been widely investigated as a radiosensitizer for treatment of various cancers, there is very little research on using nanoparticles encapsulating NU7441 for improving the effects of radiation therapy. Our group had earlier

investigated PLGA NPs encapsulating NU7441 and conjugated with R11 to specifically target and treat PC3 prostate cancer cells [126]. Colony formation results for the R11-tagged NU7441-PLGA NPs revealed a survival fraction of about 0.5 after radiation exposure, compared to about 0.7 for non-drug loaded R11-PLGA NPs. On the other hand, we observed a survival fraction of 0.15 for EPHNPs and 0.32 for HNPs, potentially due to the burst release of the drug from the radiation responsive NPs that enhanced drug availability in the cancer cellular environment.

Besides NU7441, other radiosensitizers such as β-lapachone loaded onto gold NPs have also been investigated for cancer therapy [148]. *In vitro* therapeutic efficacy studies of these NPs observed significant decrease in A549 cell viability, an observation like ours. However, *in vivo* therapeutic efficacy studies including exposure to radiation were not reported. Wen et al. [149] investigated curcumin loaded into poly(N-vinylpyrrolidone)-poly(caprolactone) (PVP-PCL) NPs as radiosensitizers to treat lung cancer. These NPs also observed significant reduction in A549 cell survival upon exposure to radiation and curcumin loaded PVP-PCL NPs, illustrating the advantages of incorporating radiosensitizers in nanoparticles. However, these NPs did not possess any targeting capabilities like our EPHNPs which may affect the localization of these NPs in the tumor tissues, thereby affecting the bioavailability of the drug loaded NPs and inducing off-target toxicities. Similarly, Ataxia-telangiectasia mutated protein (ATM) inhibitor KU55933 loaded PLGA NPs in combination with radiation exposure, also impaired the survival of A549 lung cancer cells, but did not significantly different from free KU55933 of equivalent doses [150]. EPHNPs, on the other hand, exhibited significant reduction in cancer cell survival compared to free NU7441, possibly due to the presence of targeting moieties on the NPs that improve the NP internalization by lung cancer cells. Thus, the combination of the radiation responsive nanoparticles with the

targeting moieties on the NPs and not just the drug plays a significant role in enhancing the targeting, internalization and therapeutic efficacy of the NPs.

The limitations of this study mainly involve the use of hyaluronic acid. Hyaluronic acid also susceptible to degradation by enzymes like hyaluronidase that are also present in the tumor microenvironment, which may cause some degree of drug leakage in the tumor microenvironment [151]. Hyaluronic acid also expresses CD44 that binds to CD44 receptors present not only on tumor cells, but also on certain healthy cells like hepatic endothelial cells [152]. This correlates with our biodistribution study, where we observed some degree of NP accumulation in the liver. Another limitation of our design lies in the coatings of platelet cell membranes that may induce activation of resident platelets in the tumor microenvironment or those in circulation [153]. An alternative to platelet membranes, include those derived from red blood cells [154], macrophages or monocytes [155], and cancer cell [156] membranes among others that have been investigated in the past by several research groups. Other limitations include the lack of *in vivo* therapeutic and toxicity analysis of the EPHNPs with radiation therapy.

3.5. SUMMARY

To summarize, radiation-responsive NPs specifically targeting the lung cancer cells via platelet membrane cloaking and EphA2 targeting were formulated and characterized. The particles exhibited a hydrodynamic diameter of about 250 nm. Furthermore, these NPs demonstrated a radiation (dose) dependent release of NU7441, an ability that controlled the drug release when

needed, that would prevent associated side-effects of the toxic drugs on healthy cells and tissues. They were cyto-compatible to AT1 healthy lung cells and observed hemo-compatibility to human blood. Importantly, the presence of platelet membranes and EphA2 antibodies on the NP surface, significantly enhanced the uptake of these NPs into lung cancer cells, as confirmed spectrophotometrically and via fluorescence imaging. Additionally, the NU7441-loaded EPHNPs in combination with radiation also significantly induced *in vitro* lung cancer cell death compared to those by radiation alone, free NU7441 and NU7441-loaded HNPs. Thus, the NU7441 loaded radiation-responsive NPs coated with platelet membranes and EphA2 antibodies can potentially be utilized as an enhanced and localized radiation therapy strategy for lung cancer treatment. The future studies for this research include investigation about the therapeutic efficacy of concurrent chemo-radiation therapy using *in vivo* in lung tumor animal models and toxicity of the NPs to healthy organs and tissues.

CHAPTER 4: MULTIFUNCTIONAL DUAL STIMULI-RESPONSIVE CORE-SHELL NPs FOR COMBINED CHEMO-RADIOTHERAPY TO TREAT LUNG CANCER

4.1. INTRODUCTION

Individual chemotherapy and radiation therapy are the conventional treatments for lung cancer. However, these strategies face several limitations that affect their therapeutic efficacy, including rapid relapse, poor drug bioavailability and off-target side-effects, which severely affect the drug dosage used to achieve the maximal therapeutic efficacy [87]. Cancer cells are also inherently resistant to chemotherapeutic drugs, resulting in minimal therapeutic efficacy and eventually leading to expansion and proliferation of cancer cells [157]. For instance, cisplatin is an FDA approved chemotherapeutic drug for the treatment of NSCLC. Cisplatin crosslinks with purine bases in DNA, to cause DNA damage and subsequent initiation of apoptosis in cells [99]. However, cisplatin is extremely toxic to normal tissues, leading to side-effects like nephrotoxicity, neurotoxicity and ototoxicity, in addition to being severely limited in its therapeutic actions due to cisplatin resistance in cancer cells [97, 158]. Additionally, the DNA self-repair mechanisms of cancer cell DNA severely limit the benefits of radiation therapy, often resulting in poor overall survival in lung cancer patients [87].

Concurrent chemo-radiotherapy (CRT) can overcome these limitations, by enhancing the effectiveness of radiation therapy. CRT is concurrent administration of a chemotherapeutic agent and radiation therapy to control tumor growth and subsequently improve patient responses to cancer therapy [159]. The most commonly investigated and successful drug for combined

treatment with radiation is cisplatin, due to its effectiveness in patients with widespread NSCLCs [160]. CRT combining cisplatin and radiation, has been investigated clinically in several studies to study its effectiveness to treat NSCLC, where concurrent cisplatin and radiation treatment significantly improved the five-year survival rate of patients undergoing treatment compared to sequential chemo-radiotherapy (where the patient is administered with the chemotherapeutic drug, followed by radiation therapy after a few chemotherapy drug dosing regimens) and radiation therapy alone [49, 161].

However, a major disadvantage of CRT is the increased risks of side-effects such as anemia, acute esophagitis and neutropenia, thus limiting the drug dosages that can be implemented without causing toxicity to the patients, while maintaining the drug within the therapeutic window [49]. The systemic administration of cisplatin is also limited by severe toxicity, especially when combined with radiation. Similarly, other major chemotherapeutic drugs like carboplatin, paclitaxel and docetaxel are also administered in significantly lower doses when combined with radiation [160]. Additionally, the addition of chemotherapy regimen to a radiation therapy regimen may not be sufficient to achieve the desired therapeutic efficacy. Thus, there is an increasing need to develop strategies that can achieve adequate therapeutic efficacy, while reducing the toxicity associated with the treatment.

Recent developments in multi-compartment nanoparticles (NPs) for cancer therapy and their unique characteristics such as controlled drug releases of various drugs for combined therapies and targeting capabilities have made them suitable carriers for CRT. Multi-compartment NPs or core-shell NPs are composed of two or more materials that are combined to form a core and shell of the NP. Varieties of core-shell materials have been investigated for drug delivery

applications, such as metal based NPs coated with either polymeric shell or a silica shell, multi-shell NPs, hollow shell NPs and organic core-shell NPs among others [162]. For example, multifunctional core-shell NPs for lung cancer chemo-radiotherapy were developed for treatment of lung cancer [87]. These NPs comprised of a folic acid-functionalized poly (N-isopropyl acrylamide)/carboxymethyl chitosan shell encapsulating gemcitabine hydrochloride (gem), coated onto a PLGA core loaded with NU7441. These NPs exhibited dual temperature and pH responsive gem release kinetics from the shell and sustained NU7441 release kinetics from the core. Additionally, these NPs observed enhanced therapeutic efficacy when combined with radiation therapy, compared to that by radiation alone.

In this project, we will aim to develop dual-drug loaded, dual-stimuli responsive core-shell nanoparticles (DSNPs) that can deliver chemotherapeutic agents and radiosensitizers concurrently for concurrent chemo-radiotherapy to treat lung cancers. In this research, we investigated the combination of NU7441+cisplatin, a CRT drug regimen that has investigated before [87]. We utilized a GSH-sensitive polymer (PU 1.8SS) synthesized by our lab to form the core NP, which encapsulate and deliver the chemotherapeutic drug, cisplatin [68]. Due to the presence of reducible disulfide linkages in the backbone of the polymer, the elevated levels of GSH in cancer cells trigger the release of cisplatin from the NPs [68]. These NPs were coated with a radiation-responsive shell made of hyaluronic acid. Hyaluronic acid is a natural polymer, composed of glyosidic bonds in its backbone that degrade in the presence of reactive oxygen species (ROS) and free radicals generated during radiation therapy [79]. The shell encapsulated NU7441, a radiosensitizer, which would be released from the shell in response to radiation exposure, to synergistically enhance the therapeutic effects of radiation therapy **(Figure 1.3)**. To improve the targeting capabilities of the

NPs, we functionalized these NPs with antibodies against EphA2 receptors that are highly expressed on the surface of lung cancer cells lines, while being poorly expressed on healthy lung cells [89, 91, 118]. To keep the design of the NPs simple, platelet membranes were not utilized in the core-shell NP design. We solely utilized antibodies against EphA2 receptors for targeting lung cancer cells.

4.2. EXPERIMENTAL SECTION

4.2.1 Synthesis of DSNPs

Core-shell NPs comprised of a GNP core and HNP shell were synthesized via electrostatic layer-by-layer coating technique, where the negatively charged GNPs are coated with an intermediate positively charged layer, followed by coating with negatively charged HA, thus forming a sandwich of alternating negative and positive charged layers. Cisplatin (Cayman Chemicals) loaded GNPs were synthesized as described earlier in section 2.2.1. 10 mg of these NPs were dispersed in 10 mL of 10mM sodium chloride (NaCl) solution and vortexed to thoroughly suspend the NPs. 250 µL of polyallylamine hydrochloride (PAH, 1000µg/mL in 10mM NaCl; MilliporeSigma) was added to this solution to coat a positive charge on the GNPs and allowed to react for 30 minutes at room temperature while stirring, following which the NP suspension was centrifuged at 15,000 RPM for 30 minutes to collect the PAH coated GNPs. The pelleted NPs were suspended in 10 mL of dI water, and 1 mL of hyaluronic acid (10 mg/mL in dI water; Lifecore Biomedical) containing 2mg of NU7441 (Tocris) was added to the NP suspension

to initiate the coating of drug loaded HA onto the GNPs. The solution was allowed to stir overnight at room temperature, followed by centrifugation at 15,000 RPM for 30 minutes and lyophilized for 2 days to collect the DSNPs.

Antibody (Ab) conjugation onto the DSNPs was performed via carbodiimide crosslinker chemistry. Briefly, 5mg of lyophilized NPs were suspended in 4mL of 2% 2-ethanesulfonic acid (MES; MilliporeSigma) buffer (~pH 5.0), and 20 mg of 1-Ethyl-3-(3-dimethylaminopropyl) carbodiimide (EDC; MilliporeSigma) was added to this suspension and allowed to react at room temperature for 30 minutes. Twenty mg of N-hydroxysuccinimide (NHS; MilliporeSigma) was then added to this suspension and allowed to react at room temperature for another 30 minutes (this reaction activates ester groups on the surface of the NPs for conjugating of ligands/antibodies onto NPs). Eleven µg of Ab solution was then added to the above NP suspension, and the conjugation reaction performed overnight 4°C, followed by dialysis to remove unconjugated Abs, and lyophilization to obtain the Ab/targeting ligand-conjugated NPs. Antibody conjugation efficiency was determined by Bradford protein assays and calculated by the following equation;

$$Ab\ coating\ efficiency = \frac{Amount\ of\ Ab\ used - amount\ of\ Ab\ in\ supernatant}{Amount\ of\ Ab\ used} X\ 100\%$$

…. (4.1)

4.2.3 Characterization of nanoparticles

Particle size was measured using the Dynamic Light Scattering (DLS) technique via the ZetaPALS zeta potential analyzer (Brookhaven Instruments Inc.). NU7441 loading efficacy into the shell and cisplatin loading efficiency into the core of the DSNPs were determined by indirect

method. Briefly, the amounts of NU7441 and cisplatin in the supernatants were determined by a UV-Vis spectrophotometer (Tecan) at an absorbance of 288 nm and 346 nm, respectively.

The amount of drug loaded into the NPs was determined by the following**:**

$$Drug\ loading\ efficacy = \frac{Drug\ amount\ used - Drug\ \ in\ supernatant}{Drug\ \ amount\ used} X\ 100\%$$

…. (4.2)

To study the drug release kinetics, DSNPs were exposed to either of the 4 conditions, no treatment (1X-PBS), GSH (5 mM), radiation (5 Gy) and a combination of GSH (5 mM) and radiation (5 Gy). The purpose of this study was to observe the synergistic cisplatin release (from the GSH sensitive core) and NU7441 release (from the radiation responsive shell). To initiate the drug release, 1 mg/mL of DSNPs were resuspended in either 1X-PBS (0 mM GSH) or 1X-PBS containing 5 mM of GSH (6 replicates each). 3 replicates from each GSH concentrations were then exposed to radiation (0 Gy or 5 Gy). The NPs were then incubated at 37˚C between predetermined timepoints. At each time-point, the NP suspensions were centrifuged at 15,000 RPM for 25 minutes. The supernatants containing the released drugs were collected and stored at -20˚C, following which the NPs were resuspended in 1X-PBS (± 5mM GSH) and incubated until the next time point. The amounts of NU7441 released were calculated using a standard curve of NU7441 (absorbance 234 nm), followed by normalizing the drug released against the amount of NU7441 loaded into the NPs. Similarly, cisplatin was calculated using a standard curve of cisplatin (absorbance 310 nm), followed by normalizing the drug released against the amount cisplatin loaded into the NPs. A sample size of n=3 per group was used for this study.

4.2.3 Investigating the therapeutic efficacies of dual drug combinations

The therapeutic efficacy of dual drug combinations compared to single drug administrations, were determined by studying the A549 cancer cell killing ability of the drugs via MTS assays (72 hours of drug exposure) and colony formation assays (10 days of drug exposure). To study the drug therapeutic efficacy via MTS assays, A549 lung cancer cells were seeded at a seeding density of 20,000 cells/well in a 48 micro-well plate and allowed to attach overnight. The following day, cells were treated with free NU7441, free cisplatin (0.5 µg/mL and 1 µg/mL drug concentration) or a combination of the drugs (NU7441+cisplatin). Untreated cells and cells treated with 1% Triton X-100 were regarded as the negative and positive controls, respectively. For this study, we used a sample size of n=4 per treatment group. 72 hours later, cell viability was determined by MTS assays (Promega Corporation) following the manufacturer's protocol.

To observe the survival of cancer cells upon exposure to the drugs, we performed colony formation assays (CFA). To perform these studies, A549 lung cancer cells were seeded on 60 mm petridishes, and *in vitro* CFA studies were performed as described previously [108]. The cells were treated with free NU7441 and cisplatin or the drug combinations (100 ng/dish) and incubated at 37˚C for a period of 10 days. Once the cancer cell colonies had reached a colony of at least 50 cells, the cells were washed with phosphate buffered saline, and stained with crystal violet (MilliporeSigma) dye (0.5% w/v in 6% v/v glutaraldehyde). The number of colonies in each dish were then counted. A sample size of n=3 per treatment group was used for this study.

4.2.4 Cellular uptake of nanoparticles

Cellular uptake of DSNPs and E-DSNPs was determined by measuring the amount of fluorescently-labeled NPs that get internalized by lung cancer cells. DSNPs and E-DSNPs loaded with a fluorescent dye, Coumarin-6 (MilliporeSigma), were synthesized as described earlier. Coumarin-6 was used here to facilitate fluorescent mediated detection of NPs in the cells. To study *in vitro* cellular uptake of these NPs, A549 human lung cancer cells were seeded at a seeding density of 10,000 cells/well in a 96 micro-well plate and allowed to attach overnight. Next day, the cells were incubated with DSNPs or E-DSNPs at different concentrations (0, 25, 50, 100, 250 and 500 µg/ml; n=4 per concentration per group) at 37°C for 2 hours. Post 2 hours, cells were imaged using a fluorescence microscope. The cells were also washed 3X with sterile 1X-PBS and lysed using 1% Triton X-100. The amount of NPs internalized were determined by measuring the fluorescence intensity of coumarin-6 (translated to µg of NPs) at a wavelength of λex 458 nm and λem 540 nm and normalized against the amount of total protein from cells per well, which was determined using bicinchonic acid assays (BCA) following the company's instructions (Pierce™ BCA Protein Assay Kit, ThermoFisher Scientific). Furthermore, fluorescence imaging was used to image E-DSNP and DSNP uptake into A549 lung cancer cells. Briefly, A549 cells were seeded at a cell seeding density of 150,000 cells on glass coverslips and allowed for attaching overnight. The following day, the cells were exposed to 1mg/mL of DSNPs or E-DSNPs encapsulating coumarin-6 for 2 hours. The cells were washed three times with 1X-PBS, and fixed for 15 minutes in 4% paraformaldehyde. The fixed cells were washed with 1X-PBS to remove excess paraformaldehyde and their nucleus stained with nucBlue® (ThermoFisher Scientific) dye. The cells were then observed under a fluorescence microscope (Cytoviva Inc).

4.2.5 In vitro therapeutic efficacy

A proof-of-concept study to determine the benefits of using dual drugs vs. single drugs was first performed using MTS assays. The *in vitro* therapeutic efficacy of double drug-loaded E-DSNPs compared to single drug-loaded DSNPs in the absence of radiation were determined. The purpose of this study was to first determine the enhanced therapeutic efficacy of dual drug loaded NPs, against single drug loaded NPs. The drug combination was chosen from the results obtained from section 4.2.3. Briefly, A549 and H460 lung cancer cells were seeded at a seeding density of 20,000 cells/well in a 48 micro-well plate and allowed to attach overnight. The following day, cells were treated with either the free single drugs (0.5 or 1 µg/mL drug concentration), or combined free drugs, or drug-loaded NPs, i.e. E-DSNPs with NU7441, E-DSNPs with cisplatin and E-DSNPs with NU7441+cisplatin. Untreated cells and cells treated with 1% Triton X-100 were regarded as the negative and positive controls respectively. 72 hours later, cell death was determined by MTS cell viability assays. In addition, the toxicity of DSNPs vs. E-DSNPs (without radiation) to healthy lung cells (AT1) was also studied by assessing the cell viability of the AT1 cells via MTS cell viability assays. For this study, the cells were treated with 500 µg/mL of drug loaded NPs for 2 hours, after which the media was aspirated, cells were washed 2X with media to remove left-over NPs and the cells replenished with fresh media (this was done to prevent any excess non-specific uptake of the NPs).

The *in vitro* therapeutic efficacies of dual-drug loaded E-DSNPs compared to single drug loaded E-DSNPs in the presence of radiation were determined by studying the viability of A549 lung cancer cells after treatment by MTS assays. The study was performed as described above, this time with exposure to 5 Gy radiation in addition to the DSNPs. 72 hours after exposure, cell

viability was determined by MTS assays. To observe the survival of cancer cells upon exposure to the drugs, we performed colony formation assays (CFA). To perform these studies, A549 lung cancer cells were seeded on 60 mm petridishes, and *in vitro* CFA studies were performed as described previously [108]. The cells were treated with free NU7441+ cisplatin (100 ng/mL of each drug/dish), DSNPs (loaded with NU7441+cisplatin) and E-DSNPs (loaded with NU7441+cisplatin) and the vehicle, following which they were irradiated (3 sets, each treated at either 2, 5 or 10 Gy) and incubated at 37˚C for a period of 10 days. Another set of replicates were also generated, without exposure to radiation (0 Gy). This set served as a control for the study. Once the cancer cell colonies had reached a colony of at least 50 cells, the cells were washed with tap water, and stained with crystal violet (MilliporeSigma) dye (0.5% w/v in 6% v/v glutaraldehyde). The number of colonies in each dish were then counted, and survival fraction of the cells was calculated and plotted. To calculate the survival fraction of A549 cells, the number of surviving colonies at a radiation dose (S_D) was normalized (S_D/S_0) to the number of surviving colonies at 0 Gy radiation (S_0).

4.2.5. Cytotoxicity analysis of nanoparticles

Healthy lung alveolar Type 1 epithelial cells (AT1) cells were seeded at a density of 8000 cells/well in a 96 microwell plate and incubated overnight to facilitate cell attachment. Next day, the cells were incubated with varying concentrations (n=4 per concentration) of non-drug loaded DSNPs (0, 50, 100, 200, 500, and 1000 µg/ml). Following 24 hours incubation, the cell viability

was determined using MTS cell viability assays (CellTiter 96®AQueous One Solution Cell Proliferation Assay, Promega Corporation).

4.2.6 Hemo-compatibility analysis of nanoparticles

A hemolysis evaluation of the non-drug loaded DSNPs was conducted as described previously [109]. Human blood from a donor was acquired following methods approved by the Institutional Review Board at the University of Texas at Arlington. After collection, human blood was incubated with DSNPs at a NP concentration of either 100 µg/ml or 1000 µg/ml, 0.9% saline (as negative control), or distilled water (as positive control) for 2 hours at 37˚C. The samples were then centrifuged at 1000 g, following which absorbance readings were taken at 545 nm using a UV-Vis spectrophotometer. The percentage of hemolysis was calculated using the following equation:

$$Hemolysis = \frac{Abs\ of\ sample - Abs\ of\ negative\ control}{Abs\ of\ positive\ control - Abs\ of\ negative\ control} \times 100\%$$

…. (4.3)

To study the blood clotting kinetics, non-drug loaded DSNPs at concentrations of 100 or 1000 µg/ml), water (negative control) and 0.9% saline (positive control) were added to blood activated with 0.1M calcium chloride ($CaCl_2$) and incubated at room temperature. At pre-determined time points (10, 20, 30, and 60 minutes), water was added to the tubes to lyse the red blood cells (RBCs) that were not a part of the formed clot. Absorbance readings of supernatant were taken at 540 nm using a UV-Vis spectrophotometer. The blood clotting kinetics were also

observed visually, and photographs acquired. A sample size of n=8 per group was used for the hemolysis and blood clotting studies.

4.2.7 Statistical analysis

Results were analyzed statistically using 2-way ANOVA and Fisher's post-hoc analysis (Statview 5.0 software) with $p<0.05$ considered as a significant value. All results were displayed as mean ± SD, and quadruplet samples (n=4) were used for each experiment if not specified.

4.3. RESULTS

4.3.1 Nanoparticle characterization

The GSH NP core, non-drug loaded DSNPs and dual-drug loaded DSNPs observed a diameter of 187± 28 nm, 223 ± 31 nm and 297 ± 27 nm respectively, by dynamic light scattering technique **(Figure 4.1 A)**. Conjugation of antibodies against EphA2 further increased the NP size to 323 ± 21 nm. Scanning electron microscopy (SEM) imaging of the DSNPs observed a spherical morphology of the NPs**(Figure 4.1 B)**.

4.3.2 Physico-chemical characteristics of DSNPs

A)	Size (nm)
GNPs	187± 28
DSNPs without drug	223 ± 31
DSNPs with dual drug-loading	297 ± 27
E-DSNPs with dual drug-loading	323 ± 21

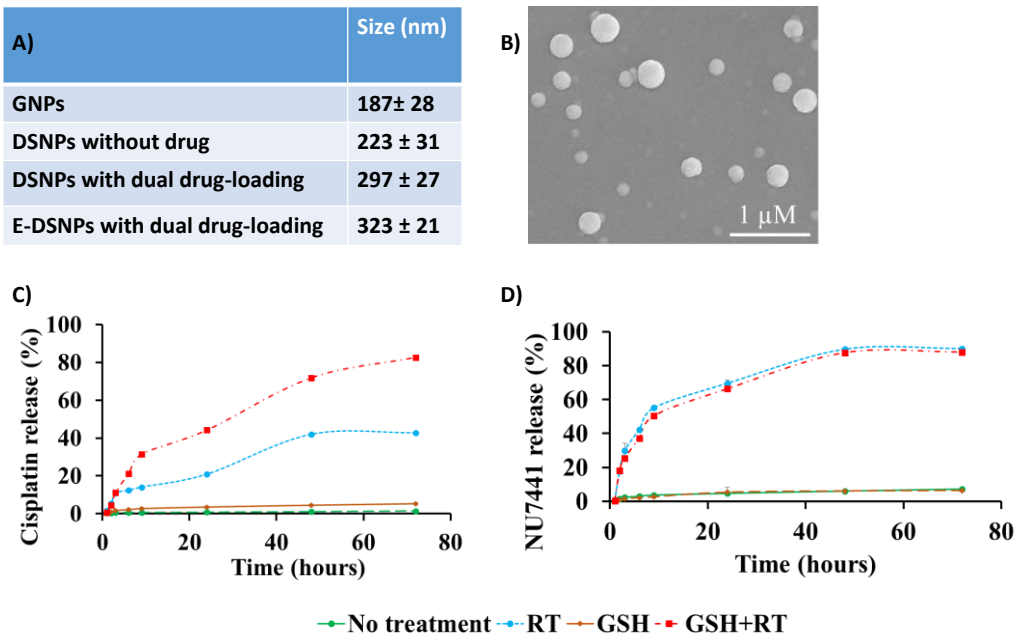

Figure 4.1. *In vitro* characterization of E-DSNPs. **A)** Dual drug-loaded E-DSNPs exhibited hydrodynamic diameter up to ~ 300nm. **B)** SEM imaging observed a spherical morphology of the NPs. **C)** Exposure of E-DSNPs to combined radiation and GSH permitted elevated cisplatin release from the core of the NPs, compared to that by radiation alone. **D)** E-DSNPs exhibited higher NU7441 release from the shell, when exposed to combined GSH and radiation, and that by radiation alone. Exposure to GSH alone did not have any effect on the drug release characteristics of cisplatin or NU7441.

NU7441 and cisplatin loading efficacies into the DSNPs were measured indirectly via a UV-vis spectrophotometer at an absorbance of 288nm and 346nm and was calculated to be about 71% and 56% respectively. Drug release of NU7441 and cisplatin from the DSNPs under GSH (5 mM) and radiation (5 Gy) exhibited radiation responsive and glutathione responsive drug characteristics **(Figure 4.1 C and D)**. DSNPs exposed to 1X-PBS alone, produced negligible NU7441 and cisplatin release. Similarly, DSNPs exposed to GSH alone, also observed poor cisplatin and NU7441 release. The poor cisplatin release could potentially be due to the HA layer acting as a shield to prevent drug leakage from the GSH sensitive core. Radiation alone, on the other hand triggered the degradation of the HA shell, characterized by the significant increase in

NU7441 (~ 90%) and cisplatin (~ 40%) within 72 hours. Furthermore, NPs treated with GSH and radiation experienced nearly 100% cisplatin and NU7441 release within 72 hours, as a result of radiation degrading the radiation responsive shell, thus exposing the GSH sensitive core to GSH in the solution.

4.3.3 In vitro tumor killing efficacy of drug combinations

The *in vitro* therapeutic efficacies of drug combinations were investigated using MTS cell viability assays and colony formation assays. MTS assay was used to study the effect of combined NU7441 and cisplatin, over a 72 hour period **(Figure 4.2A)**. The combination of free NU7441 and cisplatin reduced the viability to A549 cells to 40%, compared to NU7441 and cisplatin alone (cell viability reduced to 60% and 55% respectively). We also examined the efficacy of a combined

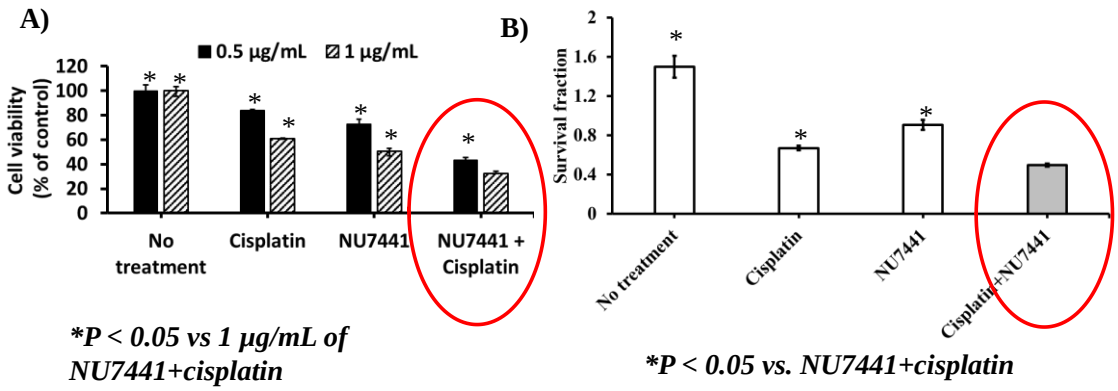

Figure 4.2: *In vitro* investigation of dual-drug treatment. **A)** A549 cell viability after 72 hours treatment with drug combinations (circled), observed significant decline compared to free drugs. **B)** Treatment of A549 lung cancer cells with individual free drug vs. combined free drugs (circled) revealed lower cancer colony survival as a result of the combined treatment than that with individual

drug regimen vs. individual drug therapy, by evaluating their ability to reduce survival of A549 lung cancer cell colonies via colony formation assays as described previously **(Figure 4.2B)**. The

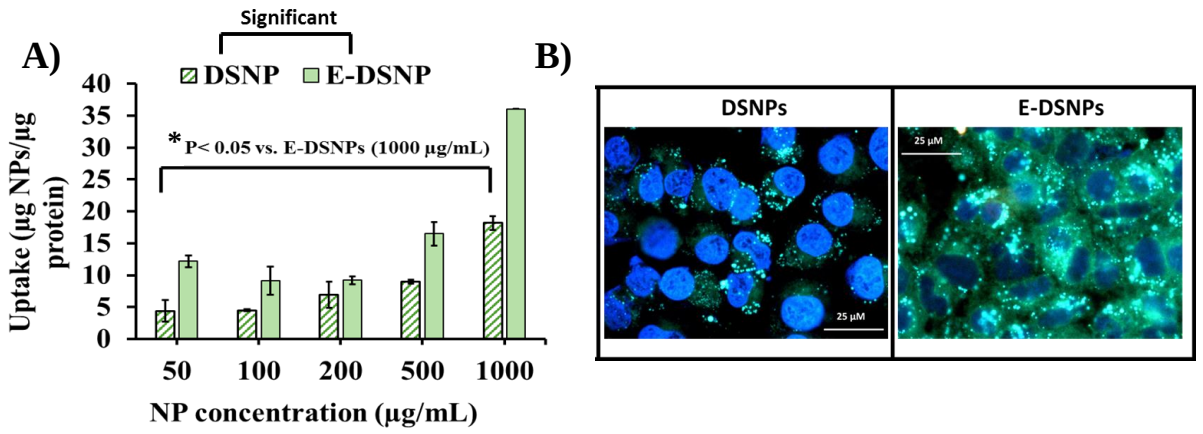

Figure 4.3. *In vitro* uptake of DSNPs. **A)** Spectrophotometric analysis of E-DSNP uptake into A549 cells showed dose dependent uptake, in addition to nearly a fold-increase in NP uptake compared to untargeted DSNPs. **B)** Fluorescence imaging also observed significant enhancement in NP internalization of the anti-EphA2 tagged DSNPs into A549 cancer cells compared to that of the untargeted DSNPs. Nucleus of the cells were stained blue with nucBlue® dye.

results observed a significant decrease in the survival fraction (SF) post treatment with combinations of radiosensitizers and chemotherapeutic drugs compared to the single drugs alone. The combination of NU7441+cisplatin were significantly more toxic (SF: 0.49) than NU7441 alone (SF: 0.90) or cisplatin alone (SF: 0.67).

4.3.4. Investigation of E-DSNP uptake into lung cancer cells

Spectrophotometric analysis of NP uptake into A549 cells found that DSNPs and E-DSNPs consisted of NP dose-dependent uptake into A549 lung cancer cells **(Figure 4.3A)**. Importantly, E-DSNPs significantly improved NP uptake, with nearly a 50% increase in NP uptake at the highest NP concentration. Similar findings were observed using fluorescence microscope, where EphA2 targeted NPs exhibited a distinct difference in NP localization (in terms of higher green intensity as a result of FITC in the NPs) in the A549 cells **(Figure 4.3B)**.

4.3.4 In vitro tumor killing efficacy of NPs

In vitro therapeutic efficacy of E-DSNPs in the absence of radiation were investigated in A549 and H460 lung cancer cells, to observe the benefits of dual drug therapy compared to that of single drug **(Figure 4.4)**. The E-DSNPs loaded with NU7441 and cisplatin significantly reduced the viability of H460 cells (20% cell viability), out-performing the therapeutic efficacy of either E-DSNPs encapsulating either NU7441 (32% cell viability) or E-DSNPS encapsulating cisplatin (cell viability 34%). The dual drug-loaded E-DSNPs also observed significant improvement in H460 cell death compared to free combined drugs (NU7441+cisplatin) (cell viability: ~ 20% and 35% respectively). A similar trend in therapeutic efficacy was observed for A549 lung cancer cells treated with dual-drug loaded E-DSNPs compared to either E-DSNPs encapsulating NU7441 only or E-DSNP loaded with cisplatin only (cell viability: ~ 30%, 50% and 40% respectively). The dual drug-loaded E-DSNPs also

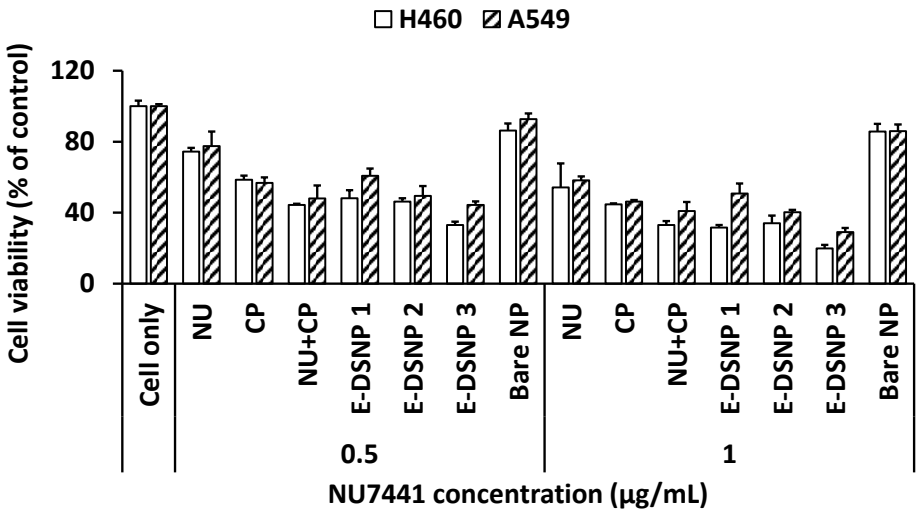

Figure 4.4. *In vitro* tumor killing efficacies of E-DSNPs. Dual drug loaded DSNPs observed significantly lower cell viability compared to DSNPs encapsulating NU7441 only or cisplatin only (DSNP1: DSNP with NU7441 only; DSNP 2: DSNP with cisplatin only and DSNP 3: DSNP with NU7441+ cisplatin). NU: NU7441 and CP: cisplatin.

observed significant improvement in A549 cell death compared to free combined drugs (NU7441+cisplatin) (cell viability: ~ 29% and 41% respectively).

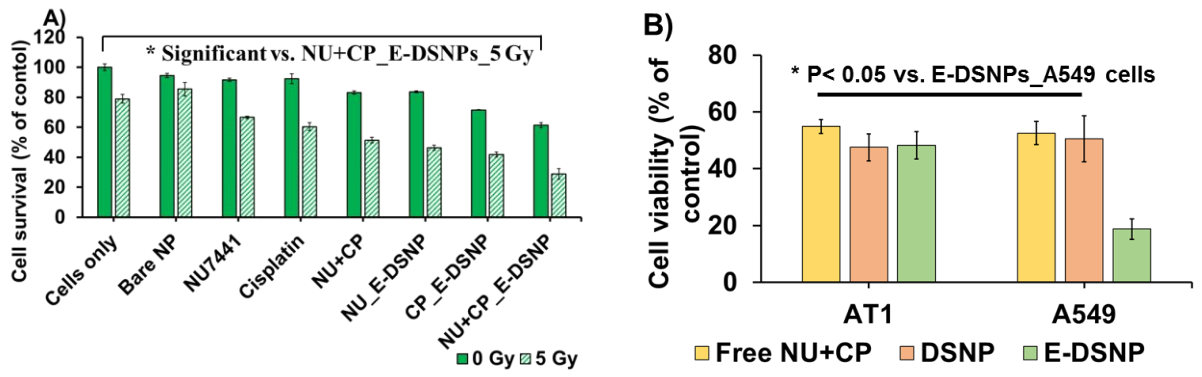

Figure 4.5. Investigation of *in vitro* cancer cell killing ability of dual-drug loaded E-DSNPs. **A)** *In vitro* therapeutic efficacy of dual drug loaded E-DSNPs with 5 Gy radiation treatment observed significantly lower cell viability of A549 lung cancer cells compared to cells treated with E-DSNPs without radiation treatment and single drug loaded NPs or free drug controls (± RT). **B)** E-DSNPs exert higher toxicity to A549 cells due to targeting via EphA2 receptors, but produce similar cancer cell death as untagged controls in AT1 cells due to poor targeting efficiency. NU: NU7441 and CP: cisplatin.

In vitro therapeutic efficacy of dual-drug loaded E-DSNPs in combination with radiation exposure, were investigated in A549 lung cancer cells, to observe the benefits of dual drug therapy compared to that of single drug **(Figure 4.5A)**. The dual drug loaded E-DSNPs significantly reduced the viability of A549 cells (~61% cell viability), out-performing the therapeutic efficacy of E-DSNPs encapsulating NU7441 alone (~84% cell viability) or E-DSNP loaded with cisplatin alone (~71% cell viability). The therapeutic efficacy of dual drug-loaded E-DSNPs was further improved by combining the NPs with radiation (5 Gy), where the cell viability significantly reduced (~29%) compared to radiation alone (~80% viability), free dual drugs (~51% viability) and E-DSNPs encapsulating either NU7441 only (~46% viability) or cisplatin only (~41% viability). Importantly, the efficacy of combining cisplatin and NU7441 with concurrent radiation treatment was clearly observed.

The therapeutic efficacy and associated toxicities of NU7441 and cisplatin loaded E-DSNPs vs. DSNPs to A549 lung cancer cells and AT1 lung epithelial cells were also determined by MTS cell viability assays **(Figure 4.5B)**. A549 cells treated with dual drug-loaded E-DSNPs and dual drug-loaded DSNPs observed reduced cell survival, although E-DSNPs significantly enhanced A549 cell death (~18% cell viability) compared to DSNPs (~50%) and free NU7441+cisplatin (~53%). However, in case of AT1 cells, free NU7441+cisplatin, DSNPs and E-DSNPs each reduced the cell viability to about 50%, potentially due to poor binding of the E-DSNPs to AT1 cells, thus producing similar cell death as the untagged DSNPs.

The tumor cell killing capability of E-DSNPs were also tested by colony formation assays. Photomicrographs **(Figure 4.6A)** represent cancer cell colonies from various treatment groups exposed to increasing doses of radiation exposure. The surviving fraction of A549 cells treated

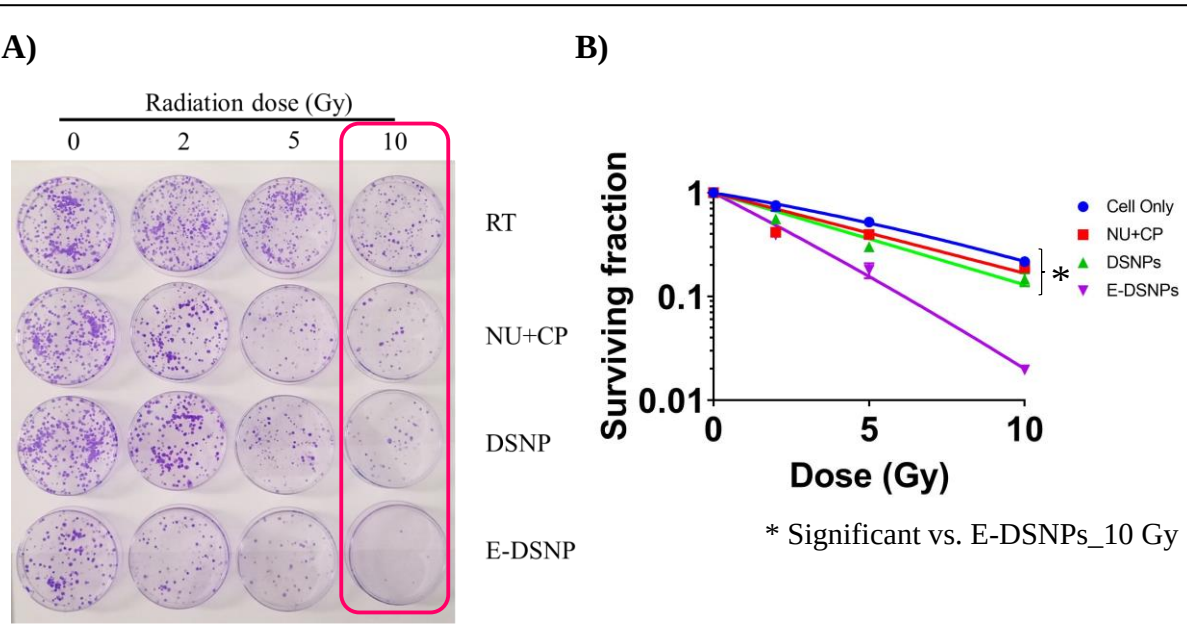

Figure 4.6. Colony formation assays to study the therapeutic effects of E-DSNPs. **A)** Photomicrographs of A549 lung cancer cell colonies. **B)** graphs depicting survival fractions of cancer cells treated with concurrent 10Gy radiation and dual drug loaded E-DSNPs treatment to nearly complete loss of tumor cell survival compared to that by radiation, free drugs and dual drug loaded untargeted NPs. NU: NU7441 and CP: cisplatin.

with dual-drug loaded E-DSNPs concurrently with radiation observed a radiation-dose dependent response, where the survival fraction of the cells were reduced to 0.39, 0.17, 0.01 (nearly 100% loss of cancer cell survival) when exposed to 2 Gy, 5 Gy and 10 Gy respectively. Cell treated with free drugs noted a survival fraction of 0.41, 0.39, 0.18 upon exposure to 2 Gy, 5 Gy and 10 Gy respectively. Untargeted DSNPs consisted of survival fraction of 0.55, 0.30, 0.14 upon exposure to 2 Gy, 5 Gy and 10 Gy respectively. Thus, concurrent CRT with our E-DSNPs as drug carriers could significantly improve lung tumor cell killing.

4.3.5 In vitro characterization of E-DSNPs

The cytotoxicity of DSNPs at increasing concentrations were determined by MTS cell viability assays. The DSNPs observed over 85% cyto-compatibility at the highest NP concentration of 1000 µg/mL to AT1, confirming the cyto-compatibility of the NPs to healthy lung cells **(Figure 4.7A)**.

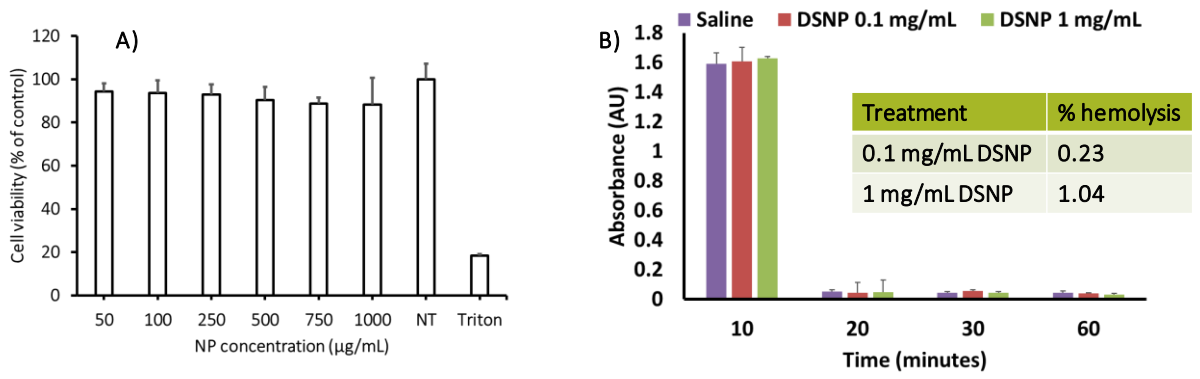

Figure 4.7. *In vitro* characterization of DSNPs. **A)** In vitro cyto-compatibility Of the NPs observed over 90% alveolar type-I cell viability via MTS assays. **B)** DSNPs observed a blood clotting trend similar to that of saline control.

Hemo-compatibility of the E-DSNPs was analyzed by investigating the hemolysis of blood and clotting profile of whole blood exposed to the NPs. E-DSNPs exhibited less than 5% hemolysis, which is below the acceptable range (by FDA). An increase in hemolysis was observed with increase in NP concentration. E-DSNPs exhibited a hemolysis of about 0.2 % and 1 % at a NP concentration of 0.1 mg/mL and 1 mg/mL respectively. Additionally, the blood clotting trend was like that of the control group (0.9% saline). These results confirm the hemo-compatibility of the E-DSNPs **(Figure 4.7B)**.

4.4. DISCUSSION

We have reported an innovative dual-stimuli responsive core-shell NPs that comprise of a glutathione responsive core encapsulating a chemotherapeutic drug and a radiation sensitive shell loading with a radiosensitizer, for multiple drug delivery for CRT. These NPs had several exciting features, namely their stimuli-responsiveness that permited enhanced release of radiosensitizer during concurrent radiation therapy, followed by cisplatin release in the intracellular environment. Furthermore, the incorporation of EphA2 provided targeting of the NPs to the lung cancer cells, while sparing the healthy cells thus reducing the chances of off-target drug toxicity. These NPs were loaded with radiosensitizer NU7441 and chemotherapeutic drug cisplatin for enhanced chemo-radiotherapy of lung cancer, and functionalized with EphA2 antibodies to impart lung cancer cell targeting functionalities to the NPs. Our results demonstrate the retention of stimuli responsive nature of the polymers in the DSNPs, where the GSH responsive core observed significant increase in drug release in GSH solutions, while the radiation responsive shell observed

significant increase in release of NU7441 with the increase in exposed radiation dose. Additionally, we observed an increased cisplatin and NU7441 release from the core and shell respectively when exposed to radiation and glutathione. Importantly, dual drug-loaded E-DSNPs and DSNPs combined with radiation significantly improved lung cancer cell death compared to NPs encapsulating single drugs or free single or dual-drugs (with or without radiation) thus emphasizing the benefits of: 1) synergistic radiation therapy concurrent with dual drug therapy and 2) utilizing NPs responsive to dual stimuli for delivering multiple drugs.

Ephrin transmembrane receptors A2 is a member of the Eph family, which is the largest family of tyrosine kinase receptors [163]. EphA2 highly expressed on lung cancer cells, plays a major role in cancer recurrence and metastasis and often results in poor prognosis and survival of NSCLC patients [91]. Due to the over-expression of EphA2 receptors on cancer cells, we functionalized the DSNPs with antibodies against EphA2 receptors to improve the localization and enrichment of the NPs in the tumor regions. The in vitro enhancement in uptake of E-DSNPs, correlates with our findings from the *in vitro* uptake studies and *in vivo* biodistribution studies from chapters 2 and 3. Furthermore, compared to the folate conjugate core-shell NPs developed earlier by our group [87], we observed nearly 25 times higher NP internalization into A549 cancer cells. Similarly, EphA2 targeting also outperformed CD44 and folate targeting by hyaluronic acid micelles synthesized by Liu et al. [164]. As reported by this study, the addition of folate groups to hyaluronic acid micelles did not improve the uptake of the micelles, conjugation of EphA2 to the hyaluronic acid backbone, resulted in a fold-increase in NP uptake. These results once again highlight the superior and highly specific targeting capability of EphA2.

The synergistic radiation and glutathione responsiveness of the shell and core of the NPs were confirmed. The HA shell acts as a shield to drug leakage from the GSH core, as evidenced by the lack of cisplatin release in the absence of radiation. NU7441 release from the shell demonstrated a sharp burst release when treated with radiation. The GSH responsiveness of the core is similar to previous reports of redox responsive NPs containing disulfide linkages in the polymer backbone, where addition of glutathione enhances drug release from the NPs [112]. Radiation induced release of NU7441 from the shell also follows similar reports of ROS induced drug release from hyaluronic acid based NPs [141]. Chiang et al. [165] reported a single nanocarrier responsive to ROS and GSH levels in the environment. Nearly 100% of campothecin was released from these NPs within 50 hours when exposed to either 100 μM of H_2O_2 or 20 mM of GSH; however, drug release in response to both stimulus together was not studied. Some NP designs incorporating multiple drugs into a single structure for dual drug release have also been investigated. Zhang et al. [166], utilized Poly (lactic-co-glycolic acid)-poly (ethylene glycol) (PLGA-PEG) NPs co-delivering cisplatin and wortmannin (wtmn) to enhance the efficacy of radiation therapy, while reducing side-effects. However, these NPs observed poor drug encapsulation efficiency of about 12.5% and 40% for wtmn and cisplatin respectively, potentially due to the two drugs being loaded into the same NPs resulting in the one drug interfering with the loading of the other drug. The DSNPs, on the other hand, are two-compartment nanoparticles thus loading of one drug does not affect the loading of the other, as evidenced by the higher drug encapsulation efficiencies of cisplatin (~ 56%) and NU7441 (~ 71%).

Various NP formulations for chemo-radiotherapy have been investigated with the central purpose of enhancing therapeutic efficacy, while reducing toxicity to the healthy tissues. Core-

shell nanoparticle structures have gained popularity due to their multi-compartment design that permits the loading of multiple drugs and synergistic drug release. Kim et al. [167], fabricated pluronic-based core-shell NPs encapsulating doxorubicin (dox) in the shell for chemotherapy and gold NPs in the core for radiosensitization of SSC-7 oral cancer cells. The combination of 5 Gy radiation and the dox loaded NPs observed a fold-reduction in the *in vivo* tumor volume, compared to mice treated with the NPs alone without radiation. However, the combined treatment did not result in a complete tumor ablation, with tumor volumes exhibiting a slightly increasing trend with time. Although *in vitro* therapeutic efficacies of these NPs combined with radiation was not investigated, the NPs decreased the viability of SSC-7 cells in a dox dose dependent manner in this study. However, the dox loaded NPs were not as effective as free dox at killing the cancer cells (cancer cell viability of ~ 50% and 30% after 2 days of treatment with the NPs and free dox respectively). E-DSNPs, on the other hand, produced a more distinct cancer cell killing efficacy, with nearly a fold-reduction in cancer cell viability compared to the free drugs, even in the absence of radiation. A single compartment design delivering cisplatin and wtmn lowered the survival of ovarian cancer cells in a radiation dose-dependent manner, with significant increases in sensitization enhancement ratios (SER) from 1.00 to 1.29 for untreated cells and cells treated with dual drug loaded NPs respectively [166]. The core-shell E-DSNPs also observed significant loss in cell viability (up to ~ 60%) compared to untreated cells without any radiation exposure. Furthermore, radiation treatment reduced the cell viability to 18% (i.e. ~ 82% cell death), potentially be due to the addition of targeting antibodies against EphA2 transmembrane receptors that enhanced the preferential localization of the NPs.

The application of NPs for CRT have revolutionized pre-clinical cancer treatment, due to the ability to amplify the benefits of both radiation and chemotherapy alone. Lung cancer chemotherapy using the campothecin loaded ROS/GSH responsive NPs by Chiang et al. [165], observed a drug concentration dependent decrease in A549 lung cancer cell viability to about 60% within 48 hours. Similarly, our dual-drug loaded E-DSNPs also decreased A549 cell viability to nearly 30%. Furthermore, E-DSNPs encapsulating NU7441 only reduced the cell viability by 50%, while E-DSNPs encapsulating cisplatin only reduced the cell viability to 40%. However, exposure to radiation produced a fold-decrease in cell viability compared to cells treated with E-DSNPs without radiation exposure. Similarly, PLGA NPs encapsulating NU7441 and conjugated with R11 to specifically target and treat PC3 prostate cancer cells, revealed a survival fraction of about 0.5 after radiation exposure, compared to about 0.7 for non-drug loaded R11-PLGA NPs [126]. On the other hand, E-DSNPs combined with radiation reduced the survival fraction of A549 lung cancer cells to less than 0.008, compared to 0.41 by E-DSNPs without radiation treatment. These results further signify the advantages of dual drug treatment from core-shell NPs and synergistic radiation therapy for reducing the survival of cancer cells.

Although we have been able to show the improved therapeutic efficacy of the DSNPs and E-DSNPs, there are some limitations to address. One limitation, is that the HA coating on the GNPs may not be sufficient to cover the whole surface of the NPs, which may affect the expected release kinetics of the two drugs. Thus, a future strategy could be to add multiple layers of HA to facilitate complete coverage of the GSH core. However, this may also result in larger NPs, thus affecting their internalization into cancer cells [147]. This chapter also falls short of *in vivo* tumor reduction and biodistribution studies.

4.5. SUMMARY

In summary, we have synthesized dual drug loaded, dual stimuli responsive NPs, that exhibit both radiation-responsive release of NU7441 from the shell, and glutathione-responsive release of cisplatin from the core NPs for concurrent chemo-radiotherapy. These NPs are cyto-compatible and hemo-compatible, in addition to exhibiting enhanced uptake because of the EphA2 targeting moieties on the DSNPs. We also observe an enhancement in the therapeutic efficacy of dual drug loaded DSNPs, compared to those with single drug, thus emphasizing on the improved therapeutic characteristics of these NPs. Furthermore, the therapeutic efficacy of E-DSNPs in conjunction with concurrent radiation, supports the benefits of utilizing E-DSNPs for lung cancer chemo-radiation therapy.

CHAPTER 5: SUMMARY AND FUTURE STUDIES

The goal of this research is to develop core-shell NPs consisting of a glutathione-responsive core and a radiation-responsive shell for cisplatin and NU7441 release, respectively, for use in concurrent chemo-radiation therapy to treat lung cancer. We have approached this goal in a step-by-step manner, by fabricating and characterizing the core and shell of the NPs in separate aims (Aim 1 and 2 respectively), followed by evaluation of the final composite NPs in aim 3. Our results demonstrated the stimuli-responsive nature of each polymer, in terms of enhanced drug release from each layer upon exposure to its respective stimulus. In addition to these findings, the drug release studies performed in aim 3 also fulfill the expected order of drug release from the NPs exposed to both radiation and glutathione. Furthermore, we also evaluated EphA2 receptor targeting to enhance the localization of the NPs at the lung tumor site. Via *in vitro* targeting and *in vivo* biodistribution studies, we observed that the EphA2 targeted NPs not only accumulated more in the lung cancer cells, but also substantially avoided uptake into healthy cells. Subsequently we did observe improved tumor killing abilities of the EphA2 targeted NPs in all three aims. We also observed improved therapeutic efficacies of the NPs from aims 2 and 3 in conjunction with radiation. Furthermore, the *in vivo* therpaeutic efficacy studies in a subcutaneous tumor model in aim 1, observed enhanced lung tumor reduction, when treated with anti-EphA2 tagged GNPs encapsulating cisplatin. Thus, to study the *in vivo* tumor reduction capabilities of EPHNPs and E-DSNPs with concurrent radiation therapy, we will use a subcutaneous tumor model as a proof-of-concept. If successful, we will investigate lung tumor reduction by these NPs in an orthotopic lung tumor model, and utilize inhalation delivery via a nebulizer for NP delivery to the lung tumors.

Although, we have seen success in the development and characterization of the E-DSNPs, there are some limitations associated with the nanoparticle design. For instance, there is some degree of cisplatin leakage from the EGNPs in the absence of glutathione stimulus. To overcome this limitation, we can investigate other variations of the PU-SS polymer, by varying the amount of disulfide linkages in the polymer backbone. Furthermore, to improve the *in vivo* tumor reduction ability of the NPs, we may utilizing different antibody coating techniques or varying the amount of antibody:nanoparticle ratios, that may improve the antibody conjugation efficiency on the NPs and subsequently NP localization in the tumor. Additionally, to improve the therapeutic efficacies of the NPs, we can incorporate higher amounts of drugs into the NPs and/or use layer-by-layer technique to incorporate the drugs onto the NPs. In addition, cisplatin resistance has also been reported to result in tumor relapse, due to either enhanced DNA repair, altered cellular uptake of cisplatin, increased cellular export of cisplatin or drug inactivation in the tumor cells [168]. Thus, therapeutic efficacies may also be improved by utilizing other FDA approved and/or clinically investigated single-drugs or drug-combinations, such as CDK 4/6 inhibitors, histone deacetylate inhibitors, paclitaxel, carboplatin, gemcitabine, and others.

REFERENCES

[1] Siegel RL, Miller KD, Jemal A. Cancer statistics, 2018. CA: Cancer J. Clin. 2018;68:7-30.

[2] Sukumar UK, Bhushan B, Dubey P, Matai I, Sachdev A, Packirisamy G. Emerging applications of nanoparticles for lung cancer diagnosis and therapy. Int Nano Lett. 2013;3:45.

[3] Goldstraw P, Ball D, Jett JR, Le Chevalier T, Lim E, Nicholson AG, et al. Non-small-cell lung cancer. Lancet. 2011;378:1727-40.

[4] Wistuba II, Gazdar AF, Minna JD. Molecular genetics of small cell lung carcinoma. Semin Oncol. 2001;28:3-13.

[5] Wistuba, II, Berry J, Behrens C, Maitra A, Shivapurkar N, Milchgrub S, et al. Molecular changes in the bronchial epithelium of patients with small cell lung cancer. Clin Cancer Res. 2000;6:2604-10.

[6] Doll R, Hill AB. Lung cancer and other causes of death in relation to smoking. Br Med J. 1956;2:1071-81.

[7] Ozlu T, Bulbul Y. Smoking and lung cancer. Tuberks Toraks. 2005;53:200-9.

[8] Husgafvel-Pursiainen K, Hackman P, Ridanpää M, Anttila S, Karjalainen A, Partanen T, et al. K-ras mutations in human adenocarcinoma of the lung: Association with smoking and occupational exposure to asbestos. Int J Cancer. 1993;53:250-6.

[9] McDonald JW, Taylor JA, Watson MA, Saccomanno G, Devereux TR. p53 and K-ras in radon-associated lung adenocarcinoma. Cancer Epidemiol Biomarkers Prev. 1995;4:791.

[10] Spitz MR, Wei Q, Dong Q, Amos CI, Wu X. Genetic susceptibility to lung cancer. Cancer Epidemiol Biomarkers Prev. 2003;12:689.

[11] Mounika P. Helicobacter pylori infection and risk of lung cancer: A meta-analysis. Lung Cancer Int. 2013;2013:6.

[12] Miller KD, Siegel RL, Lin CC, Mariotto AB, Kramer JL, Rowland JH, et al. Cancer treatment and survivorship statistics, 2016. CA: Cancer J. Clin. 2016;66:271-89.

[13] Zappa C, Mousa SA. Non-small cell lung cancer: current treatment and future advances. Transl lung cancer res. 2016;5:288-300.

[14] Kato H. Photodynamic therapy for lung cancer — A review of 19 years' experience. J. Photochem. Photobiol. 1998;42:96-9.

[15] Saha SP, Kalathiya RJ, Davenport DL, Ferraris VA, Mullett TW, Zwischenberger JB. Survival after pneumonectomy for stage III non-small cell lung cancer. Oman Med J. 2014;29:24-7.

[16] Harada H, Okada M, Sakamoto T, Matsuoka H, Tsubota N. Functional advantage after radical segmentectomy versus lobectomy for lung cancer. Ann Thorac Surg. 2005;80:2041-5.

[17] Ginsberg RJ, Rubinstein LV. Randomized trial of lobectomy versus limited resection for T1 N0 non-small cell lung cancer. Ann Thorac Surg. 1995;60:615-23.

[18] Fernandez FG, Kosinski AS, Furnary AP, Onaitis M, Kim S, Habib RH, et al. Differential effects of operative complications on survival after surgery for primary lung cancer. J Thorac Cardiovasc Surg. 2018;155:1254-64.e1.

[19] Handy JR, Jr., Asaph JW, Skokan L, Reed CE, Koh S, Brooks G, et al. What happens to patients undergoing lung cancer surgery? Outcomes and quality of life before and after surgery. Chest. 2002;122:21-30.

[20] Ziarnik E, Grogan EL. Post-lobectomy early complications. Thorac surg clin. 2015;25:355-64.
[21] Babu A, Templeton AK, Munshi A, Ramesh R. Nanoparticle-based drug delivery for therapy of lung cancer: Progress and challenges. J Nanomater. 2013;2013:11.
[22] Scagliotti G, Hanna N, Fossella F, Sugarman K, Blatter J, Peterson P, et al. The differential efficacy of pemetrexed according to NSCLC histology: a review of two Phase III studies. Oncologist. 2009;14:253-63.
[23] Sandler A, Gray R, Perry MC, Brahmer J, Schiller JH, Dowlati A, et al. Paclitaxel-carboplatin alone or with bevacizumab for non-small-cell lung cancer. N Engl J Med. 2006;355:2542-50.
[24] Wheatley-Price P, Shepherd FA. Targeting angiogenesis in the treatment of lung cancer. J Thorac Oncol. 2008;3:1173-84.
[25] Wheatley-Price P, Shepherd FA. Epidermal growth factor receptor inhibitors in the treatment of lung cancer: reality and hopes. Curr Opin Oncol. 2008;20:162-75.
[26] Shepherd FA, Rodrigues Pereira J, Ciuleanu T, Tan EH, Hirsh V, Thongprasert S, et al. Erlotinib in previously treated non-small-cell lung cancer. N Engl J Med. 2005;353:123-32.
[27] Lu J, Liong M, Zink JI, Tamanoi F. Mesoporous silica nanoparticles as a delivery system for hydrophobic anticancer drugs. Small. 2007;3:1341-6.
[28] Gu FX, Karnik R, Wang AZ, Alexis F, Levy-Nissenbaum E, Hong S, et al. Targeted nanoparticles for cancer therapy. Nano Today. 2007;2:14-21.
[29] Luqmani YA. Mechanisms of drug resistance in cancer chemotherapy. Med Princ Pract. 2005;14 Suppl 1:35-48.
[30] Landoni F, Maneo A, Colombo A, Placa F, Milani R, Perego P, et al. Randomised study of radical surgery versus radiotherapy for stage Ib-IIa cervical cancer. Lancet. 1997;350:535-40.
[31] Ko EC, Raben D, Formenti SC. The integration of radiotherapy with immunotherapy for the treatment of non-small cell lung cancer. Clin Cancer Res. 2018; 24:5792-5806
[32] Mesbahi A. A review on gold nanoparticles radiosensitization effect in radiation therapy of cancer. Rep Pract Oncol Radiother. 2010;15:176-80.
[33] Baskar R, Dai J, Wenlong N, Yeo R, Yeoh K-W. Biological response of cancer cells to radiation treatment. Front Mol Biosci. 2014;1:24.
[34] Timmerman R, Paulus R, Galvin J, Michalski J, Straube W, Bradley J, et al. Stereotactic body radiation therapy for inoperable early stage lung cancer. Jama. 2010;303:1070-6.
[35] De Ruysscher D, Belderbos J, Reymen B, van Elmpt W, van Baardwijk A, Wanders R, et al. State of the art radiation therapy for lung cancer 2012: A Glimpse of the Future. Clin Lung Cancer. 2013;14:89-95.
[36] Chemotherapy in non-small cell lung cancer: a meta-analysis using updated data on individual patients from 52 randomised clinical trials. Non-small Cell Lung Cancer Collaborative Group. Br Med J. 1995;311:899-909.
[37] Mattonen SA, Palma DA, Johnson C, Louie AV, Landis M, Rodrigues G, et al. Detection of local cancer recurrence after stereotactic ablative radiation therapy for lung cancer: Physician performance versus radiomic assessment. Int J Radiat Oncol Biol Phys. 2016;94:1121-8.
[38] Citrin DE, Mitchell JB. Altering the response to radiation: Sensitizers and protectors. Semin oncol. 2014;41:848-59.
[39] Sunada S, Kanai H, Lee Y, Yasuda T, Hirakawa H, Liu C, et al. Nontoxic concentration of DNA-PK inhibitor NU7441 radio-sensitizes lung tumor cells with little effect on double strand break repair. Cancer Sci. 2016;107:1250-5.

[40] Yu L, Shang Z-F, Hsu F-M, Zhang Z, Tumati V, Lin Y-F, et al. NSCLC cells demonstrate differential mode of cell death in response to the combined treatment of radiation and a DNA-PKcs inhibitor. Oncotarget. 2015;6:3848-60.
[41] Davidson D, Amrein L, Panasci L, Aloyz R. Small Molecules, inhibitors of DNA-PK, targeting DNA repair, and beyond. Front Pharmacol. 2013;4:5.
[42] Seiwert TY, Salama JK, Vokes EE. The concurrent chemoradiation paradigm—general principles. Nature Clin Prac Oncol. 2007;4:86.
[43] Seiwert TY, Salama JK, Vokes EE. The chemoradiation paradigm in head and neck cancer. Nat Clin Pract Oncol. 2007;4:156-71.
[44] Choy H, Kim DW. Chemotherapy and irradiation interaction. Semin Oncol. 2003;30:3-10.
[45] Miller ED, Fisher JL, Haglund KE, Grecula JC, Xu-Welliver M, Bertino EM, et al. The addition of chemotherapy to radiation therapy improves survival in elderly patients with stage III non–Small cell lung cancer. J Thorac Oncol. 2018;13:426-35.
[46] Gandara DR, Chansky K, Albain KS, Gaspar LE, Lara PN, Jr., Kelly K, et al. Long-term survival with concurrent chemoradiation therapy followed by consolidation docetaxel in stage IIIB non-small-cell lung cancer: a phase II Southwest Oncology Group Study (S9504). Clin Lung Cancer. 2006;8:116-21.
[47] Gandara DR, Chansky K, Albain KS, Leigh BR, Gaspar LE, Lara PN, Jr., et al. Consolidation docetaxel after concurrent chemoradiotherapy in stage IIIB non-small-cell lung cancer: phase II Southwest Oncology Group Study S9504. J Clin Oncol. 2003;21:2004-10.
[48] Furuse K, Fukuoka M, Kawahara M, Nishikawa H, Takada Y, Kudoh S, et al. Phase III study of concurrent versus sequential thoracic radiotherapy in combination with mitomycin, vindesine, and cisplatin in unresectable stage III non-small-cell lung cancer. J Clin Oncol. 1999;17:2692-9.
[49] O'Rourke N, Roque IFM, Farre Bernado N, Macbeth F. Concurrent chemoradiotherapy in non-small cell lung cancer. Cochrane Database Syst Rev. 2010:CD002140.
[50] Brigger I, Dubernet C, Couvreur P. Nanoparticles in cancer therapy and diagnosis. Adv Drug Deliv Rev. 2012;64:24-36.
[51] Iyer R, Hsia CCW, Nguyen KT. Nano-therapeutics for the lung: State-of-the-art and future perspectives. Curr Pharm Design. 2015;21:5233-44.
[52] Taghizadeh B, Taranejoo S, Monemian SA, Salehi Moghaddam Z, Daliri K, Derakhshankhah H, et al. Classification of stimuli–responsive polymers as anticancer drug delivery systems. Drug Deliv. 2015;22:145-55.
[53] Wang X, Zhang M, Zhang L, Li L, Li S, Wang C, et al. Designed synthesis of lipid-coated polyacrylic acid/calcium phosphate nanoparticles as dual pH-responsive drug-delivery vehicles for cancer chemotherapy. Chem Eur J. 2017;23:6586-95.
[54] Thambi T, Deepagan VG, Yoon HY, Han HS, Kim S-H, Son S, et al. Hypoxia-responsive polymeric nanoparticles for tumor-targeted drug delivery. Biomaterials. 2014;35:1735-43.
[55] Guo F, Wu J, Wu W, Huang D, Yan Q, Yang Q, et al. PEGylated self-assembled enzyme-responsive nanoparticles for effective targeted therapy against lung tumors. J Nanobiotechnol. 2018;16:57.
[56] Du J, Lane LA, Nie S. Stimuli-responsive nanoparticles for targeting the tumor microenvironment. J Control Release. 2015;219:205-14.
[57] Wang Y, Deng Y, Luo H, Zhu A, Ke H, Yang H, et al. Light-responsive nanoparticles for highly efficient cytoplasmic delivery of anticancer agents. ACS Nano. 2017;11:12134-44.

[58] Brazel CS. Magnetothermally-responsive nanomaterials: Combining magnetic nanostructures and thermally-sensitive polymers for triggered drug release. Pharm Res. 2009;26:644-56.
[59] Li Y, Tong R, Xia H, Zhang H, Xuan J. High intensity focused ultrasound and redox dual responsive polymer micelles. Chem Commun. 2010;46:7739-41.
[60] Traverso N, Ricciarelli R, Nitti M, Marengo B, Furfaro AL, Pronzato MA, et al. Role of glutathione in cancer progression and chemoresistance. Oxid Med Cell Longev. 2013;2013:10.
[61] Ortega AL, Mena S, Estrela JM. Glutathione in Cancer Cell Death. Cancers. 2011;3:1285-310.
[62] Mura S, Nicolas J, Couvreur P. Stimuli-responsive nanocarriers for drug delivery. Nature Mater. 2013;12:991.
[63] Gamcsik MP, Kasibhatla MS, Teeter SD, Colvin OM. Glutathione levels in human tumors. Biomarkers. 2012;17:671-91.
[64] Sun Y, Yan X, Yuan T, Liang J, Fan Y, Gu Z, et al. Disassemblable micelles based on reduction-degradable amphiphilic graft copolymers for intracellular delivery of doxorubicin. Biomaterials. 2010;31:7124-31.
[65] Wang YC, Wang F, Sun TM, Wang J. Redox-responsive nanoparticles from the single disulfide bond-bridged block copolymer as drug carriers for overcoming multidrug resistance in cancer cells. Bioconjug Chem. 2011;22:1939-45.
[66] Koo AN, Lee HJ, Kim SE, Chang JH, Park C, Kim C, et al. Disulfide-cross-linked PEG-poly(amino acid)s copolymer micelles for glutathione-mediated intracellular drug delivery. Chem Commun (Camb). 2008; 6570-72.
[67] Li Y, Xiao K, Luo J, Xiao W, Lee JS, Gonik AM, et al. Well-defined, reversible disulfide cross-linked micelles for on-demand paclitaxel delivery. Biomaterials. 2011;32:6633-45.
[68] Xu C, Huang Y, Wu J, Tang L, Hong Y. Triggerable degradation of polyurethanes for tissue engineering applications. ACS Appl Mater Interfaces. 2015;7:20377-88.
[69] Liang J, Liu B. ROS-responsive drug delivery systems. Bioeng transl med. 2016;1:239-51.
[70] Tao W, He Z. ROS-responsive drug delivery systems for biomedical applications. Asian J Pharm. 2018;13:101-12.
[71] Napoli A, Valentini M, Tirelli N, Muller M, Hubbell JA. Oxidation-responsive polymeric vesicles. Nat Mater. 2004;3:183-9.
[72] Shim MS, Xia Y. A reactive oxygen species (ROS)-responsive polymer for safe, efficient, and targeted gene delivery in cancer cells. Angew Chem Int Ed. 2013;52:6926-9.
[73] Xu H, Cao W, Zhang X. Selenium-containing polymers: promising biomaterials for controlled release and enzyme mimics. Acc Chem Res. 2013;46:1647-58.
[74] Fang R, Xu H, Cao W, Yang L, Zhang X. Reactive oxygen species (ROS)-responsive tellurium-containing hyperbranched polymer. Polym Chem. 2015;6:2817-21.
[75] Wang M, Sun S, Neufeld CI, Perez-Ramirez B, Xu Q. Reactive oxygen species-responsive protein modification and its intracellular delivery for targeted cancer therapy. Angew Chem Int Ed. 2014;53:13444-8.
[76] Kumari S, Badana AK, G MM, G S, Malla R. Reactive oxygen species: A key constituent in cancer survival. Biomark insights. 2018;13:1177271918755391.
[77] Liou G-Y, Storz P. Reactive oxygen species in cancer. Free radic res. 2010;44:479-96.
[78] Gupta SC, Hevia D, Patchva S, Park B, Koh W, Aggarwal BB. Upsides and downsides of reactive oxygen species for cancer: the roles of reactive oxygen species in tumorigenesis, prevention, and therapy. Antioxid redox signal. 2012;16:1295-322.

[79] Šoltés L, Mendichi R, Kogan G, Schiller J, Stankovská M, Arnhold J. Degradative action of reactive oxygen species on hyaluronan. Biomacromolecules. 2006;7:659-68.
[80] Alonso MJ. Nanomedicines for overcoming biological barriers. Biomed Pharmacother. 2004;58:168-72.
[81] Maeda H, Matsumura Y. Tumoritropic and lymphotropic principles of macromolecular drugs. Crit Rev Ther Drug Carrier Syst. 1989;6:193-210.
[82] Maeda H. The enhanced permeability and retention (EPR) effect in tumor vasculature: the key role of tumor-selective macromolecular drug targeting. Adv Enzyme Regul. 2001;41:189-207.
[83] Noguchi Y, Wu J, Duncan R, Strohalm J, Ulbrich K, Akaike T, et al. Early phase tumor accumulation of macromolecules: A great difference in clearance rate between tumor and normal tissues. Jpn J Appl Phys. 1998;89:307-14.
[84] Matsumura Y, Maeda H. A new concept for macromolecular therapeutics in cancer chemotherapy: Mechanism of tumoritropic accumulation of proteins and the antitumor agent smancs. Cancer Res. 1986;46:6387-92.
[85] Peer D, Karp JM, Hong S, Farokhzad OC, Margalit R, Langer R. Nanocarriers as an emerging platform for cancer therapy. Nat Nanotechnol. 2007;2:751-60.
[86] Pérez-Herrero E, Fernández-Medarde A. Advanced targeted therapies in cancer: Drug nanocarriers, the future of chemotherapy. Eur. J. Pharm. Biopharm. 2015;93:52-79.
[87] Menon JU, Kuriakose A, Iyer R, Hernandez E, Gandee L, Zhang S, et al. Dual-drug containing core-shell nanoparticles for lung cancer therapy. Sci Rep. 2017;7:13249.
[88] Peng X-H, Wang Y, Huang D, Wang Y, Shin HJ, Chen Z, et al. Targeted delivery of cisplatin to lung cancer using ScFvEGFR-heparin-cisplatin nanoparticles. ACS Nano. 2011;5:9480-93.
[89] Patel AR, Chougule M, Singh M. EphA2 targeting pegylated nanocarrier drug delivery system for treatment of lung cancer. Pharm Res. 2014;31:2796-809.
[90] Noberini R, Rubio de la Torre E, Pasquale EB. Profiling Eph receptor expression in cells and tissues: a targeted mass spectrometry approach. Cell Adh Migr. 2012;6:102-12.
[91] Brannan JM, Dong W, Prudkin L, Behrens C, Lotan R, Bekele BN, et al. Expression of the receptor tyrosine kinase EphA2 is increased in smokers and predicts poor survival in non-small cell lung cancer. Clin Cancer Res. 2009;15:4423-30.
[92] Narain A, Asawa S, Chhabria V, Patil-Sen Y. Cell membrane coated nanoparticles: next-generation therapeutics. Nanomedicine (Lond). 2017;12:2677-92.
[93] Gao W, Zhang L. Coating nanoparticles with cell membranes for targeted drug delivery. J drug target. 2015;23:619-26.
[94] Chai Z, Hu X, Lu W. Cell membrane-coated nanoparticles for tumor-targeted drug delivery. Sci China Mater. 2017;60:504-10.
[95] Sun H, Su J, Meng Q, Yin Q, Chen L, Gu W, et al. Cancer-cell-biomimetic nanoparticles for targeted therapy of homotypic tumors. Adv Mater. 2016;28:9581-8.
[96] Elaskalani O, Berndt MC, Falasca M, Metharom P. Targeting platelets for the treatment of cancer. Cancers. 2017;9:94.
[97] Sarin N, Engel F, Kalayda GV, Mannewitz M, Cinatl J, Rothweiler F, et al. Cisplatin resistance in non-small cell lung cancer cells is associated with an abrogation of cisplatin-induced G(2)/M cell cycle arrest. PLoS ONE. 2017;12:e0181081.

[98] Pignon JP, Tribodet H, Scagliotti GV, Douillard JY, Shepherd FA, Stephens RJ, et al. Lung adjuvant cisplatin evaluation: a pooled analysis by the LACE Collaborative Group. J Clin Oncol. 2008;26:3552-9.
[99] Dasari S, Tchounwou PB. Cisplatin in cancer therapy: molecular mechanisms of action. Eur J pharmacol. 2014;0:364-78.
[100] Gonzalez VM, Fuertes MA, Alonso C, Perez JM. Is cisplatin-induced cell death always produced by apoptosis? Mol Pharmacol. 2001;59:657-63.
[101] Lee W-H, Loo C-Y, Traini D, Young PM. Inhalation of nanoparticle-based drug for lung cancer treatment: Advantages and challenges. Asian J Pharm. 2015;10:481-9.
[102] Galluzzi L, Vitale I, Michels J, Brenner C, Szabadkai G, Harel-Bellan A, et al. Systems biology of cisplatin resistance: past, present and future. Cell Death Dis. 2014;5:e1257.
[103] Cao Z-T, Chen Z-Y, Sun C-Y, Li H-J, Wang H-X, Cheng Q-Q, et al. Overcoming tumor resistance to cisplatin by cationic lipid-assisted prodrug nanoparticles. Biomaterials. 2016;94:9-19.
[104] Zhou L, Wang H, Li Y. Stimuli-responsive nanomedicines for overcoming cancer multidrug resistance. Theranostics. 2018;8:1059-74.
[105] Ma Y-C, Wang J-X, Tao W, Sun C-Y, Wang Y-C, Li D-D, et al. Redox-responsive polyphosphoester-based micellar nanomedicines for overriding chemoresistance in breast cancer cells. ACS Appl Mater Interfaces. 2015;7:26315-25.
[106] Basotra M, Singh SK, Gulati M. Development and validation of a simple and sensitive spectrometric method for estimation of cisplatin hydrochloride in tablet dosage forms: Application to dissolution studies. ISRN Anal Chem. 2013;2013:8.
[107] Franken NA, Rodermond HM, Stap J, Haveman J, van Bree C. Clonogenic assay of cells in vitro. Nat Protoc. 2006;1:2315-9.
[108] Kim JC, Saha D, Cao Q, Choy H. Enhancement of radiation effects by combined docetaxel and flavopiridol treatment in lung cancer cells. Radiother Oncol. 2004;71:213-21.
[109] Xu H, Nguyen KT, Brilakis ES, Yang J, Fuh E, Banerjee S. Enhanced endothelialization of a new stent polymer through surface enhancement and incorporation of growth factor-delivering microparticles. J Cardiovasc Transl Res. 2012;5:519-27.
[110] Faustino-Rocha A, Oliveira PA, Pinho-Oliveira J, Teixeira-Guedes C, Soares-Maia R, da Costa RG, et al. Estimation of rat mammary tumor volume using caliper and ultrasonography measurements. Lab Animal. 2013;42:217.
[111] Jensen MM, Jørgensen JT, Binderup T, Kjaer A. Tumor volume in subcutaneous mouse xenografts measured by microCT is more accurate and reproducible than determined by 18F-FDG-microPET or external caliper. BMC Med Imaging. 2008;8:16.
[112] Cheng R, Feng F, Meng F, Deng C, Feijen J, Zhong Z. Glutathione-responsive nano-vehicles as a promising platform for targeted intracellular drug and gene delivery. J Control Release. 2011;152:2-12.
[113] Ryu J-H, Roy R, Ventura J, Thayumanavan S. Redox-sensitive disassembly of amphiphilic copolymer based micelles. Langmuir. 2010;26:7086-92.
[114] Dai L, Li J, Zhang B, Liu J, Luo Z, Cai K. Redox-responsive nanocarrier based on heparin end-capped mesoporous silica nanoparticles for targeted tumor therapy in vitro and in vivo. Langmuir. 2014;30:7867-77.
[115] Acharya S, Sahoo SK. PLGA nanoparticles containing various anticancer agents and tumour delivery by EPR effect. Adv Drug Deliv Rev. 2011;63:170-83.

[116] Moreno D, Zalba S, Navarro I, Tros de Ilarduya C, Garrido MJ. Pharmacodynamics of cisplatin-loaded PLGA nanoparticles administered to tumor-bearing mice. Eur J Pharm Biopharm. 2010;74:265-74.
[117] Song W, Ma Y, Wang J, Brantley-Sieders D, Chen J. JNK signaling mediates EPHA2-dependent tumor cell proliferation, motility, and cancer stem cell-like properties in non-small cell lung cancer. Cancer Res. 2014;74:2444-54.
[118] Brannan JM, Sen B, Saigal B, Prudkin L, Behrens C, Solis L, et al. EphA2 in the early pathogenesis and progression of non-small cell lung cancer. Cancer Prev Res (Phila). 2009;2:1039-49.
[119] Alvarez-Berrios MP, Vivero-Escoto JL. In vitro evaluation of folic acid-conjugated redox-responsive mesoporous silica nanoparticles for the delivery of cisplatin. Int J Nanomedicine. 2016;11:6251-65.
[120] Cheung A, Bax HJ, Josephs DH, Ilieva KM, Pellizzari G, Opzoomer J, et al. Targeting folate receptor alpha for cancer treatment. Oncotarget. 2016;7:52553-74.
[121] Garrett TPJ, Burgess AW, Gan HK, Luwor RB, Cartwright G, Walker F, et al. Antibodies specifically targeting a locally misfolded region of tumor associated EGFR. Proc Natl Acad Sci U S A 2009;106:5082.
[122] Vignard J, Mirey G, Salles B. Ionizing-radiation induced DNA double-strand breaks: A direct and indirect lighting up. Radiother Oncol. 2013;108:362-9.
[123] Javvadi P, Makino H, Das AK, Lin Y-F, Chen DJ, Chen BP, et al. Threonine 2609 phosphorylation of the DNA-dependent Protein Kinase is a critical prerequisite for epidermal growth factor receptor mediated radiation resistance. Mol Cancer Res. 2012;10:1359-68.
[124] Menon JU, Tumati V, Hsieh JT, Nguyen KT, Saha D. Polymeric nanoparticles for targeted radiosensitization of prostate cancer cells. J Biomed Mater Res A. 2015;103:1632-9.
[125] Zhao Y, Thomas HD, Batey MA, Cowell IG, Richardson CJ, Griffin RJ, et al. Preclinical evaluation of a potent novel DNA-dependent protein kinase inhibitor NU7441. Cancer Res. 2006;66:5354-62.
[126] Menon JU, Tumati V, Hsieh J-T, Nguyen KT, Saha D. Polymeric nanoparticles for targeted radiosensitization of prostate cancer cells. J Biomed Mater Res A. 2015;103:1632-9.
[127] Stankovska M, Hrabarova E, Valachova K, Molnarova M, Gemeiner P, Soltes L. The degradative action of peroxynitrite on high-molecular-weight hyaluronan. Neuro Endocrinol Lett. 2006;27 Suppl 2:31-4.
[128] Stanger BZ, Kahn ML. Platelets and tumor cells: a new form of border control. Cancer cell. 2013;24:9-11.
[129] Goubran HA, Kotb RR, Stakiw J, Emara ME, Burnouf T. Regulation of tumor growth and metastasis: the role of tumor microenvironment. Cancer Growth Metastasis. 2014;7:9-18.
[130] Heinmoller E, Weinel RJ, Heidtmann HH, Salge U, Seitz R, Schmitz I, et al. Studies on tumor-cell-induced platelet aggregation in human lung cancer cell lines. J Cancer Res Clin Oncol. 1996;122:735-44.
[131] Hu CM, Fang RH, Wang KC, Luk BT, Thamphiwatana S, Dehaini D, et al. Nanoparticle biointerfacing by platelet membrane cloaking. Nature. 2015;526:118-21.
[132] Dennis JE, Cohen N, Goldberg VM, Caplan AI. Targeted delivery of progenitor cells for cartilage repair. J Orthop Res. 2004;22:735-41.
[133] Ko IK, Kean TJ, Dennis JE. Targeting mesenchymal stem cells to activated endothelial cells. Biomaterials. 2009;30:3702-10.

[134] Jurasz P, Alonso-Escolano D, Radomski MW. Platelet–cancer interactions: mechanisms and pharmacology of tumour cell-induced platelet aggregation. Br J Pharmacol. 2004;143:819-26.
[135] Dehaini D, Wei X, Fang RH, Masson S, Angsantikul P, Luk BT, et al. Erythrocyte–platelet hybrid membrane coating for enhanced nanoparticle functionalization. Adv Mater. 2017;29:1606209.
[136] Hu Q, Sun W, Qian C, Wang C, Bomba HN, Gu Z. Anticancer platelet-mimicking nanovehicles. Adv Mater. 2015;27:7043-50.
[137] Li W, Yi X, Liu X, Zhang Z, Fu Y, Gong T. Hyaluronic acid ion-pairing nanoparticles for targeted tumor therapy. J Control Release. 2016;225:170-82.
[138] Dosio F, Arpicco S, Stella B, Fattal E. Hyaluronic acid for anticancer drug and nucleic acid delivery. Adv Drug Deliv Rev. 2016;97:204-36.
[139] Hu B, Ma Y, Yang Y, Zhang L, Han H, Chen J. CD44 promotes cell proliferation in non-small cell lung cancer. Oncol Lett. 2018;15:5627-33.
[140] Deeble DJ, Phillips GO, Bothe E, Schuchmann HP, von Sonntag C. The radiation-induced degradation of hyaluronic acid. Int J Radiat Appl Instrum C Radiat Phys Chem 1991;37:115-8.
[141] Lee H, Lee K, Kim IK, Park TG. Fluorescent gold nanoprobe sensitive to intracellular reactive oxygen species. Adv Funct Mater. 2009;19:1884-90.
[142] Philippe C, Philippe B, Fouqueray B, Perez J, Lebret M, Baud L. Protection from tumor necrosis factor-mediated cytolysis by platelets. Am J Pathol. 1993;143:1713-23.
[143] Sabrkhany S, Griffioen AW, oude Egbrink MGA. The role of blood platelets in tumor angiogenesis. Biochim Biophys Acta. 2011;1815:189-96.
[144] Hu Q, Sun W, Qian C, Wang C, Bomba HN, Gu Z. Anticancer platelet-mimicking nanovehicles. Adv Mater. 2015;27:7043-50.
[145] Mattheolabakis G, Milane L, Singh A, Amiji MM. Hyaluronic acid targeting of CD44 for cancer therapy: from receptor biology to nanomedicine. J Drug Target. 2015;23:605-18.
[146] Tran TH, Choi JY, Ramasamy T, Truong DH, Nguyen CN, Choi H-G, et al. Hyaluronic acid-coated solid lipid nanoparticles for targeted delivery of vorinostat to CD44 overexpressing cancer cells. Carbohydr Polym. 2014;114:407-15.
[147] Shang L, Nienhaus K, Nienhaus GU. Engineered nanoparticles interacting with cells: size matters. J Nanobiotechnol. 2014;12:5.
[148] Jeong SY, Park SJ, Yoon SM, Jung J, Woo HN, Yi SL, et al. Systemic delivery and preclinical evaluation of Au nanoparticle containing beta-lapachone for radiosensitization. J Control Release. 2009;139:239-45.
[149] Wen C, Zhou Y, Zhou C, Zhang Y, Hu X, Li J, et al. Enhanced radiosensitization effect of curcumin delivered by PVP-PCL nanoparticle in lung cancer. J Nanomater. 2017;2017:8.
[150] Tian X, Lara H, Wagner KT, Saripalli S, Hyder SN, Foote M, et al. Improving DNA double-strand repair inhibitor KU55933 therapeutic index in cancer radiotherapy using nanoparticle drug delivery. Nanoscale. 2015;7:20211-9.
[151] Nikitovic D, Tzardi M, Berdiaki A, Tsatsakis A, Tzanakakis GN. Cancer microenvironment and inflammation: role of hyaluronan. Front Immunol. 2015;6:169.
[152] Huang G, Huang H. Application of hyaluronic acid as carriers in drug delivery. Drug deliv. 2018;25:766-72.
[153] Zhang Y, Liu G, Wei J, Nie G. Platelet membrane-based and tumor-associated platelet-targeted drug delivery systems for cancer therapy. Front Med. 2018.

[154] Luk BT, Fang RH, Hu CM, Copp JA, Thamphiwatana S, Dehaini D, et al. Safe and Immunocompatible Nanocarriers Cloaked in RBC Membranes for Drug Delivery to Treat Solid Tumors. Theranostics. 2016;6:1004-11.
[155] Zhang Y, Cai K, Li C, Guo Q, Chen Q, He X, et al. Macrophage-membrane-coated nanoparticles for tumor-targeted chemotherapy. Nano letters. 2018;18:1908-15.
[156] Yang R, Xu J, Xu L, Sun X, Chen Q, Zhao Y, et al. Cancer cell membrane-coated adjuvant nanoparticles with mannose modification for effective anticancer vaccination. ACS Nano. 2018;12:5121-9.
[157] Baguley BC. Multiple drug resistance mechanisms in cancer. Mol Biotechnol. 2010;46:308-16.
[158] Karasawa T, Steyger PS. An integrated view of cisplatin-induced nephrotoxicity and ototoxicity. Toxicol Lett. 2015;237:219-27.
[159] Rocca JD, Werner ME, Kramer SA, Huxford-Phillips RC, Sukumar R, Cummings ND, et al. Polysilsesquioxane nanoparticles for triggered release of cisplatin and effective cancer chemoradiotherapy. Nanomedicine. 2015;11:31-8.
[160] Price KAR, Azzoli CG, Gaspar LE. Chemoradiation for unresectable stage III non-small cell lung cancer. Semin Thorac Cardiovasc Surg. 2008;20:204-9.
[161] Curran JWJ, Paulus R, Langer CJ, Komaki R, Lee JS, Hauser S, et al. Sequential vs concurrent chemoradiation for stage III non–small cell lung cancer: Randomized phase III trial RTOG 9410. J Natl Cancer Inst. 2011;103:1452-60.
[162] Ghosh Chaudhuri R, Paria S. Core/shell nanoparticles: Classes, properties, synthesis mechanisms, characterization, and applications. Chem Rev. 2012;112:2373-433.
[163] Tandon M, Vemula SV, Mittal SK. Emerging strategies for EphA2 receptor targeting for cancer therapeutics. Expert Opin Ther Targets. 2011;15:31-51.
[164] Liu Y, Sun J, Cao W, Yang J, Lian H, Li X, et al. Dual targeting folate-conjugated hyaluronic acid polymeric micelles for paclitaxel delivery. Int J Pharma. 2011;421:160-9.
[165] Chiang Y-T, Yen Y-W, Lo C-L. Reactive oxygen species and glutathione dual redox-responsive micelles for selective cytotoxicity of cancer. Biomaterials. 2015;61:150-61.
[166] Zhang M, Hagan CT, Min Y, Foley H, Tian X, Yang F, et al. Nanoparticle co-delivery of wortmannin and cisplatin synergistically enhances chemoradiotherapy and reverses platinum resistance in ovarian cancer models. Biomaterials. 2018;169:1-10.
[167] Kim K, Oh KS, Park DY, Lee JY, Lee BS, Kim IS, et al. Doxorubicin/gold-loaded core/shell nanoparticles for combination therapy to treat cancer through the enhanced tumor targeting. J Control Release. 2016;228:141-9.
[168] Amable L. Cisplatin resistance and opportunities for precision medicine. Pharmacol Res. 2016;106:27-36.

BIOGRAPHY

Born and raised in Mumbai, India, Ms. Roshni Iyer got her Bachelor of Engineering in Biomedical Engineering from The University of Mumbai in May 2010. She then moved to Arlington, Texas in August 2010 to pursue a Master of Science degree in Bioengineering at The University of Texas at Arlington (UTA), which she completed in May 2012. As a master's student she performed research in Dr. Kytai T. Nguyen's lab, with her primary research interests in using nanoparticles to treat cardiovascular diseases. Her main research topic involved development of nanoparticle coatings on angioplasty balloons for simultaneous localized nanoparticle delivery to a diseased blood vessel during angioplasty procedure.

Post-graduation, Roshni was hired as a research assistant by Dr. Connie CCW Hsia, a pulmonologist in the Internal Medicine department at University of Texas Southwestern Medical Center (UTSW). There, she evaluated the changes in lung tissue architecture, biomolecular and physiological changes upon lung injury in small animal models. Additionally, she also investigated gene therapy via inhalation drug delivery for treatments of lung injury in small and large animal models. Her job profile included comprehensive data analysis using histology, morphometry and statistical analysis. Her work at UTSW earned her a membership in the Lung repair and regeneration consortium (LRRC) by NHLBI and the American Thoracic Society (ATS), in addition to 2 publications in leading peer-reviewed journals.

In the fall of 2014, Roshni returned to UTA to pursue a doctoral degree in Bioengineering under the guidance of Dr. Kytai T. Nguyen. Here, she adapted her experience in lung based therapies towards developing nanoparticle-based therapeutic modalities for lung cancer treatment. Her major research includes development of targeted-stimuli responsive polymeric nanoparticles-

based drug delivery platforms utilizing chemotherapeutic agents and radiosensitizers for enhanced chemotherapy and radiation therapy and concurrent chemo-radio-therapy. Other research interests include antioxidant treatment using nanoparticles for repair and regeneration of injured lung tissues, local nanoparticle-delivery techniques for angioplasty-assisted treatment of cardiovascular diseases, nanoparticle-based miRNA and small molecule delivery for treatment of breast cancer and glioblastoma. During her PhD career at UTA, Roshni has maintained membership in the Society for Biomaterials and the Biomedical Engineering Society, and presented her research at over 6 international biomedical conferences. She has also published 2 papers in peer-reviewed journals and 1 book chapter, in addition to an article in submission and two other articles in preparation for submission. She has mentored 2 high-school students, 4 undergraduate students and 6 graduate students in research. Besides her research at UTA, Roshni also held the enhanced graduate teaching assistantship at UTA for the drug delivery laboratory and didactic courses (Spring 2015 to Fall 2018).